ARL 63-152

THE TRIAXIAL TENSION FAILURE OF VISCOELASTIC MATERIALS

G. H. LINDSEY
R. A. SCHAPERY
M. L. WILLIAMS
A. R. ZAK

CALIFORNIA INSTITUTE OF TECHNOLOGY
PASADENA, CALIFORNIA

SEPTEMBER 1963

AEROSPACE RESEARCH LABORATORIES
OFFICE OF AEROSPACE RESEARCH
UNITED STATES AIR FORCE

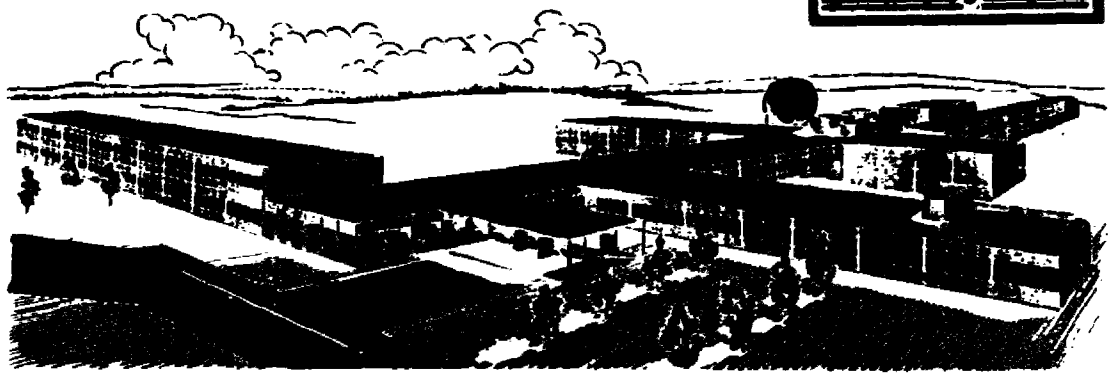

NOTICES

When Government drawings, specifications, or other data are used for any purpose other than in connection with a definitely related Government procurement operation, the United States Government thereby incurs no responsibility nor any obligation whatsoever; and the fact that the Government may have formulated, furnished, or in any way supplied the said drawings, specifications, or other data, is not to be regarded by implication or otherwise as in any manner licensing the holder or any other person or corporation, or conveying any rights or permission to manufacture, use, or sell any patented invention that may in any way be related thereto.

- - - - - - - - - -

Qualified requesters may obtain copies of this report from the Defense Documentation Center, (DDC), Cameron Station, Alexandria, Virginia.

- - - - - - - - - -

This report has been released to the Office of Technical Services, U. S. Department of Commerce, Washington 25, D. C. for sale to the general public.

- - - - - - - - - -

Copies of ARL Technical Documentary Reports should not be returned to Aerospace Research Laboratories unless return is required by security considerations, contractural obligations or notices on a specified document.

500 - October 1963 - 8-131-162

ARL 63-152

THE TRIAXIAL TENSION FAILURE OF VISCOELASTIC MATERIALS

G. H. LINDSEY
R. A. SCHAPERY
M. L. WILLIAMS
A. R. ZAK

CALIFORNIA INSTITUTE OF TECHNOLOGY
PASADENA, CALIFORNIA

SEPTEMBER 1963

Contract AF 33(616)-8399
Project 7063
Task 7063-02

AEROSPACE RESEARCH LABORATORIES
OFFICE OF AEROSPACE RESEARCH
UNITED STATES AIR FORCE
WRIGHT-PATTERSON AIR FORCE BASE, OHIO

FOREWORD

This is an interim report prepared by the Graduate Aeronautical Laboratories of the California Institute of Technology (GALCIT) for the Aerospace Research Laboratories, Office of Aerospace Research, United States Air Force under Contract No. AF 33(616)-8399, Task 7063-02, "Structures Research at Elevated Temperatures," of Project No. 7063, "Mechanics of Flight." This work is based upon analytical and experimental work accomplished from 1 January 1962 through 31 December 1962, under the cognizance of Mr. Charles A. Davies and Lt. W. J. Anderson, ARL Project Scientists.

It is a pleasure to acknowledge the assistance of Mr. Jon M. Kelly in the experimental program and preparation of the report, and also that of the Jet Propulsion Laboratory, California Institute of Technology, in providing use of their facilities for specimen preparation. The notes and data for this report are recorded in GALCIT File No. SM 63-6.

This report is distributed to the Chemical Propulsion Mailing List of 1963.

ABSTRACT

After reviewing present work in failure criteria for various stress states, this report presents both an analytical and theoretical study of triaxial failure of polymeric materials. The configuration chosen for the investigation is a thin, circular, disk-like specimen that is bonded between rigid, cylindrical bars and pulled parallel to its longitudinal axis.

Experimental observations are recorded as well as detailed descriptions of testing techniques. An analytical description of the triaxial stress state used to evaluate experimental results is determined by an approximate solution that satisfies equilibrium on the average. The analysis is in good agreement with a numerical analysis, but also includes a discussion of the effect of singular stresses near the free boundary of the specimen.

Using the minimum potential energy principle, a stability criterion for catastrophic fracture for spherical voids is made, including details of local stresses and strains at the point of fracture, for finite as well as infinitesimal strains. Preliminary correlations of these results with more general failure theories including strain rate and temperature effects for uniaxial and biaxial stress states are indicated.

TABLE OF CONTENTS

1.0 INTRODUCTION AND REVIEW OF RELATED RESEARCH

The general considerations underlying fracture in filled or unfilled viscoelastic materials were given by Williams, Blatz and Schapery[1.1], along with a description of the several types of tests in process or under development by various investigators. Within the reference of the well-known failure surface concept for either stress or strain, it was pointed out that most experimental data had been accumulated for conditions of uniaxial tension only, leaving the failure behavior under multiaxial stressing conditions open to question. Whereas there have been many studies for metal failure criteria, such as the von Mises or octahedral stress association between uniaxial and multiaxial failure, the similar connecting link for viscoelastic materials is just recently being explored. Indeed, and as will be discussed in more detail later, the failure space concept in terms of the three orthogonal principal stresses which form a three-dimensional space (σ_1, σ_2, σ_3) allows for eight different combinations of stress depending upon the octant in which the stress vector lies. Thus for a general material it would be necessary to perform tests in all of the octants corresponding to all possible tension and compression combinations of the three stresses. While material considerations such as isotropy can reduce the number of octants to be tested from eight to a minimum of two if tensile failure is the same as compressive failure, a proper application of the scientific method would require that such implied assumptions be verified by experimentation in as many multiaxial loading conditions as practicable.

The purpose of the investigation reported herein was to study in particular the failure characteristics of an unfilled viscoelastic material subjected to a triaxial tension stress field, i.e. the behavior in the Octant I, using a round, thin disk or "poker-chip" specimen. The discussion of the results is presented essentially in two parts, the experimental and the analytical interpretation. Because of the manner of testing, it was possible to observe certain aspects of flaw formation which are also described and discussed briefly. Generally speaking it was found that (1) near-hydrostatic tensile stresses could be produced and observed in the urethane rubber specimen, that (2) the experimental results could be interpreted analytically, (3) that a fundamental distinction exists between microscopic flaw initiation and overall fracture, and (4) that additional work at several strain rates and temperatures is needed to complete the association between triaxial and uniaxial failure.

1.1 The Concept of a Failure Surface in Stress or Strain Space

In general, materials may be subjected to six stress components, three normal and three shearing, which can be resolved into three principal stresses. On the other hand it is usually simplest to test under one-dimensional conditions such as tension. It is legitimate to ask the question: Having measured the strength in one combination of the three stresses ($\sigma_1 = \sigma_2 = 0$; $\sigma_3 = \sigma_{ult}$), can one then predict without further tests the failure under some other, arbitrary, combination

of the three stresses? Obviously, following a postulated failure criterion, crucial experiments are required to prove or disprove the criterion. Previous experience with metals has indicated that there is no universal criterion for all materials although considerable progress has been made. Over the years several proposed theories of failure have been advanced. Nadai[1.2] enumerates, for example, several different failure criteria, primarily as used in the study of metals, and it is worth restating them here. Each criterion defines some particular functional of the stress field or strain field, the value of which is to be determined empirically, because molecular theories of strength are not advanced to the point of calculating such limits theoretically. When the appropriate functional is exceeded, the associated yield, rupture, or fracture takes place. Seven such criteria are listed below:

a) the maximum principal stress

b) the maximum principal strain

c) the maximum principal stress difference (or shear stress)

d) the maximum principal strain difference (or shear strain)

e) the maximum total strain energy

f) the maximum distortional strain energy

g) the maximum conserved distortional strain energy

Criteria (a) and (b) utilize the fact that the maximum stress (strain) at any point in the material is the largest of the three principal stresses (strains), σ_1, σ_2, σ_3 (ϵ_1, ϵ_2, ϵ_3) at this point. In simple and biaxial tensile fields, these functionals are identical with the yield or ultimate stresses and strains for these fields respectively.

Criteria (c) and (d) stem from the observation that many materials, particularly those which evince ductile fracture (sometimes known as shear fracture) do so along a pair of planes or a cone lying in the direction of greatest shear. The maximum shear stress has the value $1/2\ (\sigma_1 - \sigma_3)$ and is obtained on a plane inclined 45^o to the direction of the principal normal stresses. This criterion is not suitable for mathematical formulation since it is necessary to determine first the maximum or minimum stresses (or strains).

An alternate criterion based on a mean value of the principal stress differences was proposed by von Mises[1.3]. This takes the form

$$\sqrt{2}\ \sigma_o = \sqrt{(\sigma_1-\sigma_2)^2+(\sigma_2-\sigma_3)^2+(\sigma_3-\sigma_1)^2} \qquad (1.1.1)$$

and σ_0 is termed the mean deviatoric stress. For both simple uniaxial tension and biaxial tension, σ_0 is identical with the yield or fracture stress. For pure shear on the other hand, the yield stress turns out to be $\sigma_0/\sqrt{3}$.

The mean deviatoric stress (or strain) has not been listed as a separate criterion, because it is also proportional to the distortional energy criterion proposed by Huber and Hencky[1.4]. They observe that

$$W_d = \frac{\sigma_0^2}{6\mu} = \frac{(\sigma_1-\sigma_2)^2+(\sigma_2-\sigma_3)^2+(\sigma_3-\sigma_1)^2}{12\mu} \qquad (1.1.2)$$

This mean deviatoric stress is also $3/\sqrt{2}$ times a quantity known as the octahedral shear stress. The total strain energy listed under (e) was

proposed by Baltrami and Haigh[1.5]. It does not prove satisfactory since there is no correlation between behavior in pure shear and in pure hydrostatic compression. The conserved distortional strain energy refers to the energy stored in a viscoelastic or plastic material, i.e. over and above the amount dissipated. The theory of application of this criterion is still not in a satisfactory state.

The important point to note is that no universal fracture criterion has been established, and that the success of a given fracture hypothesis depends in large measure upon the material with which it is associated.

Because of the many criteria for fracture, it is convenient to have a method which permits the analyst to visualize their region of possible application. Inasmuch as the three principal stresses are orthogonal and participate in all stress theories of failure, one way of presenting the criteria is in terms of principal stress space where the magnitudes of σ_1, σ_2, and σ_3 are measured along the orthogonal axes to form octants. A similar approach could be adopted for strains. The rupture of an uniaxial tensile specimen at the stress σ_3^* would therefore correspond to a point on the σ_3 axis at the particular value σ_3^*. Other combined loadings would in a similar manner correspond to other points on a rupture surface $F(\sigma_1, \sigma_2, \sigma_3) = \text{constant}$, where the object of failure testing would be to perform experiments under all different combinations of combined stresses in order to trace out the failure surface in all octants. Presumably there would be many surfaces, each corresponding to a given strain rate for which the surface was obtained.

Then, having obtained such surfaces experimentally, the analyst would proceed to check out various criteria in the different octants and the one lying closest to the test surface would be the desired failure criterion.

It is convenient to tabulate the various possibilities in the different octants. By simple permutation one has

Octant	1	2	3	Number of Positive Stresses
I	+	+	+	3
II	+	+	-	2
III	+	-	+	2
IV	+	-	-	1
V	-	+	+	2
VI	-	+	-	1
VII	-	-	+	1
VIII	-	-	-	0

By virtue of equivalence of the three principal axes, it is noted that there are four categories of octants characterized by the number of stresses of the same sign. Thus octants II, III and V are similar, and octants IV, VI, and VII are similar. This means that, for an isotropic material, only four octants need to be tested. If in addition, it is known that the compressive properties are the same as the tensile properties, then only 2 octants need be tested. On the other hand if the material is anisotropic, or if anisotropy is induced by virtue of straining, then it will be necessary to check six octants for an orthotropic material, and eight for a completely aeolotropic material.

It is not the purpose to enter an extended discussion of the various criteria at this time, especially as it is available elsewhere. (1.1, 1.6) On the other hand it is important to recognize how the triaxial tests to be reported subsequently fit into the general scheme of determining failure criteria, and in particular the character of the failure surface in Octant I.

1.2 The Nature of Viscoelastic Behavior

The most important distinguishing characteristic of viscoelastic material is its time dependence. Metals can exhibit creep, which is a time dependent deformation under load, and in a sense viscoelastic deformation is much the same. The major difference between the creep behavior of metals and polymers is recovery. Viscoelasticity usually implies complete recovery, unless the polymer is non-crosslinked such that there are no cross-ties between the molecular chains to inhibit the flow. However with respect to fracture in elastomers, in contrast to metals, it is necessary to extend the usual concept of brittle and ductile failure. Ductile fracture in metals is characterized by irrecoverable distortion and permanent set, analogous to the behavior of an uncrosslinked polymer which also evinces unlimited, unrecoverable flow. On the other hand crosslinked polymers, the type ordinarily employed as engineering components, recover completely from even very large straining although the strain at failure may reach several hundred percent compared to elastic brittle failure in metals of only a few percent. We shall therefore restrict the discussion to crosslinked polymers, and shall use the term elastic fracture as the large strain analog of small

strain fracture customarily referred to as brittle. In either case, however, the stress-strain relation is elastic, or potentially viscoelastic, with the distinguishing feature being the strain magnitude at failure. With this understanding therefore a propellant material might have a brittle fracture below the glass temperature but an elastic fracture above it. It still remains however to deduce which of the various criteria is appropriate for predicting the fracture.

Before continuing, it is appropriate to define the terms elastomer and polymer as used in this report. A polymer is a network of long molecular chains which may or may not be tied together chemically. An important characteristic of all long chain structures is the glass transition temperature T_g above which polymers behave rubberlike, and below which, glasslike. If the polymer chains are not tied together chemically, the structure is termed a plastic - - a brittle plastic below T_g and a rubbery plastic above T_g. The extent of the elastic deformation evinced prior to flow to rupture in the rubbery plastic is markedly a function of interchain entanglement and therefore of chain stiffness or structure.

If on the other hand the polymer chains are tied together chemically, the structure is termed an elastomer or rubber - - a brittle rubber below T_g and a rubbery rubber above T_g. The extent of the elastic deformation evinced prior to rupture in a rubbery rubber is markedly a function of chain length between crosslinks, and is not markedly sensitive to chain structure. Both rubbers and plastics become increasingly viscoelastic as the temperature is lowered with rubbers having lower glass transition temperatures in general than plastics, and thus becoming viscoelastic and then brittle in lower temperature ranges than plastics.

1.2.1 Linear Viscoelastic Behavior

Linear viscoelasticity, which is the type of behavior usually assumed for analytical simplicity and is fortunately a sufficiently close approximation for most cases, implies that the time dependent stress or strain response to a prescribed input force changes only in linear proportion to the magnitude of the applied force, providing the time variation of the force is unchanged.

Researchers have determined several important features of linearly viscoelastic materials. It is first important to recognize that viscoelasticity is intimately associated with the stress-strain behavior — indeed it is the stress-strain behavior. Whereas in the usual application of Hooke's law for metals, one writes that the stress is proportional to strain, with the constant of proportionality being the (time-independent) Young's modulus, one expects the constants of proportionality for viscoelastic materials to be time and rate dependent. The resulting stress-strain law can be cast into several forms such as using the hereditary integral representation[1.7], or perhaps more clearly for the present purposes in terms of spring and dashpot elements which have both a physical and thermodynamic basis[1.8]. In operational form one can write

$$\left[a_n \frac{\partial^n}{\partial t^n} + \cdots + a_0\right]\sigma = \left[b_m \frac{\partial^m}{\partial t^m} + \cdots + b_0\right]\varepsilon \quad (1.2.1)$$

where a_n, b_m are constants, associated with the elastic spring and viscous dashpot elements[1.1], which must be determined experimentally. For example if the material were strictly elastic and not time or rate

dependent, the ratio b_o/a_o would be exactly Young's modulus. The extension of this elasticity concept can be most easily seen by taking Laplace transforms of the foregoing relation to give

$$\bar{\sigma}(p) = \left[\frac{\sum b_m p^m}{\sum a_n p^n}\right] \bar{\epsilon}(p) \equiv E(p)\,\bar{\epsilon}(p) \qquad (1.2.2)$$

such that the analogy between the Laplace transformed stress and strain and the physical elasticity variables is immediately recognized, because the transform parameter p has become merely a parameter in the pseudo-elastic stress-strain law. Viscoelastic stress analysis therefore in principle amounts to solving an associated elastic problem in the Laplace transform variables[1.9], and inverting the solution, exactly or approximately[1.10], to obtain the physical stresses or displacements.

The experimental determination of the a_n, b_m material constants is not the subject of this report, but suffice to say a material characterization must be available before either a stress analysis or a strength analysis can proceed. Techniques for converting test data into a characterization form convenient for engineering use have been previously discussed by Schapery[1.10].

1.2.2 Time-Temperature Relation

In connection with the experimental data it is important to note that a fortunate experimental association between strain rate, or time, and temperature has been established[1.11]. In particular, one has the so-called WLF relation

$$\log_{10} a_T \equiv \log_{10}(t_T / t_R) = -\frac{K_1 (T - T_R)}{K_2 + (T - T_R)} \qquad (1.2.3)$$

where the near universal constants are $K_1 = 8.86$ and $K_2 = 101.8$ for temperature expressed in degrees Centigrade. T_R is a reference temperature found to be approximately $50^{\circ}C$ above the glass transition temperature of the material. In the foregoing expression t_T is the time to observe some phenomenon at the temperature T, and t_R is the time to observe the same phenomenon at the reference temperature. Thus if one measures the relaxation time under a given strain at one temperature, its value at the same strain but at a different temperature may be calculated directly from the WLF equation. Hence providing the material obeys the semi-empirical law, which has been tentatively verified for the material used in our experiments, it is possible to explore the viscoelastic behavior over a wide range of temperature by a reasonable amount of experimentation at one temperature and various imposed strains, or vica versa. While it remains to show that this correlation will apply to failure strains under triaxial stress, the fact that Smith[1.12] has found such correlation for uniaxial tension failure leads one to anticipate similar behavior in multiaxial stress

fields. But again, as indicated in previous paragraphs, because such association has not yet been established experimentally, it would be profitable to do so.

1.3 Failure Behavior in Uniaxial Tension

As discussed previously[1.1], by far the largest accumulation of data relates to fracture of a standard JANAF specimen (Figure 1.1) under simple uniaxial tension at different constant strain rates and temperatures. One common testing machine is the Instron tester which will impose constant crosshead motion through a range of speeds from 0.02 to 20 inches per minute, over a temperature range between -100°F and 160°F. The output of the machine is an automatically recorded force-time trace to fracture (Figure 1.2) which provides the basic experimental information. Depending upon the magnitude of strain to fracture, the data is converted into plots of nominal or true stress, i.e. force divided by original or actual cross sectional area, versus strain. The accuracy of the latter quantity is frequently open to question because the elongation, or crosshead separation, is not distributed evenly over the specimen length and some "effective length" must be selected. It is common practice to use an effective length of 2.7 inches for the JANAF specimen. It has been noted in an earlier[1.1] report however that Baldwin[1.13] and Jones[1.14] have had some success in using a square flat end, bonded specimen which reduces the amount of flow near the grips and hence removes part of the gage length indeterminacy. Greensmith[1.15] has reported and reviewed

another type of tensile test wherein ring or thin hoop specimens are stretched over the two Instron supports. Except for a very small length curved directly around the end supports, the entire (double length) of the specimen is in tension. This type has the definite advantage of keeping the gage length uncertainty to a minimum. It may also be noted that the specimen is easy to test, although somewhat harder to prepare, particularly for filled materials.

The uncertainty in the basic data emphasizes the desirability, and near necessity, of developing local strain indicating devices for low modulus materials. Several improvements along these lines have been attempted, such as using gage marks near the center of longer specimens, or circle patterns distributed over the length. While some increase in accuracy has been reported, the data serve also to indicate in many cases a basic nonhomogeneity in strain distribution due to the filler particles in the propellant.

Neglecting nevertheless these important experimental refinements and working only with the reduced experimental stress-strain data, one turns next to the problem of organizing the extensive test information for many temperatures and strain rates in useful form. Presuming for the most part that maximum stress, σ_m , and strain at maximum stress, ϵ_m , are the more significant quantities Smith[1, 12] has shown for a wide variety of polymers that a very reasonable correlation of ultimate tensile properties can be obtained if the data are plotted against the logarithm of the previously mentioned WLF parameter.

A set of his typical strain data is shown in Figure 1.3 , and similar stress data in Figure 1.4 . Note in the latter case that stress

has been normalized by a temperature ratio because polymer theory predicts a linear increase of retractive forces with absolute temperature. Both sets of data were normalized using the temperature shift factor, experimentally deduced from separately shifting (i) strain at ultimate stress data, (ii) maximum stress data, and (iii) modulus data, and finding all three agreed if the near universal constants $K_1 = 8.86$. $K_2 = 101.6$ and $T_R = 269^{\circ}K$ were used.

Before passing on to a consideration of fracture under multi-axial load conditions, it should be observed that the temperature shift correlation is reasonably well founded experimentally but that the limited strain rate capability of the Instron tester is not particularly well suited for verifying the correlation over wide extremes. This may be noted in Figure 1.3 where the test data at various temperatures barely overlap. One would feel much more confident if, for example, the open circle ($160^{\circ}F$) data obtained over the $1/Ra_T$ range 5 to 8 could be extended to lower values by increasing the strain rate, hence lower $1/Ra_T$, at the same $160^{\circ}F$ temperature. Bearing in mind however the limitation of the tester, approximately 20 inches per minute cross head motion maximum, it is impossible to fulfill this desire without changing the specimen, which would not be particularly acceptable.

The obvious answer is to inquire if higher rate testers would be available. Several have been developed. One of these is the Allegheny Instrument Company device[1.16] which is generally well known. Another is one developed by E. I. DuPont de Nemours and described in a recent paper by Jones[1.17]. Basically this latter machine, which achieves

high loading rates by means of a controlled explosion of smokeless powder in the head, can strain JANAF specimens up to approximately 200, 000 inches per minute. While it is premature to generalize, indications from this and other high speed tester work are that the theoretical WLF shift factor for ultimate fracture of tensile JANAF specimens is sufficiently valid for engineering purposes.

1.4 Related Multi-Axial Testing

Inasmuch as the uniaxial testing procedures for simple JANAF tension specimens are well known and data reduction techniques widely disseminated, the subject has been rather shortly dismissed. On the other hand, from a structural standpoint as distinguished from the quality control objective, the important subject of the fracture behavior of viscoelastic materials subjected to biaxial and triaxial loadings needs considerable amplification, but suffers from lack of experimental data. At the present time, it is proposed to discuss some experiments in this area with particular emphasis upon their suitability for viscoelastic materials and due regard for testing equipment convenience.

1.4.1 Pressurized Tensile Tests

Perhaps one of the simplest extensions of the present uniaxial tensile test using the Instron tester is to enclose the specimen in a leak proof container filled with air or liquid maintained at an arbitrary compressive pressure. Within the same criticisms of the basic test with no external pressure, a triaxial tension-compression stress field

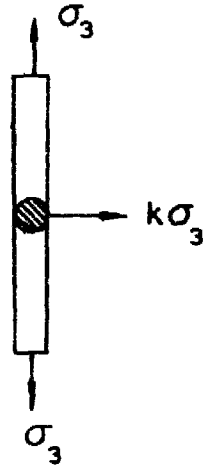

can be imposed. Suppose that the geometry is as shown on the sketch. Then the stress and strain analysis for the central portion of the specimen subjected to the uniaxial tensile stress gives

$$\sigma_3 = \sigma \; ; \qquad \epsilon_3 = \frac{\sigma_3}{E}\left[1 - 2\nu k\right] \tag{1.4.1}$$

$$\sigma_1 = \sigma_2 = k\sigma_3 \; ; \quad \epsilon_1 = \epsilon_2 = \frac{\sigma_3}{E}\left[-\nu + (1-\nu)k\right] \tag{1.4.2}$$

One would expect therefore an apparent uniaxial modulus for this tri-axial field of

$$E_a = \frac{E}{1 - 2\nu k} \tag{1.4.3}$$

where, because in the tests as described k is negative corresponding to a compressive stress, the apparent modulus would be smaller than the uniaxial modulus.

Some unpublished data of Kruse[1.18] suggests that for a filled material, the failure under these conditions agrees equally well with failure data in uniaxial tension expressed either as octahedral shearing stress or uniaxial ultimate tensile strain.

1.4.2 Diametral Compression of a Disk

Fitzgerald[1.19] has suggested that the disk type specimen may also be used in an alternate manner to examine a mixed tension-compression biaxial stress field. If a circular disk of uniform thickness, h, is loaded in diametral compression by a load, P, the stresses at the center are of opposite sign and equal to[1.20]

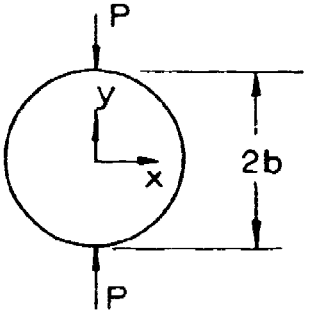

$$\sigma_x(0,0) = \frac{P}{\pi bh} \qquad (1.4.4)$$

$$\sigma_y(0,0) = -\frac{3P}{\pi bh} \qquad (1.4.5)$$

Furthermore the diametral extension, 2u(b, 0) along the horizontal (y = 0) plane is

$$2u(b,0) = \frac{P}{Eh}\left[\frac{4}{\pi} - 1 + \nu\right] \qquad (1.4.6)$$

Providing there is not local failure at the point of load application, this specimen has the advantage that the critical stresses occur at the center and may be easily observed. Furthermore, measurements of the horizontal extension permit an indirect check on the accuracy of the foregoing formulas. Presumably as long as the extension stays linear with the applied load, even though the deformations near the point of application may be large, one would feel justified in using these stress formulas based upon infinitesimal deformation theory. From the standpoint of fracture, Fitzgerald has found[1.19] that the character of failure at the center changes from tensile to shear depending upon the

the temperature of the test. This latter point, of course, emphasizes its potential significance as a sensitive test for determining a fracture criterion.

Incidentally, it may be observed in passing that the range of central stresses which can be imposed, i.e. $\sigma_y / \sigma_x = -3$ from the preceding equations, could be extended by the use of elliptical instead of circular specimens, although at some expense in experimental simplicity. The results of a combined theoretical and experimental investigation using the elliptical specimens have been reported by Brisbane.[1.21]

1.4.3 Torsion of Rod Specimens

Among the various types of mechanical testing, torsion stands as particularly important. There are several reasons for this. First of all, a cylindrical specimen subjected to a small angle of twist undergoes pure shear; the applied torque is directly proportional to the measured twist angle per unit length, the proportionality constant being the shear modulus. Thus the torsion properties for small strain should be independent of Poisson's ratio.

As the shear strain is increased, however, new effects enter the picture. Finite elastic theory predicts a lengthening of the specimen known as the Poynting effect.

It may be deduced that

$$\lambda^3 = 1 + \frac{K^2}{4}(b^2 - a^2) \qquad (1.4.7)$$

where $\lambda = \ell/\ell_o$ is the axial extension ratio

a, b are the inner, outer radius of the cylinder respectively

k is the angle of twist per unit length

One obtains the preceding relation by application of finite elastic theory to the strain transformation defined by

$$\bar{r} = \frac{r}{\sqrt{\lambda}}$$
$$\bar{\theta} = \theta + kz$$
$$\bar{z} = \lambda z$$

where the bars refer to the deformed coordinates of material points. The undetermined constant which enters into the theory because of the incompressibility condition is determined by setting the integral of the axial stress over the end face equal to zero. Figure 1.5 shows a plot of $\lambda^3 - 1$ vs k^2, taken from recent data [1.22] on filled polyurethane. Note the excellent straight line correlation in agreement with theory. The theoretical value of the slope is 1/8 in^2/rad^2, whereas the measured value turns out to be 1/7 in^2/rad^2. Considering the assumptions made in deriving the extension ratio λ, the agreement is excellent. The most important observation that can be deduced from this is that the elastic properties of the binder predominate at least up to three percent shear strain. A similar type of verification is provided by the recent data of Bergen, Messersmith and Rivlin on filled rubbers [1.23].

On the other hand, indications are that the elongation will decrease as the twist is increased further. This is to be expected since the pullaway of the binder from the filler will tend to convert the local shear into local simple tension around the filler particles. What effect

this will have upon fracture in torsion is not known. It is suspected that the fracture criterion will not be as simple for a filled elastomer as an unfilled one, therefore torsion should provide an excellent way to check out the applicability of the distortion strain energy criterion. Furthermore, torsion under superimposed hydrostatic pressure could then be used to check out the importance of anisotropy.

1.4.4 Hollow Tube Tests

Providing a satisfactory strain measurement is available, the behavior of an internally pressurized thin or thick walled cylinder up to and including burst would yield fracture information under biaxial tension, for zero axial stress, or with the added triaxiality depending upon the nature of a finite longitudinal stress. This type of specimen was first used with mixed success at the U. S. Naval Ordnance Test Station[1.24] employing an oil for the pressurization. The major difficulties aside from such obvious ones as preventing leakage, are to obtain an accurate strain history and to measure the applied time varying pressure. These tests can be used upon either thin or thick walled cylinders, and with or without being enclosed in a case. In some cases it will be more convenient to check out a thin case-bonded design using externally mounted wire strain gages and inferring the tube strains by working backward using the theoretical solution. For most purposes however, the resultant case-to-grain stiffness is so high that accuracy is poor.

It should also be mentioned that it is possible to extend the rod torsion tests mentioned in the preceding section to hollow cylinders,

preferably thin walled because of the relative accuracy with which the theoretical solution is known. Another test variation using the hollow tube is the possibility of using this geometry to examine the effect of orthotropy of multi-layered cylinders. Some preliminary analysis along these lines was presented by Pister and was reported in Reference 1.1.

1.4.5 Crack Initiation in Sheet Material

A general review of fracture initiation and propagation in viscoelastic materials has recently been presented by Williams[1.25], where one of the important conclusions was that it now appears possible to understand the mechanics of tearing fracture. In much the same manner as the controlling mechanism of ductile or brittle fracture in plastic distortion vs. surface tension, one finds that the viscous dissipation of energy, not surface tension, is fundamental to tearing in viscoelastic materials. Similar to experiments in metal fracture, it is found that experiments are most conveniently carried out in sheet specimens containing one or more initial cracks. A common configuration for metal sheet specimens not yet used extensively for viscoelastic media is the tensile strip containing a crack perpendicular to the load.* This test in conjunction with Griffith fracture theory[1.26] can be used to determine critical crack length, i.e., to find what size or flaw a given material of specified thickness will sustain under a specified external stress before it becomes unstable and propagates catastrophically. For catastrophic propagation of a brittle fracture Griffith deduced that, for an internal crack of length 2b in an infinite

* See W. G. Knauss, "Rupture Phenomena in Viscoelastic Materials," Ph. D. Dissertation, California Institute of Technology, June 1963.

sheet, the applied stress σ_0 must exceed σ_{cr}, where

$$\sigma_{cr.} = \sqrt{\frac{4ET}{\pi(2b)}} \tag{1.4.8}$$

where T is the characteristic surface tension of the material, pounds per inch. For glass $T \sim 10^{-3}$ pounds per inch.

Viscoelastic materials with their higher internal dissipation are however not usually thought of as brittle materials except in the glassy regions where the above relation might of course be expected to apply. In a fundamental paper Rivlin and Thomas [1.27] proposed an extension of the Griffith hypothesis for the rupture of rubber and found it was possible to correlate the tearing, providing T was interpreted not necessarily as surface energy but merely as a "characteristic energy"

$$T = -\left.\frac{\partial V_{cr.}'}{\partial A}\right|_{\ell} \tag{1.4.9}$$

where the internal strain energy at tearing is V_{cr}', the cross-sectional area of the specimen is $A = 2bh$, and the energy changes are evaluated or measured at a fixed length, i.e. clamped ends.

Their initial work was extended by various collaborators [1.28 - 1.33] who find that an energy criterion does seem to exist as measured upon various geometries and loading conditions. The fact that T is relatively constant, at a fixed strain rate, for various geometries is encouraging. If one approximates their data analytically, it is found that [1.29], for GR-S gum vulcanizate material,

$$T \doteq 6\times10^{5}\left(\frac{3.6}{t\,\text{sec}}\right)^{\frac{1}{6}} \qquad \text{at} \quad 90^{\circ}C \qquad (1.4.10)$$

and

$$T \doteq 40\times10^{5}\left(\frac{0.48}{t\,\text{sec}}\right)^{\frac{1}{6}} \qquad \text{at} \quad 25^{\circ}C \qquad (1.4.11)$$

where t is the time to failure, which reflects the strain rate sensitivity, and T is in ergs per cm^2. (10^7 ergs/cm^2 ≐ 60 in-lbs/in^2).

They further observe that T can be approximated by the relation [1.29]

$$T \approx W_d d \qquad (1.4.12)$$

where W_d is approximately the critical strain energy density for failure as determined in an initially uncracked tensile specimen, $W^{o}_{d} \cong \sigma_0^2/(2E)$, and d is the apparent size of the flaw or the diameter of the crack or razor blade cut at the crack point in the unloaded position. And finally, Greensmith[1.29] presents some data which suggests that W^{o}_{d} may be approximated at 25°C by

$$W^{o}_{d} = 500\times10^{5}\left(\frac{100}{t\,\text{sec}}\right)^{\frac{1}{6}} \qquad (1.4.13)$$

so that dividing the values at 25°C, there results

$$d \approx 0.03\,\text{cm.} \approx 0.01\,\text{in.} \qquad (1.4.14)$$

which is of the order of the measurements also observed by Braden and Gent[1.34, 35]. In principle then one may obtain the characteristic tearing energy by measuring the energy density required to fail a tensile specimen and reduce it by the diameter of the flaw.

It is possible to arrive at their results for a flat sheet by an alternate interpretation in terms of the characteristic average stress distance, δ, which is the distance from the crack tip beyond which the classical elastic solution is valid. If the σ_x and σ_y [1.25] are averaged locally in the vicinity of the crack point, one can deduce an average local stress

$$\bar{\sigma} = \sigma_0 \sqrt{\frac{2b}{\delta}} \qquad (1.4.15)$$

so that the factor $(2b/\delta)^{1/2}$ is essentially a stress concentration factor. Distortion strain energy is computed, taking account of the stress field at the crack $\sigma_x = \sigma_y$ and $\sigma_z = 0$, to find for a Poisson's ratio of one-half

$$W_d = \sigma_x^2(0,0)/(6\mu) \cong \bar{\sigma}^2/(6\mu) \qquad (1.4.16)$$

so that using the value of $\bar{\sigma}$ and assuming incompressibility, the critical strain energy density at failure in this specimen becomes

$$W_d = \frac{\sigma_0^2}{2E}\frac{2b}{\delta} \qquad (1.4.17)$$

But using the classic Griffith formula in the form

$$T = \left(\frac{\sigma_0^2}{2E}\right)\pi b$$

one finds

$$T = \frac{\pi}{2} W_d \delta \qquad (1.4.18)$$

which of course is the same form as $T \approx W_d d$ but associates a characteristic distance within the material, i.e. δ, perhaps a molecular chain bundle diameter, with failure.

It is also possible to show the connection with local radius of curvature[1.37] by working with the general solution for the crack field [1.36]. By integrating the elastic stress field to find the displacements, one can compute in particular the displacements of the crack boundary for the deformed, i.e. loaded, specimen. For the internally cracked specimen the shape of the crack or hole is elliptical[1.38] and the radius of curvature at the sharp point of the crack, R, can be associated with the applied stress as

$$R = 4\, b \left(\frac{\sigma_0}{E}\right)^2 \qquad (1.4.19)$$

and hence in terms of the average local stress, $\bar{\sigma}$,

$$2R = d = \delta\left(\frac{2\bar{\sigma}}{E}\right)^2 \qquad (1.4.20)$$

so that one has the further comparison

$$T = \frac{\pi}{2} W_d\, d \left(\frac{E}{2\bar{\sigma}}\right)^2 \qquad (1.4.21)$$

which would also agree with $T \approx W_d d$ if the local value of averaged stress at the crack approached values of half the tensile modulus*.

It should be emphasized that these latter associations have been made after utilizing the assumptions of infinitesimal elastic deformations for sheet specimens whereas the work of Rivlin et al. includes large strain measurements on various geometries. Nevertheless it is encouraging to see that the effects predicted by more sophisticated stress analysis are not inconsistent with these other experiments and analyses.

1.5 Biaxial Failure in Sheet Specimens

Failure experiments under biaxial tension, which contribute data for the limiting planes of Octant I of the failure surface, can be most easily performed using a pressurized membrane. On the other hand, even a thin membrane has finite thickness and hence in trying to resist bending, particularly near the supporting edge, the specimen often tends to fracture under combined bending and stretching stresses (1.18, 1.39). Also the contribution to the stress field due to the clamping pressure at the support, necessary to prevent the specimen from pulling out of the test fixture when the pressure is applied, tends to make the correlation of analysis and experiment difficult. On the other hand if the failure takes place near the center of the, say, circular membrane specimen, incidentally usually implying rounding off the support edges in order to induce failure away from the edge,

---

* This type of assumption has been invoked by H. Neuber, Theory of Notch Stresses, in estimating the maximum stress at a crack point in metals.

useful data should result if the applied strain rate can be controlled.

1.5.1 The Homogeneous Biaxial Test

Another type of test, explored in a related GALCIT program [1.40] is one wherein equal biaxial tension has been imposed, without normal pressure, by merely applying unifo m displacement around the edges of a square sheet specimen whose sides are glued to wire hooks approximately one half inch apart. The other ends of these hooks are attached to small ball bearings which are supported, and are allowed to slide on, two V-shaped guides which can be seen in Figure 1.6 . As the load is applied to the guides this arrangement produces the homogeneous biaxial extensions described above. There is of course always some non-homogeneous deformation of the specimen near the edges; however, by painting square grids on the surface and observing their deformation it was found that these edge effects propagated only a small distance into the specimen. The biggest problem with these tests is the premature fracture in the vicinity of the hooks. This problem was eventually solved by changing the design and spacing of the hooks.

1.5.2 The Strip Tension Test

A second biaxial, but not equal, tensile field specimen tested at GALCIT[1.40, 41] consisted of a rectangular sheet specimen bonded on its longer edges to steel plates which are then connected to the testing machine grips, (Figure 1.7) A tensile stress σ_z is applied perpendicular to the longer edges of the specimen. The stress normal to the

sheet, σ_y, is zero. Under these conditions a major portion of the specimen between the plates is subject to plane strain conditions along most of its longer length, i.e. $\epsilon_x = 0$, $\epsilon_y = \nu\epsilon_z$, $\epsilon_z = \sigma_z(1-\nu^2)/E$. Near the ends of course the conditions are not plane strain; however the end effects can be reduced by increasing the length of the specimen.

The first strip experiments performed were not very successful in producing failure data since premature cracks were formed near the ends of the specimen. This problem was subsequently corrected by redesigning the plates, which were glued to specimens, so as to have rounded-off corners instead of sharp ones. Further improvement was obtained by designing "dog-bone" shape specimens (1.42). These specimens have a low stress in the vicinity of the plates and the failure always occurs in the center portion of the specimens. A mold has now been made which enables casting a number of these specimens simultaneously.

In all of these experiments the extension and the load were measured on the Instron machine, the strain was then calculated by assuming that the extension was uniformly distributed over the total strained width of the specimens. The changes of thickness of the specimens were measured by the micrometer device referred to above. This device consisted of two micrometers, capable of reading to 10^{-4} inches, fixed on an aluminum U-shaped bracket. The micrometers were electrically isolated from the bracket and connected to opposite terminals of a dry battery. The specimens were coated with a conductive fluid and therefore when both micrometer spindles were

touching the specimen the electrical circuit was complete; this permitted very accurate thickness readings.

1.5.3 Comparative Data

The latter two tests have proven reasonably efficient for assessing both the mechanical characterization and the failure characteristics of several materials such as[1.40, 41, 43]

a) SBR - 1500 rubber (1.75 % S)

b) SBR - 1500 rubber (3 % S)

c) Polyurethane foam rubber (47 % voids by volume, 40μ diameter)

d) Natural rubber (2 % sulphur)

e) Natural rubber (4 % sulphur)

f) CIS - 4

g) Paracril - B

h) Neoprene - GNA

i) Butyl - 217

The mechanical (stress-strain) characterization of the material involves the determination of the form of the strain energy function, which procedure is discussed in reference (1.44). The evaluation of the failure data and a determination of the failure criterion from the experimental data is described in reference (1.45). The first step in obtaining the form of the strain energy function[1.44] is to assume the basic form of this function which is completely defined up to certain unknown parameters. From this form of the energy function the stress-strain relations are then calculated using finite elastic theory. The constitutive

laws thus obtained are then compared to the experimental data from the uniaxial, biaxial and triaxial tests. This comparison enables the evaluation of the unknown parameters in the assumed energy function. The failure surface obtained from the experimental data is shown in Figure 1.8 , which is taken directly from reference (1.45). It can be seen from this figure how the failure surface is developed from the four different types of tests. The uniaxial tests define the points at which the failure surface intercepts the three stress axes and the biaxial tests, both the strip and the homogeneous, define the lines of intersections along the three stress planes. The data from the triaxial tests produce points which define the actual shape of the failure surface throughout the octant itself.

The procedure for carrying out the latter two kinds of biaxial tests has been developed to high efficiency, and a large amount of data has been obtained for the purpose of mechanical characterization and for defining failure criteria for several materials.[1.46] Most of the experiments however have been conducted at room temperatures and slow loading rates. It remains, therefore, to extend this work over a range of temperatures and loading rates. The Instron testing machine including a temperature cabinet is now operational and thus the complete test facility will permit experiments to be conducted in the temperature range from -100 to + 250°F.

1.6 Triaxial Tension Failure

It has previously been indicated that one of the important combined stress fields was that of triaxial tension. Fracture under

this loading condition, Octant I, would contribute heavily toward determining the overall fracture surface. In particular if the material could be considered as isotropic and homogeneous, thus probably excluding filled materials, a definition of the failure surface in this octant would give one fourth of the information necessary for defining the complete surface, because as shown earlier only four of the eight octants would be independent.

The production of a triaxial tension field is not easy unless only small stresses are desired, in which case vacuum pressure can be used. Usually however fracture stresses exceed 15 psi and one must resort to more complicated means of producing the desired triaxial condition. A commonly proposed method is that of a thin disk cemented between two relatively rigid platens which are pulled in tension. The dimensions of the specimen give rise to its designation as a "poker chip" test. As fortunately the material to be tested is rather soft compared to easily available much harder platen materials*, the softer disk sandwiched between the harder bars will be restrained, because of its thinness, from its usual contraction perpendicular to the load and hence generate a triaxial tension stress field.

The elementary analysis for this case may be made by assuming the disk infinitely thin such that the external radius is sufficiently far from the center to assume the only non-zero displacement, w, is in the x_3 axial direction. Under these conditions, one is led to deduce for small deformations

---

* Note that it would not be practical to test steel for its triaxial tensile behavior.

$$\sigma_3 = \sigma \quad ; \quad \epsilon_3 = \frac{\sigma(1-2\nu)(1+\nu)}{E(1-\nu)} \tag{1.6.1}$$

$$\sigma_1 = \sigma_2 = \frac{\nu}{1-\nu}\,\sigma \quad ; \quad \epsilon_1 = \epsilon_2 = 0 \tag{1.6.2}$$

so that the apparent axial modulus becomes

$$E_a = E\left[\frac{1-\nu}{(1-2\nu)(1+\nu)}\right] \tag{1.6.3}$$

where it may be noted that for rubbery materials, which are characteristically nearly incompressible, i.e., $\nu \approx 1/2$, the triaxial tension approaches hydrostatic with a consequent infinite apparent axial stiffness.

In the following sections, the results of GALCIT tests of a viscoelastic rubber will be discussed in some detail, from first the theoretical and then the analytical standpoint. Before that however it may be mentioned that similar exploratory tests, also using poker chip specimens, have been carried out for rubber foams[1.43, 45]. It was tentatively established that the failure criterion was the mean hydrostatic stress. Thus the first octant failure surface for the foam in question would be a plane cutting the three principal stress axes at the uniaxial failure stress, or more generally

$$\sigma_{critical} = \sigma_{uni} = \frac{1}{3}\left[\sigma_1 + \sigma_2 + \sigma_3\right] \tag{1.6.4}$$

It would be premature of course to assume that the same criterion would hold in general, but in principle this example serves to illustrate the direction which further correlation will take for the solid viscoelastic rubber specimens now to be described.

REFERENCES

1.1 Williams, M. L.; Blatz, P. J.; Schapery, R. A.: Fundamental Studies Relating to Systems Analysis of Solid Propellants. GALCIT SM 61-5, California Institute of Technology, February 1961. (ASTIA Report No. AD 256-905.)

1.2 Nadai, A.: Theory of Flow and Fracture of Solids. p. 175, McGraw-Hill Book Company, Inc. 1950.

1.3 Mises, R. V.: Die Differential und Integral-Gleichungen der Mechanik and Physik, Vol. 2, p. 605, 1927.

1.4 Hencky, H.; Angew, Z.: Math.Mechanick, Vol. 4, p. 323, 1924.

1.5 Haigh, B. P.: Engineering, Vol. 190, p. 158, 1920.

1.6 Blatz, P. J.: The Yield Surface in Normal Stress or Normal Strain Space. Proceedings of JANAF Meeting, September 1960.

1.7 Alfrey, T. Jr.: Mechanical Behavior of High Polymers. Interscience Publishers Inc. New York 1948.

1.8 Schapery, R. A.: Irreversible Thermodynamics and Variational Principles with Applications to Viscoelasticity. ARL 62-418, August 1962, Aeronautical Research Laboratories, Wright-Patterson Air Force Base, Ohio.

1.9 Lee, E. H.: Viscoelastic Stress Analysis. Structural Mechanics Proceedings of the First Symposium on Naval Structural Mechanics, Edited by J. N. Goodier and N. J. Hoff, Pergamon Press, 1960.

1.10 Schapery, R. A.: Approximate Methods of Transform Inversion for Viscoelastic Stress Analysis. GALCIT SM 62-2, January 1962, California Institute of Technology. To be published in the Proceedings of the Fourth U. S. National Congress of Applied Mechanics, held June 1962.

1.11 Williams, M. L.; Landel, R. F.; Ferry, J. D.: The Temperature Dependence of Relaxation Mechanisms in Amorphous Polymers and Other Glass-Forming Liquids. Journal of American Chemical Society, Vol. 77, pps 3701-3707, 1955.

1.12 Landel, R. F.; Smith, T. L.: Viscoelastic Properties of Rubber-like Composite Propellants and Filled Elastomers. ARS Journal May, 1961, p 599.

1.13 Baldwin, J. B.; Cooper, M. H.: Preliminary Report on a Bonded Tensile Specimen. Bulletin 19th Meeting of JANAF Physical Properties Panel, September 1960, p. 151.

1.14 Jones, J. W.; Daniel, D.; Johnson, D. A.: Propellant Viscoelastic Characterization in Creep and Stress Relaxation Tests. 20th Meeting Bulletin of JANAF Panel on Physical Properties of Solid Propellants, Vol. 1, November 1961. p. 193.

1.15 Greensmith, H. W.: Rupture of Rubber. VII. Effect of Rate of Extension in Tensile Tests. Journal of Applied Polymer Science, Vol. 3, No. 8, p. 175, 1960.

1.16 Brettschneider, H.; Dale, W.: Experience with the Alinco High Rate Tensile Tester. Bulletin of 17th Meeting of JANAF Physical Properites Panel, p. 43, May 1958.

1.17 Jones, J.: Tensile Testing of Elastomers at Ultra High Strain Rates. Presented at High Rate Symposium, Boston, Massachusetts, January 1960.

1.18 Kruse, R. B.: Unpublished data, Thiokol Chemical Corporation, Huntsville, Alabama. March 1962.

1.19 Fitzgerald, J. E.: A Biaxial Test for Solid Propellants. Bulletin of 19th Meeting of JANAF Physical Properties Panel, September 1960.

1.20 Timoshenko, S.; Goodier, J. N.: Theory of Elasticity. McGraw-Hill Book Company, Inc., New York, 1951.

1.21 Brisbane, J. J.: Stress Distribution in an Elliptical Disk with Concentrated Loads Acting Along the Axes of Symmetry. Quarterly Progress Report No. P-61-25, Rohm and Haas Company, January 26, 1962.

1.22 Dowler, W.; Lewis, G.; Stimpson, L. D.: Torsion Testing of Solid Propellants. Bulletin of 18th Meeting of JANAF Physical Properties Panel, p. 27, June 1959.

1.23 Bergen, N.; Messersmith, W.; Rivlin, R. S.: The Stress Relation for Biaxial Deformation of Filled High-Polymers. ASME Meeting, New York City, December 1959.

1.24 Ordahl, D. D.: Burst Tests on Solid Propellants. (NOTS Burst Test) Bulletin of 8th Meeting of JANAF Physical Properties Panel, p. 7, July 1953.

1.25 Williams, M. L.: The Fracture of Viscoelastic Material. To be published in Fracture of Solids, Edited by Drucker, D. C. and Gilman, J. J., Interscience Publishers. 1963.

1.26 Griffith, A. A.: The Phenomena of Rupture and Flow in Solids. Philosophical Transactions of the Royal Society (London), Series A, Vol. 221, pp 163-198, 1921. See also: The Theory of Rupture. Proceedings of the First International Congress for Applied Mechanics, pp. 55-63, 1924.

1.27 Rivlin, R. S.; Thomas, A. G.: Rupture of Rubber. I. Characteristic Energy for Tearing. Journal of Polymer Science, Vol. 10, no. 3, p. 291, 1953.

1.28 Greensmith, H. W.: Rupture of Rubber. VII. Effect of Rate of Extension in Tensile Tests. Journal of Applied Polymer Science, Vol. 3, no. 8, p. 175, 1960.

1.29 Greensmith, H. W.: Rupture of Rubber. VIII. Comparison of Tear and Tensile Rupture Measurements. Journal of Applied Polymer Science, Vol. 3, no. 8, p. 183, 1960.

1.30 Thomas, A. G.: Rupture of Rubber. II. The Strain Concentration at an Incision. Journal of Polymer Science, Vol. 18, p. 177, 1955.

1.31 Greensmith, H. W.; Thomas, A. G.: Rupture of Rubber. III. Determination of Tear Properties. Journal of Polymer Science, Vol. 18, p. 189, 1955.

1.32 Greensmith, H. W.: Rupture of Rubber. IV. Tear Properties of Vulcanizates Containing Carbon Black. Journal of Polymer Science, Vol. 21, p. 175, 1956.

1.33 Thomas, A. G.: Rupture of Rubber, VI. Further Experiments on the Tear Criterion. Journal of Polymer Science, Vol. 3, no. 8, p. 168, 1960.

1.34 Braden, M.; Gent, A. N.: The Attack of Ozone on Stretched Rubber Vulcanizates. I. The Rate of Cut Growth. Journal of Applied Polymer Science, Vol. 3, no. 7, p. 90, 1960.

1.35 Braden, M.; Gent, A. N.: The Attack of Ozone on Stretched Rubber Vulcanizates. II. Conditions for Cut Growth. Journal of Applied Polymer Science, Vol. 3, no. 7, p. 100, 1960.

1.36 Inglis, C. E.: Stresses in a Plate Due to the Presence of Cracks and Sharp Corners. Transactions of the Institute of Naval Architects (London), Vol. LV, pp. 219-230, 1913.

1.37 Williams, M. L.: Discussion of "Analysis of Stresses and Strains Near the End of a Crack Traversing a Plate (Journal of Applied Mechanics, Sept. 1957, by G. R. Irwin)". Journal of Applied Mechanics, Vol. 25, no. 2, p. 299, June 1958.

1.38 Ang, D. D.; Williams, M. L.: Combined Stresses in an Orthotropic Plate Having a Finite Crack. Journal of Applied Mechanics September, 1961, pp 372-378.

1.39 Spangler, R.: Unpublished data. DuPont Eastern Laboratories, Gibbstown, N. J., September, 1961.

1.40 Blatz, P. J.; Ko, W. L.; Zak, A. R.: Fundamental Studies Relating to the Mechanical Behavior of Solid Propellants, Rocket Grains and Rocket Motors. GALCIT SM 61-19, October 1961, California Institute of Technology.

1.41 Blatz, P. J.; Ko, W. L.; Zak, A. R.: Fundamental Studies Relating to the Mechanical Behavior of Solid Propellants, Rocket Grains and Rocket Motors. California Institute of Technology, GALCIT SM 61-15, June 1961.

1.42 Progress Report No. 11, June 11, 1962, Contract No. AF 33(616)-8399, for the period 1 May 1962 - 31 May 1962, GALCIT 119.

1.43 Blatz, P. J.; Ko, W. L.; Zak, A. R.: Fundamental Studies Relating to the Mechanical Behavior of Solid Propellants, Rocket Grains and Rocket Motors. GALCIT SM 62-27, California Institute of Technology, November 1962.

1.44 Blatz, P. J.; Ko, W. L.; Zak, A. R.: Fundamental Studies Relating to the Mechanical Behavior of Solid Propellants, Rocket Grains and Rocket Motors. GALCIT SM 62-14, California Institute of Technology, February 1962.

1.45 Blatz, P. J.; Ko, W. L.; Zak, A. R.: Fundamental Studies Relating to the Mechanical Behavior of Solid Propellants, Rocket Grains and Rocket Motors. GALCIT SM 62-23, California Institute of Technology, May 1962.

1.46 Ko, W. L.: Application of Finite Elastic Theory to the Behavior of Rubber-Like Materials," Ph. D. Dissertation, California Institute of Technology, June 1963.

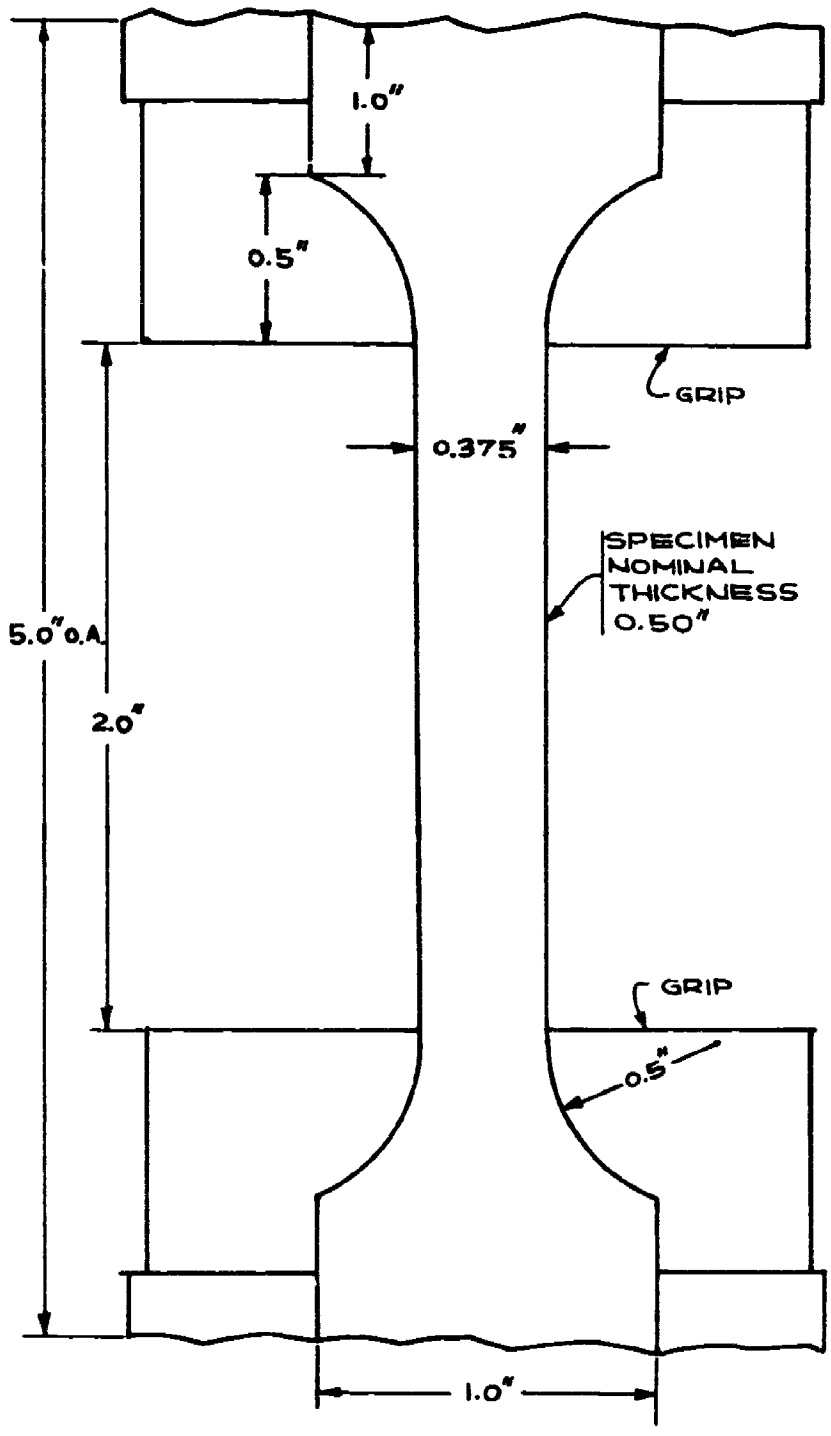

FIG. 1.1 STANDARD JANAF TENSILE SPECIMEN

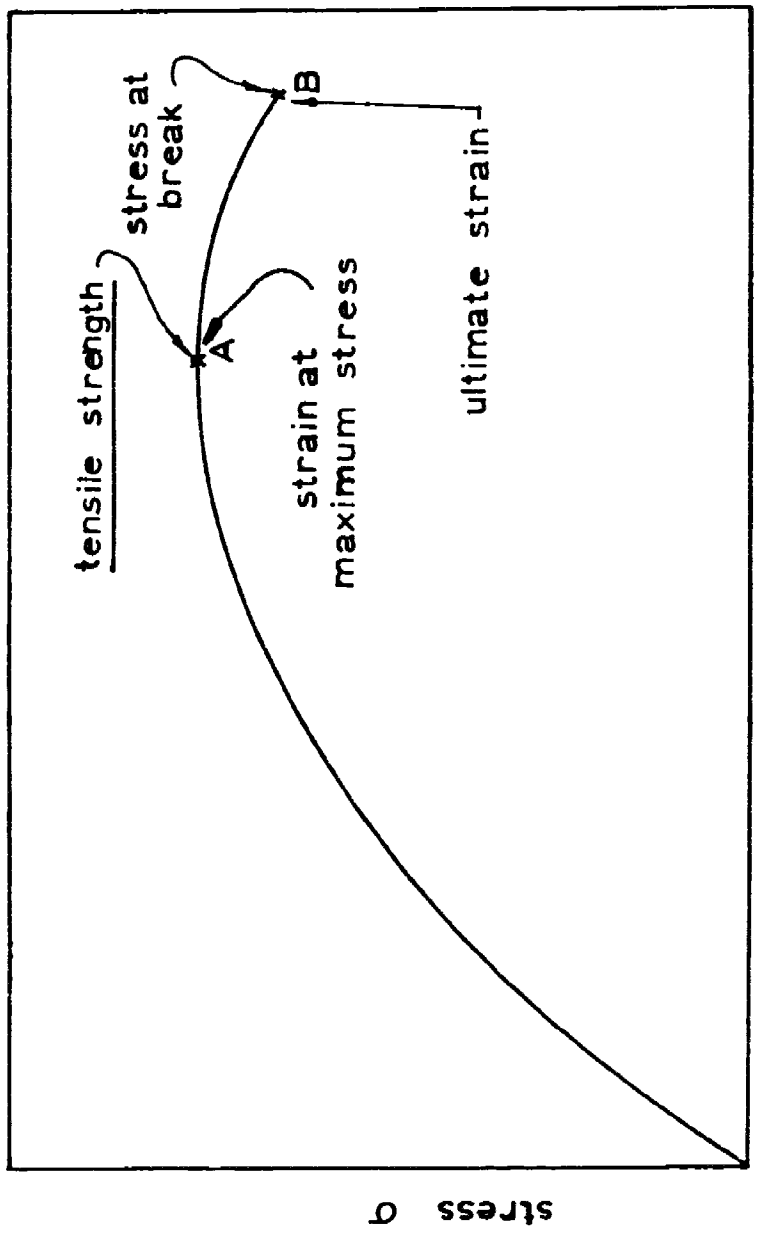

Fig. 1.2. Typical Reduced Instron Tensile Curve.

Fig. 1.3. Ultimate strain master curve (Landel and Smith Jet Propulsion Laboratory, External Publication No. 655, June 1959).

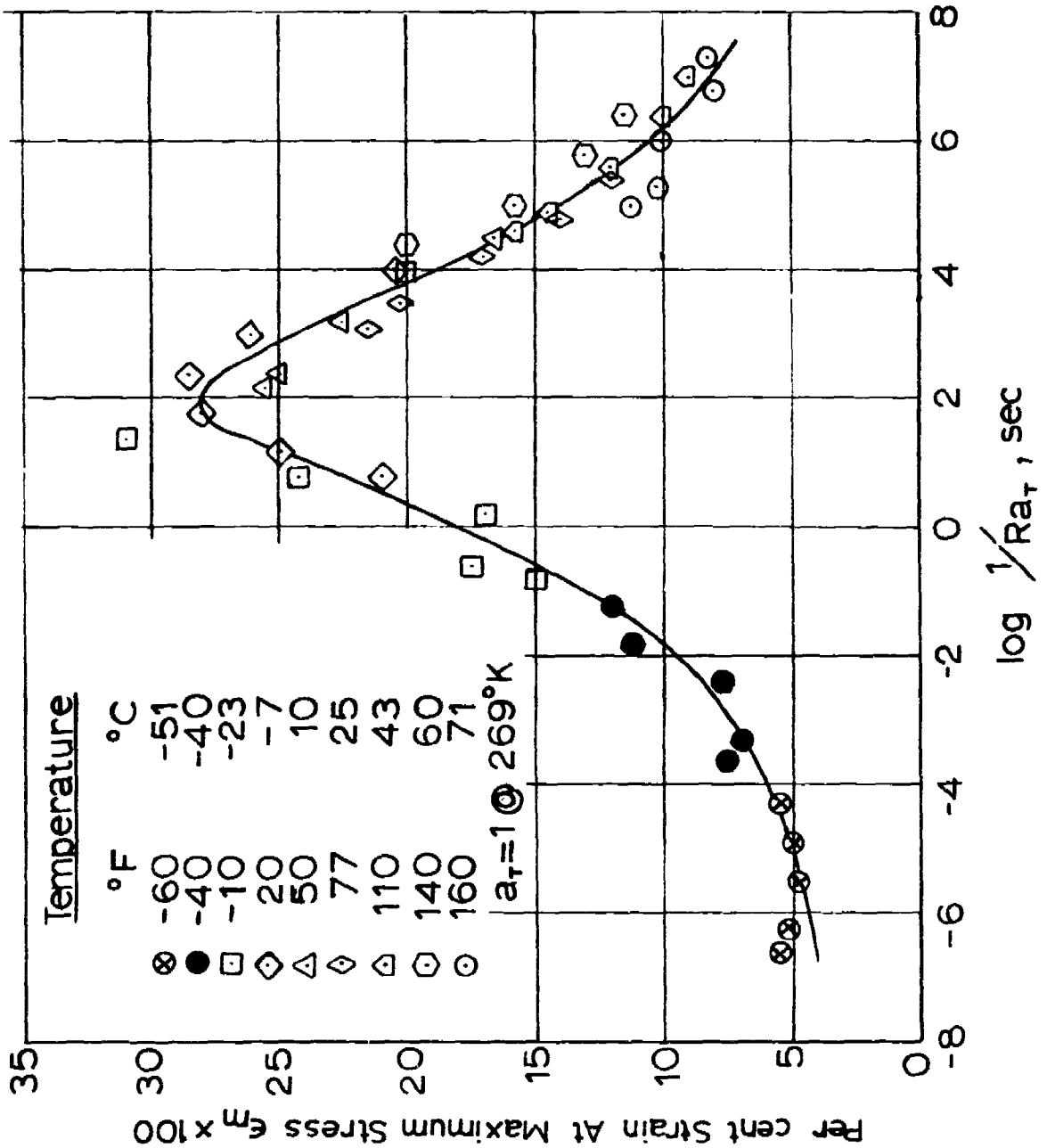

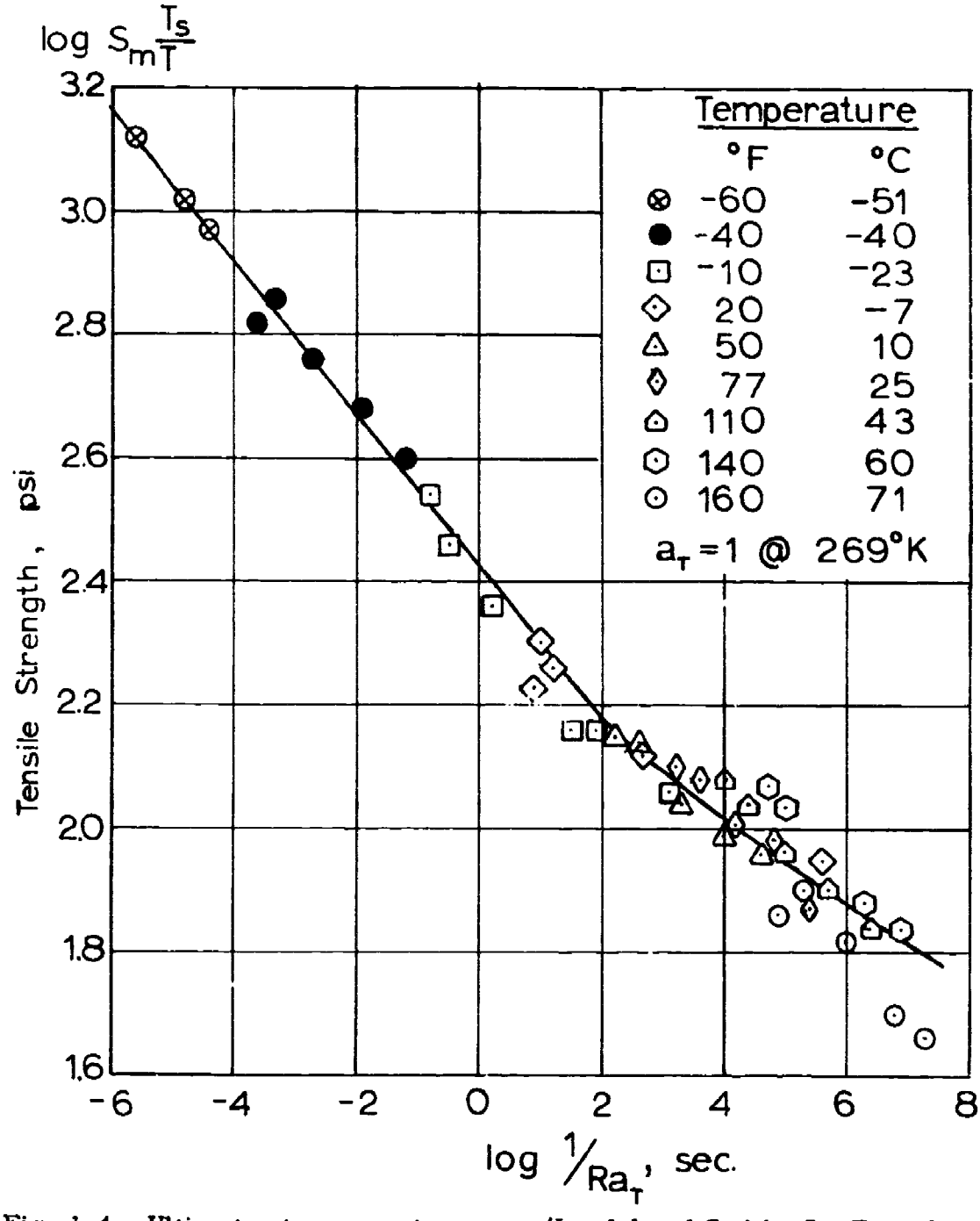

Fig. 1.4. Ultimate stress master curve (Landel and Smith, Jet Propulsion Laboratory, External Publication No. 655, June 1959).

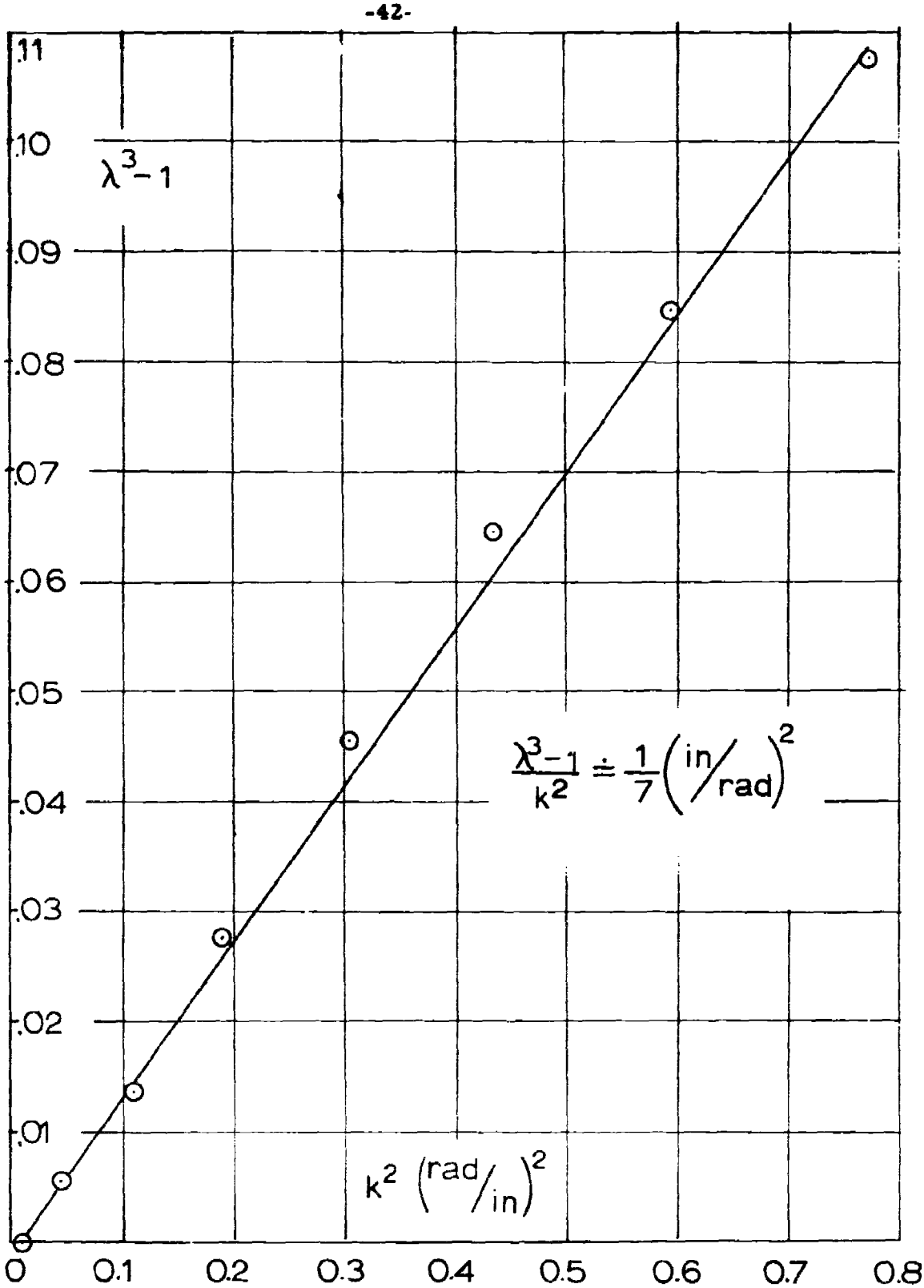

Fig. 1.5. Axial Elongation as a Function of Torsional Shear.

Fig. 1.6 Homogeneous-Biaxial Tension

Fig. 1.7 Strip-Biaxial Tension

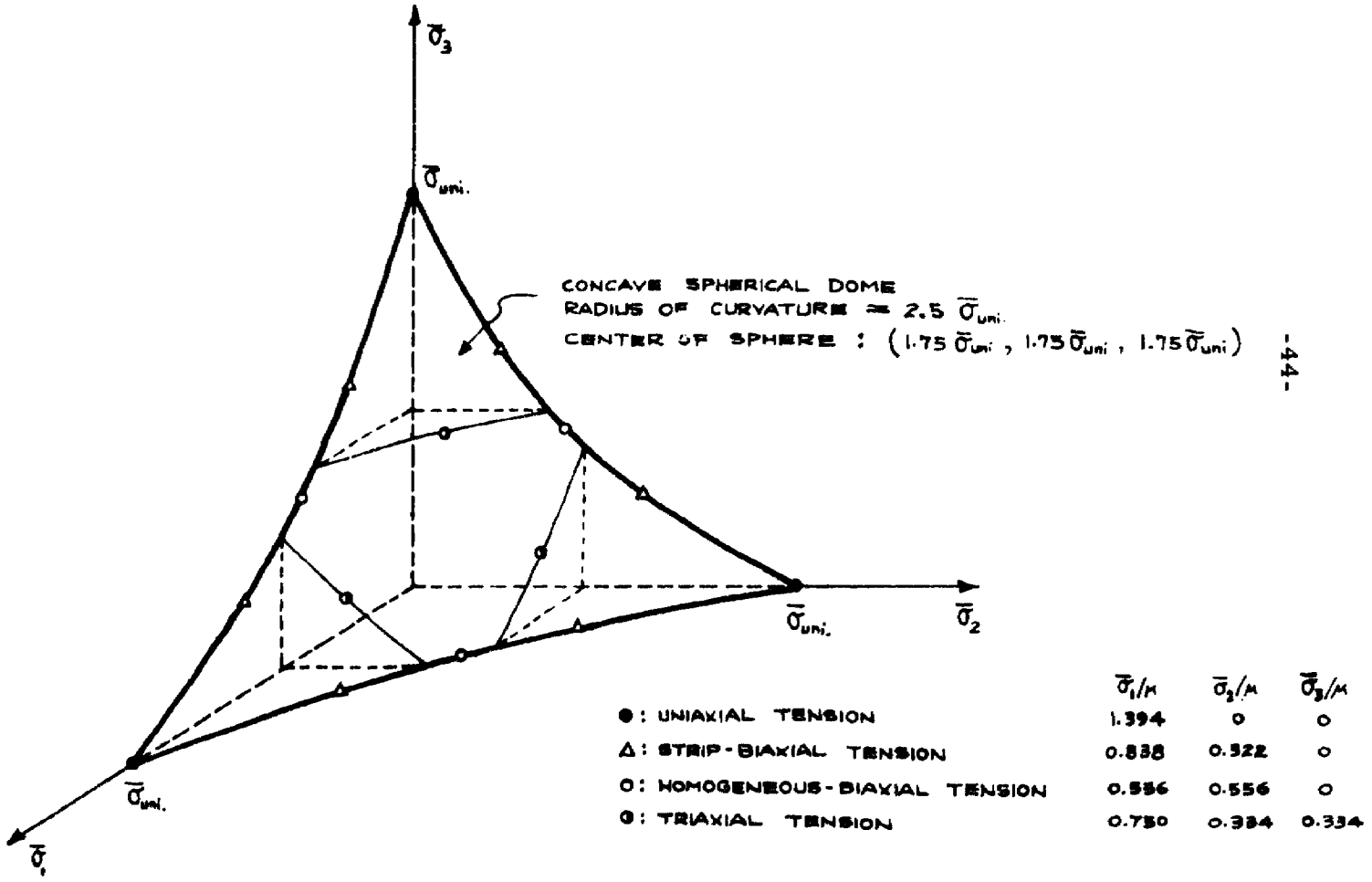

FIG. 1.8. **Failure Safe Surface Based on Experimental Data in Normal True Stress Space.**

2.0 EXPERIMENTAL ANALYSIS OF THE TRIAXIAL POKER-CHIP SPECIMEN

2.1 Objectives of the Test

In the preceding sections of this report, an overall review of the methods of failure analysis for viscoelastic materials has been presented along with details relating to the basic research necessary in formulating a sound theory. As was pointed out, an array of multiaxial testing techniques is needed to establish the desired failure surface in stress or strain space. In particular, a large portion of the surface to be defined requires a knowledge of failure under triaxial loading. Although there have been some very elaborate testing machines designed which will apply loads in three directions, they do not constitute a panacea of triaxial testing. There seems to be considerable difficulty in actually running such tests and little, if any, data has yet been published.

2.1.1 Related Work From the Literature

The primary experimental effort reported in this section pertains to a simple tensile-type test on a thin, circular disk poker-chip specimen that is pulled parallel to its longitudinal axis to produce the basic triaxial, tensile stress field described in 1.6. Such a configuration is not new, for it was used by Yerzley [2.1] as early as 1937 as a technique for determining the integrity of rubber to metal bonds. While his interest was solely in the bond strength and not in the stress field produced in the rubber itself, his results seem to have

prompted Gent and Lindley[2.2, 2.3] to pursue a similar test on carbon-filled rubber disks loaded in compression and tension.

2.1.2 Advantages of the Poker-Chip Test

At GALCIT the poker-chip test has been used with several modifications to those referenced above, to study the failure of materials in triaxial tension. The test as a whole presents a good many obstacles to the researcher that are not easily solved, both in the experimental and the analytical facets, but once these are conquered, the inherent simplicities yield a valuable, useful triaxial test. Because of its unique configuration, and the incompressibility of the material, rubbery specimens, which usually have large deformations during testing, are limited to relatively small strains all of the way to failure. This provides an additional benefit in that infinitesimal elasticity theory can be used in the analytical work without introducing large errors. It will be shown later that by measuring tensile modulus and an apparent modulus in the poker-chip test, one can also obtain Poisson's ratio and bulk modulus directly. So not only is the objective of the test one of failure study but also mechanical properties can be a valuable by-product.

2.2 Description of the Experimental Apparatus

A schematic of the experimental set-up is given in Figure 2.1 where it can be seen that a major consideration of the test construction has centered on visual observation of the specimen. By employing Lucite cylinders as grips, the experimenter can view or photograph

in full detail the history of failure via the mirrors set at 45° in the heads of the machine attachments. The experiments at GALCIT have been performed primarily upon a transparent polyurethane. Thus one can inspect the internal regions of the specimen and obtain a more accurate definition of the failure process. This factor is particularly significant in the study of fracture initiation where threshold conditions are a principal interest.

Variations of Experimental Set-Up.

More translucent materials, such as propellant binders, have also been employed with success by introducing a bright light into the optical system to illuminate the specimen internally and thus facilitate later detailed comparisons of failure in unfilled and filled systems.

Another option of this test arrangement is the ease with which photoelastic information can be obtained by introducing polarizers, analyzers, quarter-wave plates, and appropriate light sources into the system. Additional comments about this facet of the test will appear in subsequent sections.

Enumeration and Solution of Experimental Difficulties.

We turn now to the details of preparing specimens, setting up the experiment, and conducting a successful poker-chip test. Invariably there are a multitude of bothersome practical difficulties encountered that, though seemingly insignificant, can vitally effect the

outcome of the experiment. For this reason, several of the experimental fine points should be mentioned.

2.2.1 Material Description

The usual specimen material used in this series of experiments was a rather elastic (as opposed to viscous) polyurethane rubber produced commercially as Solithane 113 by the Thiokol Chemical Corporation. It can be characterized as a relatively brittle type rubber, exhibiting at room temperature an elastic mode of failure. (See section 1.1) It possesses a tensile modulus of 500 - 600 psi at a relaxation time of the order of one second in triaxial tension. It was selected for study because of its excellent optical properties, which permit close scrutiny of the failure process, and it also seems to have failure modes similar to many filled materials. The raw material is a pre-polymer, requiring a catalyst to free the chain ends and start the polymerization process. The pre-polymer with catalyst must be cast into the desired shape and allowed to cure as polymerization continues to completion, which requires about an hour at 150°C plus another two weeks in a desiccator at room temperature.

2.2.2 Casting Procedures

Some investigators have successfully cast polyurethane directly on the Lucite testing grips; however, we elected to cast the specimen material into sheets first and then bond to the Lucite grips afterward. Consequently, several factors of importance relative to casting were uncovered:

(a) Mold releases containing silicon will leave enough residue on the specimen to prevent the formation of a good bond regardless of the cleaning agent used to remove it.

(b) Polished brass, steel, Lucite, aluminum, Pyrex glass and micarta were all successfully used as mold materials, but polished aluminum was found to be the most desirable when cost, weight, etc. were all considered.

(c) Degassing the pre-polymer after it is mixed with the catalyst considerably reduces the number of bubbles produced in the casting, and tends to make the finished product more nearly colorless.

(d) The surface quality of the cast sheet is directly related to the surface quality of the mold, but as will be discussed later, when the material is bonded to the Lucite grips, the wetting property of the bonding agent eradicates surface imperfections in the cast sheet. Therefore the mold surface need be polished only to the degree necessary to allow the rubber to be removed from the mold without requiring a mold release.

2.2.3 Size Considerations

The actual thickness dimension of the cast sheet is dictated by the individual material characteristics as well as the limitations

imposed by the testing apparatus. In an approximate analysis of the stress field, to be discussed in detail later, it was found that for materials with Poisson's ratio near 0.5, a diameter to thickness aspect ratio, D/L, of approximately 200 to 1 is needed to obtain an area of constant stress in the central portion of the poker-chip. This peculiar situation results from the end effect, which is very strong for incompressible materials as opposed to the usual expectations from the St. Venant principle. Such an aspect ratio is not a practical one because of load limitations on the testing machine, and an aspect ratio of D/L = 20 was found to be a reasonable compromise. In our tests, D = 2 in.

Of course, there are other considerations which may dictate particular values of the specimen diameter. For instance, if a filled system is used, the thickness must be adjusted so that the particle size is not of the same order of magnitude. Such a condition may require that poker-chips of the order of four or five inches be used to yield meaningful results.

2.2.4 Bonding Procedure

A very critical facet of the experimental techniques of the poker-chip test is the bonding procedure. Precautions must be taken in order to produce a bond of sufficient strength that it will not allow the specimen to tear away from the grips before an internal failure is produced. First, after the poker-chips are roughly cut to size from the cured sheets, they are cleaned with a cloth slightly dampened

in methyl alcohol. If used sparingly, this procedure will produce virtually no swelling in the rubber, but it is an absolutely essential part of the bonding procedure. Second, the Lucite grips must be roughened and properly cleaned before attaching the specimen. The emery paper abrasive must not be a silicon compound or it will ruin the surface for bonding. Aluminum Oxide paper was found to work very nicely.

Third, Eastman 910 adhesive was applied to the grips, and the specimen carefully laid between them so that the air bubbles could be squeezed out under the periphery. A weight of 5 lbs or so was needed to prevent the rubber from warping away from the Lucite. Because some of the Eastman 910 is absorbed into the surface of the specimen causing some differential contraction, the bonding agent is always applied directly to the Lucite rather than to the rubber material. Bonding is also a polymerization process and a 24 hour cure under the weight is allowed. Fourth, the grips must be perfectly square and flat, not only for a good bond, but also so that the test is free of bending stresses which may arise from misalignment.

When the final assembly described above is complete, an observer can focus his attention on the inside of the specimen by viewing through a perfectly transparent window produced by the wetting phenomena of the Eastman 910 at the interfaces of Lucite and rubber.

2.3 Experimental Observations

In a previous report[2.4] descriptions were given of the phenomena observed in the poker-chip test. The field remains seemingly

undisturbed until at an average applied stress of 300 psi very small internal bubbles pop into the field at random locations near the center of the disk. After several have appeared in this region, more will emerge at distances farther from the center as the load is increased. Upon immediate release of the load, the bubbles flatten into penny-shaped cracks with their planes generally parallel to the load direction. These tiny voids grow into cracks that propagate along principal stress trajectories and eventually hook-up to form large cracks. This behavior is in contrast to the behavior of a very viscous material that was tested a couple of times for comparison. In this case, the bubbles formed as before, but they never did join up or run into cracks even though the field was virtually filled with them. Also the energy release associated with each bubble was greater for the viscous material because a much more definite jump occurred in the stress strain record.

When the specimen is pulled far enough to be completely separated, a very rough surface of failure is manifested, and each bubble formation with its accompanying plane of failure can be studied and analyzed. Figure 2.2a shows a typical surface.

2.3.1 Effects of Bending

If the grips are rotated or loaded antisymmetrically in any degree, bending stresses will be superposed on the regular stress field. When such is the case, a different mode of failure is observed.

From many tests of Solithane poker-chips with $D/h = 20$, under the influence of bending there were several factors about the

brittle fracture that were reproduced in virtually every test. The fracture initiated at a point r/R * 0.40 to 0.41 in. in the form of a penny-shaped crack that was inclined 45° to the mid-plane of the poker-chip. As is typical of brittle fracture, the process was quite

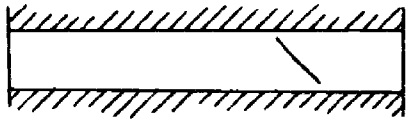

rapid, and the penny-shaped crack bursts into the field from a small nucleus that measures approximately 0.01 in after the fracture surface has been formed and the load has been released. The actual nucleus from which the fracture grows is probably much smaller. In addition the nucleus was not located at the mid-plane; rather, it was often found to be well off of the centerline, but still in the material and not at the interface. (See Figure 2.2b).

2.3.2 Crack Propagation in a Triaxial Field

The continuation of the disk-like rupture into a propagating crack is much less rapid, and, as load is increased, the crack extends from two extremes of the initially inclined disk and propagates along a principal normal stress trajectory. (See Figure 2.2 c). However, it now is straightened up from the initial plane of 45° to 90° and enlargements have shown the front of the crack to be well up into the specimen as pictured. As can be seen from the figure, below, the crack front is quite blunt in this plane. However as seen from the figure

while looking down the axis of the poker-chip, the crack is very sharp. The crack itself resembles a wedge being pushed through the material along a curved path.

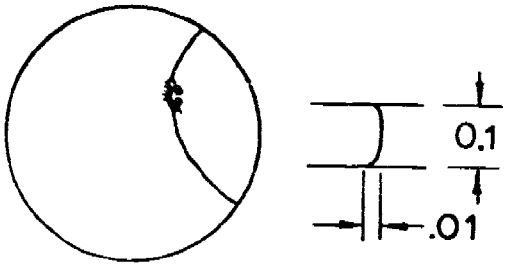

If the specimen is subjected to large strains, Enough energy is stored that even after one failure has occurred, there is still enough energy to produce another. The same process is repeated with the second nucleation of failure being less catastrophic and smaller in size but still on a 45^{o} angle and still propagating along a principal stress trajectory, see figure below.

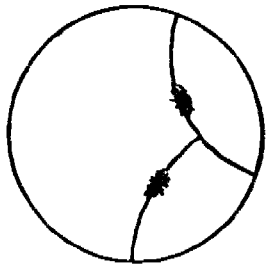

2.3.3 Related Application

Use of the Lucite bars has permitted direct observation of the entire process in order to better describe the phenomena; however, if the material were opaque, the initial part of the failure could be detected from the blips in the stress-strain curve, see figure below. There is enough energy released in each one of the catastrophic bursts that a definite discontinuity is recorded on the chart. Gent and Lindley [2.2, and 2.3] observed a

similar phenomenon, but they also heard a popping noise as the individual failures occurred.

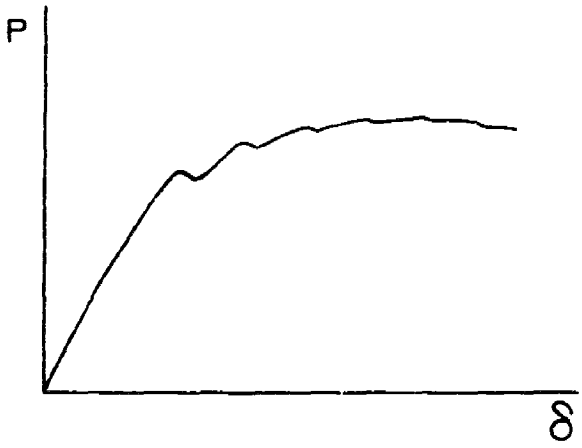

It is felt particularly desirable to make this complete study on a transparent material of this type, because it lends itself to many means of observation. Understanding gained in this way can then be applied to other materials that cannot be observed internally.

2.4 Related Experimental Observations

2.4.1 Filled Systems

In an effort to progress from simple to the more complex materials in understanding triaxial fracture, we have first concentrated upon studying unfilled continuous systems, from which knowledge we hope to proceed to the more complicated filled systems. Investigators at North American Aviation, Rocketdyne Inc., have also been observing triaxial failure of propellant by means of the poker-chip test. Figure 2.3 shows typical results obtained by Britton and Ratliff[2.5] for some of their filled polymers. It turns out that certain similarities exist between the nature of their failures and those of the unfilled polyurethane when bending was known to occur.

(a) Initiation appears to originate away from the center of the specimen,

(b) fracture occurs on a 45^{o} plane, and

(c) propagation of the crack is along a principal stress trajectory.

Thus it would appear that a good deal of useful information concerning the mechanism of failure in the filled systems can be ascertained from the behavior of this brittle type of homogeneous, isotropic polyurethane. In addition Britton and Ratliff[2.5] have determined the failure stress of mixed bi-material combinations vs. reduced strain rate, using the a_T shift factor for uniaxial tension as reference. Figure 2.4 shows their results, which indicates the possibilities of such correlations of triaxial to uniaxial data. Continued effort in this direction is indicated for the future.

2.4.2 Photoelastic Technique

Another related experimental phenomenon worthy of comment at this point is that photoelastic data can be recorded for later comparison with the stress analysis. By passing a monochromatic light beam through the systems and with the appropriate polarizing apparatus, fringe patterns in the poker-chip can be observed[2.4]. Virtually no fringes are seen until fracture occurs, after which several orders are observed. Thus far they have only been used qualitatively for areas of high stress and comparison of fringe patterns around cracks in triaxial stress fields to those in plane sheets. No actual calibration has yet been made to determine their value, although future work along these lines is anticipated. In this connection, the stress analysis given in the next section, which is expressed in terms

of average stresses through the thickness of the poker-chip, can probably be related to the fringe patterns. This relation would be expected because birefringence is a two-dimensional effect, and the presence of fringes in a three-dimensional stress field will reflect an average retardation through the third (thickness) dimension. If such a correlation can be effected, additional credence will be given to the approximate stress analysis as well as the usefulness of the fringes in defining local stresses.

REFERENCES

2.1 Yerzley, F. L.: "Industrial Engineering Chemistry," 1939, Vol. 31, p. 950.

2.2 Gent, A. N; Lindley, P. B.: "Proceedings of Institution of Mechanical Engineers," 1959, Vol. 173, no. 3, p. 111.

2.3 Gent, A. N.; Lindley, P. B.: "Proceedings of the Royal Society, A, Vol. 249, p. 195.

2.4 Williams, M. L.; Schapery, R. A.: Studies of Viscoelastic Media. ARL 62-366, Aeronautical Research Laboratories, Wright-Patterson Air Force Base, Ohio, June 1962.

2.5 Britton, S. C.; Ratliff, O. D.: Personal communication.

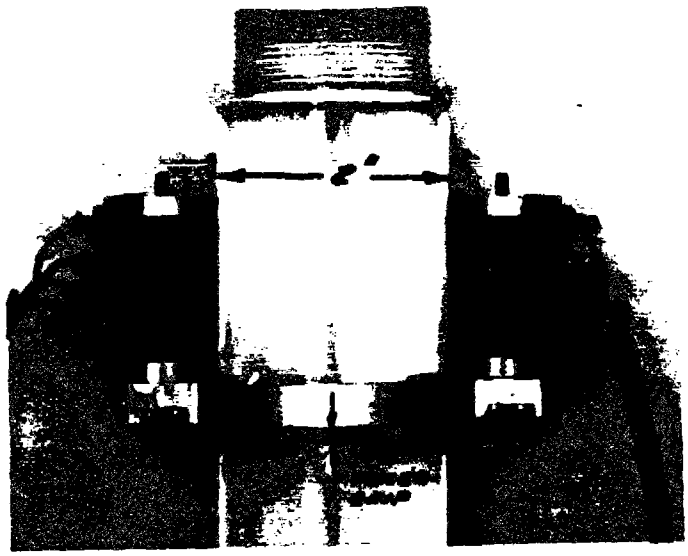

Close-up of Test Specimen
and Microformers

Test Assembly.

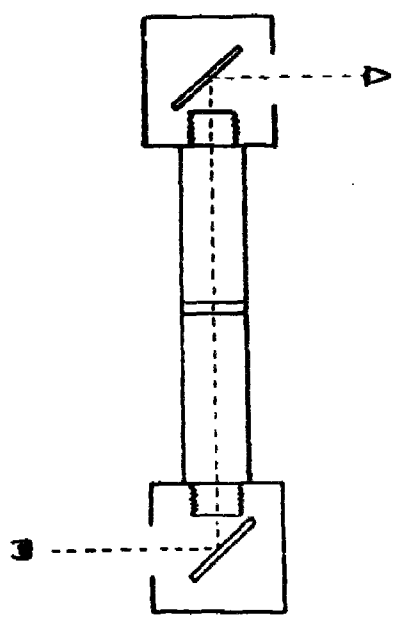

Schematic of Test
Assembly

Fig. 2.1. Experimental Apparatus for Triaxial Tension Test.

a. Fracture Surface

b. Initial Fracture 20X

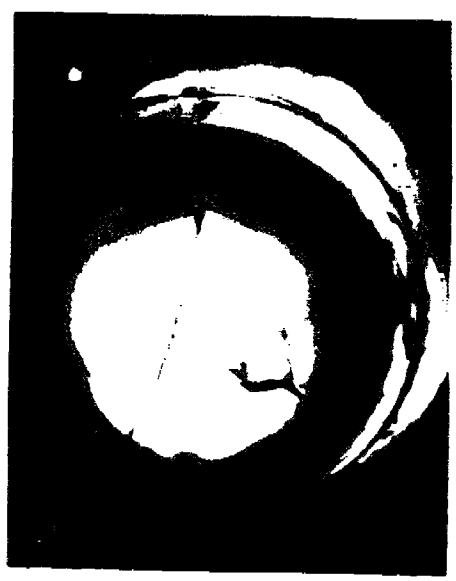

c. Propagation of the Failure Surface

Fig. 2.2. Triaxial Tension Fracture of Unfilled Material.

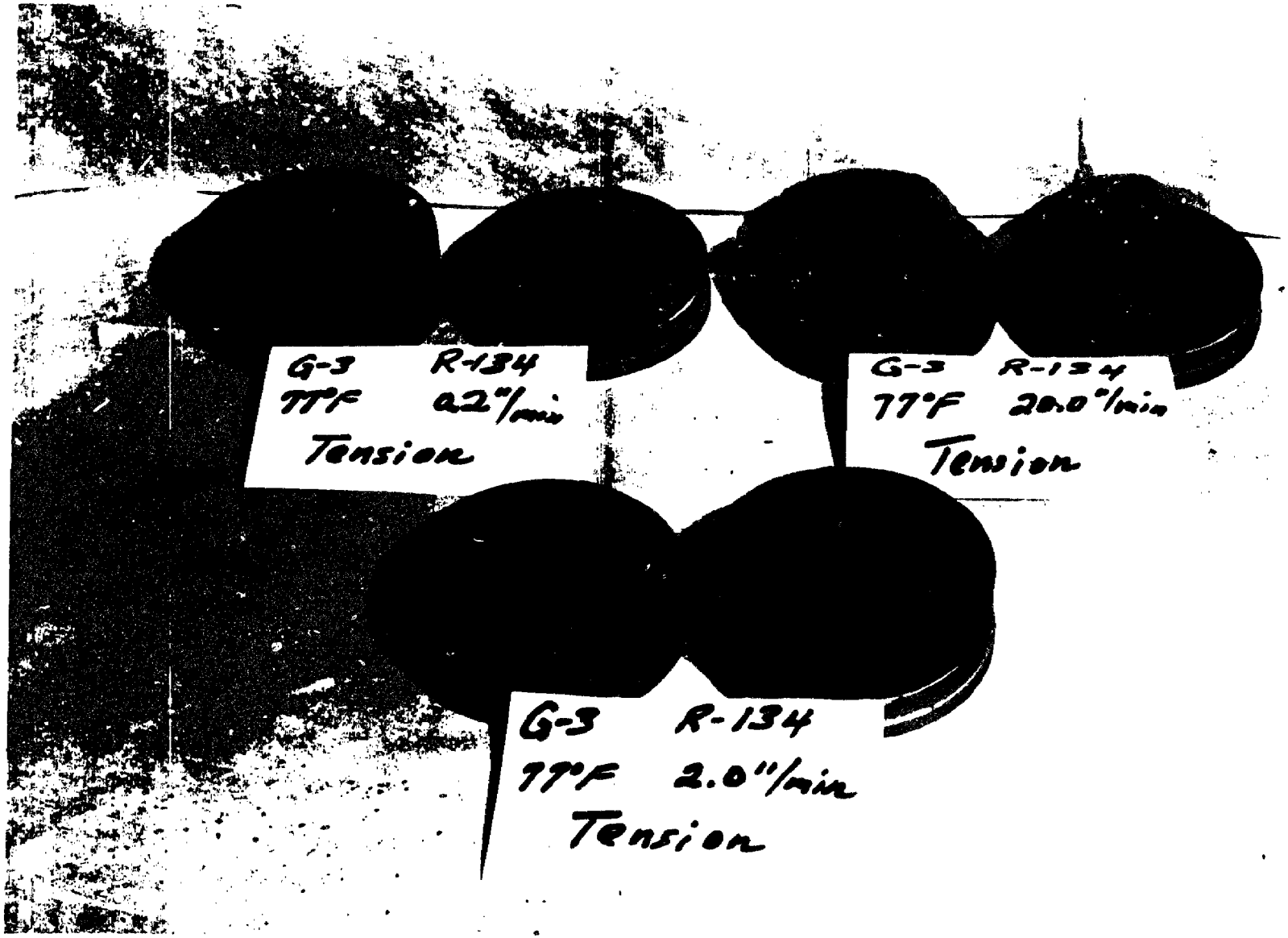

Fig. 2.3. Triaxial Tension Fracture of Propellant Materials.

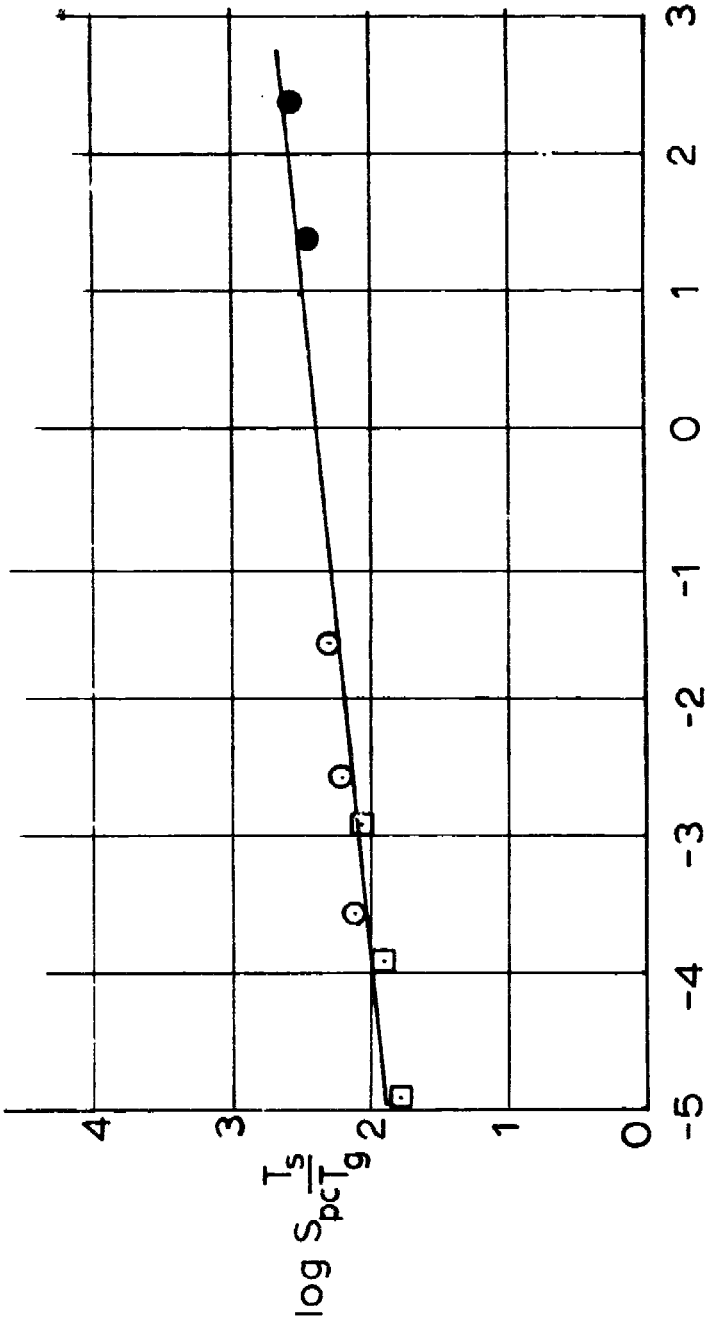

Fig. 2.4. Reduced Failure Data for Mixed Bi-material Combinations.

3.0 THEORETICAL ANALYSIS OF THE TRIAXIAL POKER-CHIP SPECIMEN

In this section various methods for the theoretical analysis of the poker-chip specimen will be discussed. First, the existing solutions relating to this problem will be reviewed and secondly, a new approximate solution will be developed.

3.1 Review of Related Solutions

The mathematical model of the poker-chip configuration, Figure 3.1, leads to a mixed boundary value problem that is almost intractable from the standpoint of classical elastic theory. Like many elastic problems of finite bodies with discontinuous boundary conditions, the poker-chip configuration presents many mathematical difficulties if an exact closed form solution is sought. However for such problems non-closed forms of solution are possible and several have been used.

One of the first theoretical analyses relating to this problem was published by Pickett[3.1]. In this analysis a Fourier series solution was used, where different series were assumed for the field variables, and the coefficients of the terms in such series were evaluated from the boundary conditions. Naturally the final solution was essentially in terms of a doubly infinite series, which required a significant amount of numerical work in order to obtain quantitative results. At the edges of the specimen the convergence of this solution is extremely slow, and in fact it has not been fully established whether it really exists. This problem of convergence at the corners is basic

and will arise in other methods which will be discussed. As will be developed more fully in Section 3.3, discontinuities from stress to displacement boundary conditions along the edges of the geometry may lead to mathematically infinite stresses. This situation exists for example at the right angled corner, where one surface is rigid and the other surface is free of stress. When the stress singularity does occur, and such singular behavior has not been explicitly built into the form of the formal representation of the solution, convergence and rate of convergence difficulties may be expected.

Gent and Lindley[3.2] began with an intuitive approach for an infinite slab and proposed a stress analysis, which can be shown equivalent to minimizing the potential energy for an assumed incompressible material. They then extended this line of reasoning to the circular disk, and the apparent modulus* deduced from this analysis was compared to a large amount of experimental data. Qualitatively there was good agreement, although quantitative predictions with the theory were good only for a very small range of aspect ratios. Furthermore, since the apparent modulus is essentially an average property, the corresponding internal stresses needed for failure analysis could be significantly different than the average value.

Energy methods have also been used. One of the first was a complementary energy formulation in terms of the stresses used by Williams, Blatz and Schapery [3.15]. In cylindrical coordinates

---

* Following Gent and Lindley, the apparent modulus is defined as the average axial stress divided by the applied axial strain.

$$\sigma_r = \frac{2\nu}{1-\nu} A(1-r^n) \cosh \sqrt{\frac{2\nu}{1-\nu}}\, z \tag{3.1.1}$$

$$\sigma_\theta = \frac{2\nu}{1-\nu} A\left[1-(n+1)r^n + r^{p+1} - r^2\right] \cosh \sqrt{\frac{2\nu}{1-\nu}}\, z \tag{3.1.2}$$

$$\sigma_z = \sigma_0 + \left[1-\frac{p+1}{2} r^{p-1}\right]\left[2A \cosh \sqrt{\frac{2\nu}{1-\nu}}\, z - \sigma_0\right] \tag{3.1.3}$$

$$\tau_{rz} = -A\left[r-r^p\right] \sqrt{\frac{2\nu}{1-\nu}} \sinh \sqrt{\frac{2\nu}{1-\nu}}\, z \tag{3.1.4}$$

where the four constants σ_0, p, n, and A were to be determined by minimizing the complementary energy. On the other hand, a potential energy formulation in terms of displacements has been proposed by Francis and Cantey[3.4] in which the radial and axial displacements minimizing the energy were found to be of the form*

$$u = \left[1-\left(\frac{z}{h}\right)^2\right]\left[k_0 J_1(\gamma_2 r)\right] \tag{3.1.5}$$

$$w = \left(\frac{z}{h}\right)\left[1-\left(\frac{z}{h}\right)^2\right]\left[k_1 J_0(\gamma_1 r) + k_2 J_0(\gamma_2 r)\right] \tag{3.1.6}$$

In both of these cases, however, the algebraic complexities involved in the computation were found to be rather formidable, particularly when parametric variations of aspect ratio and material constants were desired. Furthermore, as is fundamental with these particular energy solutions, the complementary principle for stress approximation

---

* Note that w=0 at z=h. This solution is to be superimposed with the constant strain solution.

usually yields poor displacements and, vice versa, the potential energy principle for displacements does not satisfy stress equilibrium. It will be shown later however that a combination of these methods can yield good engineering accuracy.

As a prelude to studying the poker-chip specimen a potential energy method[3.3] was developed for two dimensional slab problems. It made use of the careful measurements of Gent and Lindley[3.2] in which they determined the transverse displacements to be mainly parabolic functions of the longitudinal (axial) coordinate. Results of this analysis furnished an increased understanding of the complete stress distribution, including the extent of the boundary influence on the internal stresses. This solution, however, is not valid near the corners of the slab.

Finally, a very recent numerical solution to the problem has been obtained by Messner[3.5]. In this analysis a finite difference technique has been used, and the grid size has been progressively reduced until two subsequent sizes produce no appreciable change in the stress state over the portion of the specimen away from the corners. The convergence at the corners has been found to be extremely slow, and this is again due to the presence of stress singularities at these points. This type of computer program offers great practical advantages, since a solution can be obtained to any desired accuracy in a short time. However it has the disadvantage that in order to perform a parametric study, a separate calculation has to be performed for each configuration. Nevertheless as the Messner solution approaches the

exact one over most of the specimen, it affords an important basis against which to check the approximations.

3.2 A New Approximate Solution

In this section a new approximate method is developed to analyze both a thin, circular disk and a similarly loaded rectangular slab in plane strain. A relatively simple potential energy approximation is used, but to better satisfy the stress equilibrium balance, an integration of the axial equilibrium equation is incorporated. Also, the incompressibility assumption made by Gent and Lindley[3.2] is not invoked.

The slab analysis is first presented in order to evaluate the approximate analysis method employed by comparing the results with those obtained from the more accurate solutions of the variational technique. In addition these results will be used as the motivation for the simplifying assumptions made here in the approximate solution. Such a comparison was made, and good agreement was found with the energy solution[3.3]. With this basis of correlation established, similar approximations are made with more confidence for the poker-chip stresses and displacements.

Results of the analysis are given as curves, which can be used to determine the local normal and shearing stresses at the initial point of failure. Also a curve is given for the graphical determination of the bulk modulus from measuring Young's modulus and apparent modulus.*

In the limit these results reduce to Gent and Lindley's[3.2] solutions when the ratio of Young's modulus to bulk modulus is made

vanishingly small. However, there is considerable error for those values of Poisson's ratio which are typical for rubber. The effect of bending combined with pure extension is then examined by calculating stresses in a slab in which the rigid grips are rotated. The results of this calculation can be used, for example, to estimate the amount of bending that is tolerable in the disk without altering significantly the stress field due to pure extension.

Concluding remarks relate to application of the stress analysis results when viscoelastic effects are significant, and to important features of the solutions which are needed in fracture interpretation.

3.2.1 Stress Analysis of a Rectangular Slab

The slab geometry and notation is shown in Figure 3.1a; the slab is assumed to be infinitely long in the direction perpendicular to the x-y plane and, consequently, will be in a state of plane strain. The half-thickness is taken as unity for simplicity (but without loss of generality) so that the aspect ratio is equal to the half-width, a .

We suppose that the slab is bonded to rigid plates at $y = \pm 1$ and is loaded by increasing the thickness an amount 2ϵ . Except for small aspect ratios, a reasonable assumption for the x-displacement, u, is

$$u = -f(x)(1-y^2) \tag{3.2.1}$$

in which f is a function of x only. Considering the y-displacement, v, it is assumed that initially horizontal planes remain plane and horizontal after loading, and that the normal strain in the y-direction

is uniform, thus

$$v = \epsilon y \tag{3.2.2}$$

We should mention that in the earlier energy analysis[3.3] the y-strain was not required to be uniform, nevertheless, a linear displacement was found to be a very good approximation, except within one slab thickness from the free ends, regardless of aspect ratio and Poisson's ratio. The x-displacement, u, given by equation (3.2.1), however, has the same y-dependence as assumed with the energy method. Furthermore, the y-dependence of displacements (3.2.1) and (3.2.2) is identical with that assumed by Gent and Lindley[3.2]. However, they determined f by an incompressibility condition, which condition will not be used in the following analysis. Indeed, it will be seen that the incompressibility condition leads to considerable error unless the parameter $a\cdot\sqrt{E/K}$ (E and K are the uniaxial and bulk moduli, respectively) is very small relative to unity.

The displacements (3.2.1) and (3.2.2) provide the normal strains

$$\epsilon_x \equiv \frac{\partial u}{\partial x} = -f'(1-y^2) \tag{3.2.3a}$$

$$\epsilon_y \equiv \frac{\partial v}{\partial y} = \epsilon \tag{3.2.3b}$$

and shear strain

$$\gamma_{xy} \equiv \frac{\partial u}{\partial y} + \frac{\partial v}{\partial x} = 2fy \tag{3.2.3c}$$

where we define $f' \equiv df/dx$. Also, the relative volume change, $\mathcal{D}$, is

($\epsilon_z = 0$ by assumption)

$$\nu \equiv \epsilon_x + \epsilon_y = \epsilon - f'(1-y^2) \qquad (3.2.3d)$$

The function f will now be obtained from the requirement that the y-integrated equilibrium equation for the x-direction vanishes, namely

$$\frac{1}{2}\int_{-1}^{1}\left[\frac{\partial \sigma_x}{\partial x} + \frac{\partial \tau_{xy}}{\partial y}\right] dy = 0 \qquad (3.2.4)$$

Symmetry considerations require that the normal x-stress, σ_x, be an even function of y, and that the shear stress, τ_{xy}, be an odd function of y. Thus, denoting the average $\bar{\sigma}_x$ stress as

$$\bar{\sigma} \equiv \frac{1}{2}\int_{-1}^{1}\sigma_x\, dy = \int_{0}^{1}\sigma_x\, dy \qquad (3.2.5)$$

we have from equation (3.2.4),

$$\frac{d\bar{\sigma}_x}{dx} + \tau_{xy}\Big|_{y=1} = 0 \qquad (3.2.6)$$

Note that because of symmetry the integrated equilibrium equation for the y-direction,

$$\frac{1}{2}\int_{-1}^{1}\left[\frac{\partial \sigma_y}{\partial y} + \frac{\partial \tau_{xy}}{\partial x}\right] dy = 0 \qquad (3.2.7)$$

is identically satisfied.

The stresses in (3.2.6) are expressed in terms of f by using the isotropic stress-strain equations and the strains (3.2.3)

$$\bar{\sigma}_x = \int_0^1 \left[\lambda\vartheta + 2\mu\epsilon_x\right] dy = \lambda\left(\epsilon - \frac{2}{3}f'\right) - \frac{4}{3}\mu f' \qquad (3.2.8a)$$

$$\tau_{xy} = \mu\gamma_{xy} = 2\mu f y \qquad (3.2.8b)$$

λ and μ are the Lamé constants, which are related to the Young's modulus, E, the bulk modulus, K and the Poisson's ratio ν, as follows

$$\lambda = \frac{K - \frac{E}{3}}{1 - \frac{E}{9K}} = \frac{\nu E}{(1+\nu)(1-2\nu)} \qquad (3.2.9a)$$

$$\mu = \frac{\frac{E}{3}}{1 - \frac{E}{9K}} = \frac{E}{2(1+\nu)} \qquad (3.2.9b)$$

Also, it will be useful for later reference to record the following relation

$$\nu = \frac{1}{2} - \frac{E}{6K} \qquad (3.2.9c)$$

Substitution of stresses (3.2.8) into condition (3.2.6) yields a differential equation for f,

$$f'' - \left(\frac{3\mu}{\lambda + 2\mu}\right) f = 0 \qquad (3.2.10)$$

Since the shear stress (3.2.8b) must be an odd function of x, the desired solution to (3.2.10) is

$$f = A \sinh x\sqrt{M} \tag{3.2.11a}$$

where we define

$$M \equiv \frac{3\mu}{\lambda+2\mu} = \frac{\frac{E}{K}}{1+\frac{E}{3K}} = \frac{3(1-2\nu)}{2(1-\nu)} \tag{3.2.11b}$$

and A is a constant determined from the boundary condition $\overline{\sigma}_x(a)=0$ giving

$$A = \frac{3}{2} \cdot \frac{\nu}{1-\nu} \cdot \frac{\epsilon}{\sqrt{M}\cosh a\sqrt{M}}$$

or

$$f(x) = \frac{3}{2} \cdot \frac{\nu}{1-\nu} \cdot \frac{\epsilon}{\sqrt{M}} \cdot \frac{\sinh x\sqrt{M}}{\cosh a\sqrt{M}} \tag{3.2.12}$$

Combining equations (3.2.3), (3.2.12) and using the stress strain relations, the following expressions are obtained for the displacements and stresses (3.6)

$$u = -\frac{3}{2} \cdot \frac{\nu}{1-\nu} \cdot \frac{\epsilon}{\sqrt{M}} \cdot \frac{\sinh x\sqrt{M}}{\cosh a\sqrt{M}}(1-y^2) \tag{3.2.13a}$$

$$v = \epsilon y \tag{3.2.13b}$$

$$\frac{\sigma_x}{E\epsilon} = \frac{\nu}{(1+\nu)(1-2\nu)}\left[1 - \frac{3}{2}\frac{\cosh x\sqrt{M}}{\cosh a\sqrt{M}}(1-y^2)\right] \tag{3.2.14a}$$

$$\frac{\sigma_y}{E\epsilon} = \frac{\nu}{(1+\nu)(1-2\nu)}\left[\frac{1-\nu}{\nu} - \frac{3}{2}\frac{\nu}{1-\nu}\frac{\cosh x\sqrt{M}}{\cosh a\sqrt{M}}(1-y^2)\right] \quad (3.2.14b)$$

$$\frac{\tau_{xy}}{E\epsilon} = \frac{3}{2}\frac{\nu}{(1+\nu)(1-\nu)\sqrt{M}}\frac{\sinh x\sqrt{M}}{\cosh a\sqrt{M}}y \quad (3.2.14c)$$

The corresponding average stresses through the slab thickness are

$$\bar{\sigma}_x = \frac{E\epsilon\nu}{(1+\nu)(1-2\nu)}\left[1 - \frac{\cosh x\sqrt{M}}{\cosh a\sqrt{M}}\right] \quad (3.2.15a)$$

$$\bar{\sigma}_y = \frac{E\epsilon\nu}{(1+\nu)(1-2\nu)}\left[\frac{1-\nu}{\nu} - \frac{\nu}{1-\nu}\frac{\cosh x\sqrt{M}}{\cosh a\sqrt{M}}\right] \quad (3.2.15b)$$

$$\tau_{xy} = 0 \quad (3.2.15c)$$

The average normal stresses (3.2.15a), (3.2.15b) and the shear stress (3.2.14c) were previously compared to those obtained from the more elaborate energy analysis[3.3]. For an aspect ratio $a \geq 2$, the agreement between the two methods was found to be excellent except near the edges of the poker-chip where, because of the presence of the stress singularity, both methods are in error. For the high aspect ratio poker-chips, the energy method indicates that the non-average stresses, σ_x and σ_y, are practically independent of the thickness coordinate y. This explains why the stresses can be well represented by their average values across the thickness and therefore why the present approximate analysis is successful.

Simplification of the Stress Expression. As a practical matter of simplification, it can be shown that for ν very nearly equal to 1/2, typical of the experimental specimens, the following expressions are very good approximations to the average stresses (3.2.15)

$$\frac{\overline{\sigma}_x}{E\epsilon} = \frac{\nu}{(1+\nu)(1-2\nu)}\left[1 - \frac{\cosh x\sqrt{\frac{E}{K}}}{\cosh a\sqrt{\frac{E}{K}}}\right] \tag{3.2.16a}$$

$$\frac{\overline{\sigma}_y}{E\epsilon} = \frac{\nu}{(1+\nu)(1-2\nu)}\left[\frac{1-\nu}{\nu} - \frac{\nu}{1-\nu}\frac{\cosh x\sqrt{\frac{E}{K}}}{\cosh a\sqrt{\frac{E}{K}}}\right] \tag{3.2.16b}$$

and a similar approximate expression can be written for the shear stress

$$\frac{\tau_{xy}}{E\epsilon} = \frac{\nu}{(1+\nu)(1-2\nu)}\left[\frac{\sinh x\sqrt{\frac{E}{K}}}{\cosh a\sqrt{\frac{E}{K}}}\right]y \tag{3.2.16c}$$

Limit-Check of the Solution. Finally we consider the limit case $\nu = 1/2$ ($E/K = 0$) for which the stresses (3.2.16) become

$$\frac{\overline{\sigma}_x}{E\epsilon} = \frac{a^2}{2}\left(1 - \frac{x^2}{a^2}\right) \tag{3.2.17a}$$

$$\frac{\overline{\sigma}_y}{E\epsilon} = \frac{\overline{\sigma}_x}{E\epsilon} + \frac{4}{3} \tag{3.2.17b}$$

$$\frac{\tau_{xy}}{E\epsilon} = xy \tag{3.2.17c}$$

Stresses (3.2.17a) and (3.2.17c) are identical with those derived by Gent and Lindley[3.2] for an incompressible slab.

Some representative stress distributions calculated from equations (3.2.16) and (3.2.17) are shown in Figures 3.2 and 3.3; the energy solutions[3.3] are not indicated since they cannot be graphically distinguished from those in equations (3.2.16), except at $|x| \cong a$. It is of interest to mention that the value of Poisson's ratio of the rubber specimens employed in the poker-chip tests of reference (3.3) is in the neighborhood of $0.4975 \lesssim \nu \lesssim 0.4995$; thus, the corresponding stresses are significantly different from those given by Gent and Lindley[3.2].

On the basis of the excellent agreement between the slab stresses claculated from the energy method of reference 3.3, and those calculated from the above simplified method, we shall now apply the latter method to a circular disk.

3.2.2 Stress Analysis of a Circular Disk

Figure 3.1b shows a circular disk of radius (a) with its axis in the z-direction, and the faces $z = \pm 1$ bonded to rigid plates.

As in the slab problem, we assume that the disk is loaded by increasing the thickness by 2ϵ and proceed to select two displacement functions, which satisfy the boundary conditions on that part of the boundary where displacements are prescribed. Note that the third (circumferential) displacement, v, is identically zero by reasons of symmetry. Such functions are admissible functions for use in the Theorem of Minimum Potential Energy, although it should be recalled that the resultant minimization yields a result, in this case the function $g(r)$, such that the equations of equilibrium are not satisfied

unless the solution actually is exact. The displacement functions chosen are (compare reference 3.4)

$$u = -(1-z^2)\,g(r) \tag{3.2.18a}$$

$$w = \epsilon z \tag{3.2.18b}$$

in the radial and thickness directions respectively. Note that the displacement boundary conditions are satisfied at the surfaces $z = \pm 1$, and that $g(r)$ is presently an unprescribed function of the radius. The strains corresponding to these displacements are easily found to be

$$\epsilon_r = \frac{\partial u}{\partial r} = -g'(1-z^2) \tag{3.2.19a}$$

$$\epsilon_\theta = \frac{u}{r} = -\frac{g}{r}(1-z^2) \tag{3.2.19b}$$

$$\epsilon_z = \frac{\partial w}{\partial z} = \epsilon \tag{3.2.19c}$$

$$\gamma_{rz} = \frac{\partial u}{\partial z} + \frac{\partial w}{\partial r} = 2gz \tag{3.2.19d}$$

from which the z-averaged stresses are found as

$$\bar{\sigma}_r \equiv \frac{1}{2}\int_{-1}^{1} \sigma_r\, dz = \lambda\left(\epsilon - \frac{2}{3}g' - \frac{2}{3}\frac{g}{r}\right) - \frac{4}{3}\mu g' \tag{3.2.20a}$$

$$\bar{\sigma}_\theta \equiv \frac{1}{2}\int_{-1}^{1} \sigma_\theta\, dz = \lambda\left(\epsilon - \frac{2}{3}g' - \frac{2}{3}\frac{g}{r}\right) - \frac{4}{3}\mu\frac{g}{r} \tag{3.2.20b}$$

$$\bar{\sigma}_z \equiv \frac{1}{2}\int_{-1}^{1} \sigma_z\, dz = \lambda\left(\epsilon - \frac{2}{3}g' - \frac{2}{3}\frac{g}{r}\right) + 2\mu\epsilon \tag{3.2.20c}$$

$$\tau_{rz} = 2\mu g z \tag{3.2.20d}$$

where $g' \equiv dg/dr$.

The function g is found from the condition that the z-integrated equilibrium equation for the radial direction is to vanish, i.e.

$$\int_{-1}^{1} \left[\frac{\partial \sigma_r}{\partial r} + \frac{\partial \tau_{rz}}{\partial z} + \frac{\sigma_r - \sigma_\theta}{r} \right] dz = 0 \qquad (3.2.21a)$$

or,

$$\frac{d\bar{\sigma}_r}{dr} + \tau_{rz}\Big|_{z=1} + \frac{\bar{\sigma}_r - \bar{\sigma}_\theta}{r} = 0 \qquad (3.2.21b)$$

Also, note that because of symmetry the integrated equilibrium equation for the z-direction[3.6] is satisfied identically,

$$\int_{-1}^{1} \left[\frac{\partial \tau_{rz}}{\partial r} + \frac{\partial \sigma_z}{\partial z} + \frac{\tau_{rz}}{r} \right] dz = 0 \qquad (3.2.22)$$

Substitution of stresses (3.2.20) into equation (3.2.21) yields the differential equation for g, thus

$$g'' + \frac{g'}{r} - \left(\frac{1}{r^2} + M \right) g = 0 \qquad (3.2.23)$$

where M is the same definition as used previously in the slab problem, viz.

$$M \equiv \frac{3\mu}{\lambda + 2\mu} = \frac{3}{2} \frac{(1-2\nu)}{(1-\nu)} \qquad (3.2.24)$$

Since the deformation must be finite at the origin

$$g(r) = A I_1(r\sqrt{M}) \tag{3.2.25}$$

where $I_1(r\sqrt{M})$ is a modified Bessel function of the first kind, of order one. The constant A is found by using the boundary condition that $\bar{\sigma}_r(a) = 0$ from which it follows that

$$A = \frac{3}{2}\,\frac{\nu\epsilon}{(1-\nu)\sqrt{M}I_0(a\sqrt{M}) - (1-2\nu)\frac{I_1(a\sqrt{M})}{a}} \tag{3.2.26}$$

Substitution of solutions (3.2.25) into stresses (3.2.20) using (3.2.26) yields the following stresses:

$$\frac{\bar{\sigma}_r}{E\epsilon} = \left(\frac{3\nu}{1+\nu}\right)\frac{K}{E}\left[1 - \frac{I_0(r\sqrt{M})\left\{1-\frac{2}{3}M\frac{I_1(r\sqrt{M})}{r\sqrt{M}I_0(r\sqrt{M})}\right\}}{I_0(a\sqrt{M})\left\{1-\frac{2}{3}M\frac{I_1(a\sqrt{M})}{a\sqrt{M}I_0(a\sqrt{M})}\right\}}\right] \tag{3.2.27a}$$

$$\frac{\bar{\sigma}_\theta}{E\epsilon} = \frac{\bar{\sigma}_r}{E\epsilon} + \frac{1}{1+\nu}\left[\frac{I_0(r\sqrt{M}) - \frac{2I_1(r\sqrt{M})}{r\sqrt{M}}}{I_0(a\sqrt{M}) + \left(\frac{1-2\nu}{\nu}\right)\left\{I_0(a\sqrt{M}) - \frac{I_1(a\sqrt{M})}{a\sqrt{M}}\right\}}\right] \tag{3.2.27b}$$

$$\frac{\bar{\sigma}_z}{E\epsilon} = \frac{\bar{\sigma}_r}{E\epsilon} + \frac{1}{1+\nu}\left[1 + \frac{I_0(r\sqrt{M}) - \frac{I_1(r\sqrt{M})}{r\sqrt{M}}}{I_0(a\sqrt{M}) + \left(\frac{1-2\nu}{\nu}\right)\left\{I_0(a\sqrt{M}) - \frac{I_1(a\sqrt{M})}{a\sqrt{M}}\right\}}\right] \tag{3.2.27c}$$

$$\frac{\tau_{rz}}{E\epsilon} = \left(\frac{3\nu}{1+\nu}\right)\frac{K}{E}\frac{\sqrt{M}}{\left[1-\frac{2}{3}M\frac{I_1(a\sqrt{M})}{a\sqrt{M}\,I_0(a\sqrt{M})}\right]}\left[\frac{I_1(r\sqrt{M})}{I_0(a\sqrt{M})}\right]Z \qquad (3.2.27d)$$

which, it may be found, approaches a state of triaxial, hydrostatic tension at the center in the case of an incompressible material.

We expect the stresses (3.2.27) to be good approximations for $0 \leqslant \nu \leqslant 1/2$ except for the singular stresses near the free-edge r = a. While the validity of the slab stresses was restricted to a region at least one thickness away from the free edges, the end-effects are stronger in the disk, and consequently, it is reasonable to restrict the above stresses to radii less than about one and one-half thicknesses from the edge, $r \lesssim a-3$. However, just as with the slab stresses, when $E/K \ll 1$, these approximations should be quite good even closer to the boundary.

Simplification of the Stress Expression. With this restriction on the radius, equations(3.2.27) can be very well approximated by the expressions:

$$\frac{\overline{\sigma}_r}{E\epsilon} = \frac{\overline{\sigma}_\theta}{E\epsilon} \cong \frac{3\nu}{1+\nu}\left(\frac{K}{E}\right)\left[1 - \frac{I_0(r\sqrt{\frac{E}{K}})}{I_0(a\sqrt{\frac{E}{K}})}\right] \qquad (3.2.28a)$$

$$\frac{\sigma_z}{E\epsilon} \cong \frac{3\nu}{1+\nu}\left(\frac{K}{E}\right)\left[1-\frac{I_0(r\sqrt{\frac{E}{K}})}{I_0(a\sqrt{\frac{E}{K}})}\right]+\frac{1}{1+\nu}\left[1+\frac{1}{2}\frac{I_0(r\sqrt{\frac{E}{K}})}{I_0(a\sqrt{\frac{E}{K}})}\right] \qquad (3.2.28b)$$

$$\frac{\tau_{rz}}{E\epsilon} \cong \frac{3\nu}{1+\nu}\sqrt{\frac{K}{E}}\left[\frac{I_1(r\sqrt{\frac{E}{K}})}{I_0(a\sqrt{\frac{E}{K}})}\right]z \qquad (3.2.28c)$$

It is to be noted that all the normal stresses are essentially equal when Poisson's ratio is close to one-half. Furthermore, Figures 3.4 and 3.5, illustrating stresses with a = 20, show the extreme sensitivity to such Poisson's ratios.

For later purposes relating to the analysis of possible failure criteria, it will be convenient to record several of the stress combinations resulting from the simplified forms above.

Octahedral Shear Stress

$$\tau_0 = \frac{1}{3}\sqrt{(\sigma_1-\sigma_2)^2+(\sigma_1-\sigma_3)^2+(\sigma_2-\sigma_3)^2} \qquad (3.2.29a)$$

$$\tau_0 = \frac{\sqrt{2}}{3}\left[\frac{1}{1+\nu}\left(1+\frac{1}{2}\frac{I_0(r\sqrt{\frac{E}{K}})}{I_0(a\sqrt{\frac{E}{K}})}\right)\right]E\epsilon \qquad (3.2.29b)$$

Distortional Energy

$$W_{dist.} = \frac{1+\nu}{6E}\left[(\sigma_1-\sigma_2)^2+(\sigma_1-\sigma_3)^2+(\sigma_2-\sigma_3)^2\right] = \frac{3(1+\nu)}{2E}\tau_0^2 \qquad (3.2.30a)$$

$$W_{dist} = \frac{E\epsilon^2}{3(1+\nu)}\left[1+\frac{1}{2}\frac{I_0(r\sqrt{\frac{E}{K}})}{I_0(a\sqrt{\frac{E}{K}})}\right]^2 \qquad (3.2.30b)$$

Dilitational Energy

$$W_{dil} = \frac{1}{18K}\left[\sigma_1+\sigma_2+\sigma_3\right]^2 \qquad (3.2.31a)$$

$$W_{dil} = \frac{K\epsilon^2}{2(1+\nu)^2}\left[(1+\nu)+\left(\frac{1-8\nu}{2}\right)\frac{I_0(r\sqrt{\frac{E}{K}})}{I_0(a\sqrt{\frac{E}{K}})}\right]^2 \qquad (3.2.31b)$$

Total Strain Energy

$$W = \frac{E\epsilon^2}{3(1+\nu)}\left\{\left[1+\frac{1}{2}\frac{I_0(r\sqrt{\frac{E}{K}})}{I_0(a\sqrt{\frac{E}{K}})}\right]^2+\frac{1+\nu}{2(1-2\nu)}\left[1+\frac{(1-8\nu)}{2(1+\nu)}\frac{I_0(r\sqrt{\frac{E}{K}})}{I_0(a\sqrt{\frac{E}{K}})}\right]^2\right\} \qquad (3.2.32)$$

<u>Displacement Expression.</u> In addition to the stresses (3.2.28), the radial displacement,

$$u = -g(1-Z^2) = -\frac{3\nu\epsilon K\sqrt{M}\, I_1(r\sqrt{M})(1-Z^2)}{E\left[I_0(a\sqrt{M})-\frac{2}{3}M\frac{I_1(a\sqrt{M})}{a\sqrt{M}}\right]}$$

$$\cong -3\nu\epsilon\sqrt{\frac{K}{E}}\left[\frac{I_1(r\sqrt{\frac{E}{K}})}{I_0(a\sqrt{\frac{E}{K}})}\right](1-Z^2) \qquad (3.2.33)$$

is of importance since its midplane value at the boundary, r = a, can be measured experimentally, and possibly used to deduce the bulk modulus in view of the sensitivity to Poisson's ratio shown in Figure 3.6.

Furthermore, as shown in Figure 3.6, this displacement may be very large for nearly incompressible materials, even when the nominal strain, ϵ, is small. In the neighborhood of the radii for which the radial displacement is not small relative to the disk thicknesses, some error due to large strains will be introduced in the results of the present linear analysis.

Apparent Modulus. Another quantity of experimental interest is the apparent uniaxial modulus E_A, defined as the ratio of the average stress over the bonded surface σ_{zA}, required to produce the axial displacement w, to the nominal axial strain ϵ, viz.

$$E_A \equiv \frac{\sigma_{zA}}{\epsilon} = \frac{2\pi \int_0^a \overline{\sigma}_z \, r \, dr}{\pi a^2 \epsilon} \tag{3.2.34}$$

Upon substitution of σ_z, equation (3.2.27c), into (3.2.34) we find

$$\frac{E_A}{E} = \frac{3\nu}{1+\nu}\left(\frac{K}{E}\right)\left[1 - \frac{2I_1(a\sqrt{M})}{a\sqrt{M}\, I_0(a\sqrt{M})}\right]$$

$$+ \frac{1}{1+\nu}\left[1 + \frac{2I_1(a\sqrt{M})\left[1 - \frac{I_1(a\sqrt{M})}{a\sqrt{M}\, I_0(a\sqrt{M})}\right]}{a\sqrt{M}\, I_0(a\sqrt{M})\left[1 + \frac{1-2\nu}{\nu}\left(1 - \frac{I_1(a\sqrt{M})}{a\sqrt{M}\, I_0(a\sqrt{M})}\right)\right]}\right] \tag{3.2.35}$$

This apparent modulus can be conveniently employed for determination of the bulk modulus of nearly incompressible materials. Namely, given an aspect ratio a, and experimentally measured modulus E_A, the modulus ratio E/K can be deduced from a graph of equation (3.2.35), such as shown in Figure 3.7. It is observed that

E_A / Ea^2 depends on only the parameter $a\sqrt{E/K}$ for $a \gtrsim 30$. The accuracy of apparent modulus (3.2.35) is expected to be good, even for small aspect ratios. This follows from the fact that it is an average property, and therefore should not be sensitive to error in stress near the periphery*. Furthermore, E_A has the correct limiting value of E for $a = 0$.

Limit-Check of the Solution. The incompressible limit case ($\nu = 1/2$) solutions are readily found from equations (3.2.27), (3.2.33) and (3.2.35) to be

$$\frac{\sigma_r}{E\epsilon} = \frac{\sigma_\theta}{E\epsilon} = \frac{1}{4}(a^2 - r^2) \qquad (3.2.36a)$$

$$\frac{\sigma_z}{E\epsilon} = \frac{1}{4}(a^2 - r^2) + 1 \qquad (3.2.36b)$$

$$\frac{\tau_{rz}}{E\epsilon} = \frac{rz}{2} \qquad (3.2.36c)$$

where it may be noted that for a large aspect ratio, the condition ($r=0$) of triaxial hydrostatic tension is achieved. Further,

$$u = -\frac{3}{4}\epsilon r(1 - Z^2) \qquad (3.2.36d)$$

$$\frac{E_A}{E} = 1 + \frac{a^2}{8} \qquad (3.2.36e)$$

---

* The effect of sirgular stresses at the edge can be estimated, see section 3.3.

which are identical with those obtained by Gent and Lindley[3.2]. Representative behavior of stresses (3.2.36b) and (3.2.36c), and displacement (3.2.36d), is shown in Figures 3.4 - 3.6 and is denoted by $\nu = 1/2$. The apparent modulus (3.2.36e) was modified by Gent and Lindley[3.2] to approximately account for the additional strain due to dilatation. By adding the displacement obtained from the incompressible analysis to a displacement due to dilatational deformation they obtain

$$\frac{1}{E_A} = \frac{1}{K} + \frac{1}{E\left(1+\frac{a^2}{8}\right)} \tag{3.2.37}$$

which can be written as

$$\frac{E_A}{E a^2} = \frac{1}{\left(\frac{8}{1+\frac{8}{a^2}}\right)+\left(a\sqrt{\frac{E}{K}}\right)^2} \tag{3.2.38}$$

Equation (3.2.38) is shown as the dashed line in Figure 3.7. For the range of the end-effect parameter shown, it is seen that its use in predicting bulk modulus from apparent modulus data can lead to significant error.

Finally, it is interesting to present the stresses at the center of the specimen where the triaxial tension stresses exist. Using equation (3.2.27) one finds

$$\frac{\bar{\sigma}_r(0)}{E\epsilon} = \frac{\bar{\sigma}_\theta(0)}{E\epsilon} = \frac{3\nu}{1+\nu}\frac{K}{E}\left[1-\frac{1-\frac{M}{3}}{I_0(a\sqrt{M})-\frac{2}{3}M\frac{I_1(a\sqrt{M})}{a\sqrt{M}}}\right] \tag{3.2.39a}$$

$$\frac{\bar{\sigma}_z(0)}{E\epsilon} = \frac{\bar{\sigma}_r(0)}{E\epsilon} + \frac{1}{1+\nu}\left[1 + \frac{\frac{\nu}{2}}{(1-\nu)I_0(a\sqrt{M}) - (1-2\nu)\frac{I_0(a\sqrt{M})}{a\sqrt{M}}}\right] \qquad (3.2.39b)$$

For the case where the aspect ratio of the poker-chip becomes very large, that is, $a\sqrt{M} \to \infty$, the above expression can be written in the form

$$\frac{\bar{\sigma}_r(0)}{E\epsilon} = \frac{\bar{\sigma}_\theta(0)}{E\epsilon} = \frac{3\nu}{1+\nu}\frac{K}{E}\left[1 - \frac{(1-\frac{M}{3})\sqrt{2\pi a\sqrt{M}}}{\exp a\sqrt{M}}\right] \qquad (3.2.40a)$$

$$\frac{\bar{\sigma}_z(0)}{E\epsilon} = \frac{\bar{\sigma}_r(0)}{E\epsilon} + \frac{1}{1+\nu}\left[1 + \frac{\nu\sqrt{2\pi a\sqrt{M}}}{2(1-\nu)\exp a\sqrt{M}}\right] \qquad (3.2.40b)$$

The stresses represented by the equations (3.2.40) have been evaluated and plotted against the aspect ratio a in the Figure 3.8. In calculating these results it was assumed that $\nu = 0.4989$ which is the value of the Poisson's ratio for poker-chip material in the present program. One may note also that, independent of the material properties, if the aspect ratio is vanishingly small, then $\sigma_r(0) = \sigma_\theta(0) = 0$ and $\sigma_z = E\epsilon$ which is the proper solution for a uniaxial tension specimen.

Comparison of Results with Finite Difference Solution. It is interesting to compare the stress distributions obtained from the approximate solution of this section with the numerical results of

of reference 3.5. Using equations (3.2.28) the three average normal stresses and the shear stress have been computed for the case a = 10 and ν= 0.4 and 0.5 which are configurations analyzed in reference 3.5. The results of this calculation for the axial stress σ_z are shown in Figure 3.9, where the stress obtained from the two methods of solution are compared. It can be seen from these results that, although the analytical method predicts only the average normal stress $\bar{\sigma}_z$, the two methods agree very closely except at the edge of the poker-chip. At the edges both methods are not accurate because of the presence of the singularity. The agreement for the other three stresses is equally good.

3.2.3 Comparative Potential Energy Analysis for the Circular Disk

In the previous section, an analysis was presented which satisfied the displacement boundary conditions, and the z-averaged equilibrium equations and stress boundary conditions. As such the solution was expected to be a judicious compromise between a best deformation (minimum potential energy) and best stress (minimum complementary energy) approximation. It is informative to inquire at this point what type solution would result if the potential energy were minimized, particularly as the deformation functions chosen earlier, i.e. (3.2.18), are admissible functions for application of this theorem. As it will be convenient for later purposes, use the dimensional forms, viz.

$$u(r,z) = \left[1-(z/h_v)^2\right] g(r)$$

$$w(z) = (w_0/h_v)z$$

where h_v is the half-thickness of the specimen.

In the absence of body forces and with zero applied stress on the stress prescribed boundary r = a, the Minimum Potential Energy Theorem[3.13] requires that the potential energy

$$V=\int_{0}^{a}\int_{-h_v}^{h_v}\left\{\frac{\lambda}{2}\left[\epsilon_r+\epsilon_\theta+\epsilon_z\right]^2+\mu\left[\epsilon_r^2+\epsilon_\theta^2+\epsilon_z^2+\frac{\gamma_{rz}}{2}^2\right]\right\}dz\,r\,dr\cdot 2\pi \qquad (3.2.41)$$

be a minimum with respect to the variation of functionals involved in the double integral. Using the expressions for strains (3.2.19) in (3.2.41) and performing the variation by standard techniques, one finds the governing differential equation to be

$$g''(r)+\frac{1}{r}g'(r)-\left[\frac{1}{r^2}+M_v\right]g(r)=0 \qquad (3.2.42)$$

where

$$M_v\equiv\frac{5}{4}\cdot\frac{1-2\nu}{1-\nu}\cdot\frac{1}{h_v^2}$$

and the boundary condition, assuming finite deformation at r = 0,

$$g'(a)+\frac{\nu}{1-\nu}\frac{g(a)}{a}=\frac{5}{4}\frac{\nu}{1-\nu}\frac{w_o}{h_v} \qquad (3.2.43)$$

The appropriate solution of (3.2.42) is

$$g(r)=A_v I_o(r\sqrt{M_v})$$

where to satisfy (3.2.43)

$$A_v = \frac{5\nu}{4}\frac{w_o a}{h_v}\frac{1}{(1-\nu)a\sqrt{M_v}I_o(a\sqrt{M})-(1-2\nu)I_1(a\sqrt{M_v})} \qquad (3.2.44)$$

The basic similarity with (3.2.23), the z-averaged method, is very evident. For $h_v = 1$, a 5:6 ratio for M_v:M is obtained in the governing equation and nearly the same ratio is found for A_v:A. In the latter the ratio is not precisely 5 : 6 because A is a function of M. Nevertheless a qualitative idea of the difference in the two and indirectly a bound on the average error can be obtained by observing from the differential equation that

$$\frac{M_v}{M} = \frac{5}{6}\cdot\frac{1}{h_v^2} \qquad (3.2.45)$$

such that if $h = \sqrt{5/6} = 0.912$ then the governing equations for a minimum energy solution of $h_v = 0.912$, or $a_v = 1.088$ corresponds to a z-averaged stress solution in a specimen of thickness h = 1 and aspect ratio, a. Of course, if values of M_v and A_v from (3.2.42) and (3.2.44) are used in the basic solution instead of M and A from (3.2.24) and (3.2.26), then the results for the minimum potential energy solution can be immediately reproduced.

Because one is generally interested in the stress state at failure, and hence stresses that satisfy equilibrium of stress at least in

some sense — here taken as the z-average — it is recommended that the results from the previous section be used for fracture analysis.

3.2.4 The Effect of Bending

We consider now some extensions of the approximate analysis into some related areas of importance. The approximate method (Sections 3.2.1 and 3.2.2) is applied here in order to calculate stresses and displacements due to pure rotation of the grips. Only the rectangular slab is considered since its solution is obtained much more readily than the solution for bending of the disk, and the relative effects of combined bending and stretching should be indicative of the behavior of the circular disk. The solutions for pure extension are combined with the bending results and few cases are examined.

Displacement Expressions. The displacements due to grip rotation, shown in Figure 3.1c, are assumed as

$$u = -h(x)(1-y^2) \tag{3.2.46a}$$

$$v = \epsilon_b \frac{x}{a} y \tag{3.2.46b}$$

where $2\epsilon_b$ is the displacement between the grips at the boundary $x = a$.

Stress Expression. Applying the integral condition (3.2.6) and boundary condition $\sigma_x = 0$ at $x = \pm a$, we obtain the following stresses:

$$\frac{\bar{\sigma}_x}{E} = \epsilon_b \left(\frac{3\nu}{1+\nu}\right)\left(\frac{K}{E}\right)\left[\frac{x}{a} - \frac{\sinh x\sqrt{M}}{\sinh a\sqrt{M}}\right] \tag{3.2.47a}$$

$$\frac{\overline{\sigma}_y}{E} = \frac{\sigma_x}{E} + \frac{\epsilon_b}{1+\nu}\left[\frac{x}{a} + \left(1-\frac{2}{3}M\right)\frac{\sinh x\sqrt{M}}{\sinh a\sqrt{M}}\right] \qquad (3.2.47b)$$

$$\frac{\tau_{xy}}{E} = \epsilon_b\left(\frac{3\nu}{1+\nu}\right)\frac{K}{E}\sqrt{M}\left[\frac{\cosh x\sqrt{M}}{\sinh a\sqrt{M}} - \frac{1}{a\sqrt{M}}\right]y \qquad (3.2.47c)$$

where all symbols have been defined in section 3.2.1. It is easy to show that these stresses are exact when $a\to\infty$ and $\nu\neq 1/2$, or when $\nu = 0$. Also for the same reasons as given in section 3.2.1 these bending solutions can be well approximated by

$$\frac{\overline{\sigma}_x}{E} \cong \epsilon_b\left(\frac{3\nu}{1+\nu}\right)\frac{K}{E}\left[\frac{x}{a} - \frac{\sinh x\sqrt{\frac{E}{K}}}{\sinh a\sqrt{\frac{E}{K}}}\right] \qquad (3.2.48a)$$

$$\frac{\overline{\sigma}_y}{E} \cong \frac{\sigma_x}{E} + \frac{\epsilon_b}{1+\nu}\left[\frac{x}{a} + \frac{\sinh x\sqrt{\frac{E}{K}}}{\sinh a\sqrt{\frac{E}{K}}}\right] \qquad (3.2.48b)$$

$$\frac{\tau_{xy}}{E} \cong \epsilon_b\left(\frac{3\nu}{1+\nu}\right)\sqrt{\frac{K}{E}}\left[\frac{\cosh x\sqrt{\frac{E}{K}}}{\sinh a\sqrt{\frac{E}{K}}} - \frac{1}{a}\sqrt{\frac{K}{E}}\right]y \qquad (3.2.48c)$$

where $0 \leq \nu \leq 1/2$; $|x| \leq a - 2$.

The total stresses due to extension and bending are readily obtained by adding solutions (3.2.48) and (3.2.15). For example, when $\nu = 1/2$ we find

$$\frac{\sigma_y}{E\epsilon} = \frac{a^2}{2}\left(1-\frac{x^2}{a^2}\right)\left(1+\frac{1}{3}\frac{E_b}{\epsilon}\frac{x}{a}\right)+\frac{4}{3}\left(1+\frac{\epsilon_b}{\epsilon}\frac{x}{a}\right) \qquad (3.2.49a)$$

and

$$\frac{\tau_{xy}}{E\epsilon} = a\left[\frac{x}{a}+\frac{1}{2}\frac{\epsilon_b}{\epsilon}\left(\frac{x^2}{a^2}-\frac{1}{3}\right)\right] y \qquad (3.2.49b)$$

Results. Some representative results are plotted in Figures 3.10 and 3.11 for various amounts of bending strain ϵ_b, relative to the extension strain, ϵ. It is seen that for Poisson's ratio close to 1/2, the maximum normal stress, σ_y, is not significantly affected by bending if $\epsilon_b/\epsilon \lesssim 1/2$; however, the location of the maximum is more sensitive to Poisson's ratio and tends to move towards the periphery with decreasing Poisson's ratio. Also, when $\nu = 0$ and with extension and bending, σ_y becomes

$$\frac{\sigma_y}{E\epsilon} = 1+\frac{\epsilon_b}{\epsilon}\frac{x}{a} \qquad (3.2.50)$$

so that the maximum is at the boundary $x = a$.

3.3 The Effect of Corner Stress Singularities

The methods of solution for the stresses in a poker-chip, which have been discussed in Sections 3.1 and 3.2, are not able to predict the conditions at the edges where a discontinuity in the boundary exists. The reason for this is the presence of stress singularities, which give rise to rapid changes in the stresses, and consequently, the above methods

converge extremely slowly, or not at all, at these singular points. Therefore this high stress region has to be investigated by a different method which is capable of predicting the stress state in the singular regions. Such a method will be discussed in the present section, where the nature of the stress singularities in the poker-chip will be obtained.

The conditions existing at the edge of the boundary of the poker-chip are represented by Figure 3.12. Material 1 in this figure represents the grips to which the poker-chip specimen is bonded and the Material 2 represents a portion of the specimen near the edge. Material 1 extends over 180 degrees and the Material 2 over 90 degrees. This situation corresponds to the case when the grips have a larger diameter than the specimen and therefore they overlap the latter.

The analysis of the stress in this situation is based on an analytical method developed by Williams[3.7] [3.8]. This method pertains to the analysis of stresses in wedge bodies both under plane stress and plane strain conditions. This analysis was originally developed for homogeneous materials, but in reference 3.9 it was extended to the case of bi-material configurations. In reference 3.11 it was shown* that the stress singularities in bodies of revolution, under axisymmetric loading, are the same as in wedges under plane strain conditions, and therefore the analysis of reference 3.9 can be extended to the case of a poker-chip, that is to the configurations of Figure 3.12.

---

* Recently it was discovered that J. N. Goodier has presented a different proof of the same fact, see reference 3.12.

3.3.1 Analysis of the Poker-Chip Configuration

The method of solution developed in references 3.7. 3.8 and 3.9 will be reviewed here for completeness. A stress function $\chi(r,\psi)$, which satisfies the biharmonic equation

$$\nabla^4 \chi = 0 \tag{3.3.1}$$

is taken in the form

$$\chi(r,\psi) = r^{\lambda+1} F(\psi) = r^{\lambda+1}\left[a \sin(\lambda+1)\psi + b\cos(\lambda+1)\psi + c \sin(\lambda-1)\psi + d\cos(\lambda-1)\psi\right]^{*} \tag{3.3.2}$$

The polar coordinate system r, ψ is shown in Figure 3.12, where the constants λ, a, b, c, and d are at present unknown. Each material will possess a separate stress function and subscripts 1 and 2 will be used to denote the quantities belonging to Materials 1 and 2 respectively.

The boundary conditions for the present configurations are as follows:

at $\psi = 0$; the normal stress σ_ψ, the tangential stress $\tau_{r\psi}$, the radial displacement u_r, and the tangential displacement u_ψ are continuous across the material interface,

and at $\psi = -\pi/2$ and $\psi = \pi$, the surfaces are free of stresses and therefore σ_ψ and $\tau_{r\psi}$ are zero.

The stresses and displacements in the case of plane strain are related to the stress function F as follows[3.9].

---

* This λ is to be distinguished from its pervious designation as Lame's constant.

$$\sigma_r = \frac{1}{r^2}\frac{\partial^2 \chi}{\partial \psi^2} + \frac{1}{r}\frac{\partial \chi}{\partial r} = r^{\lambda-1}\left[F''(\chi)+(\lambda-1)F(\chi)\right] \qquad (3.3.3)$$

$$\sigma_\psi = \frac{\partial^2 \chi}{\partial r^2} = r^{\lambda-1}\lambda(\lambda+1)F(\psi) \qquad (3.3.4)$$

$$\tau_{r\psi} = -\frac{1}{r}\frac{\partial^2 \chi}{\partial r \partial \psi} + \frac{1}{r^2}\frac{\partial \chi}{\partial \psi} = -\lambda r^{\lambda-1}F'(\psi) \qquad (3.3.5)$$

$$U_\psi = \frac{1}{2\mu} r^{\lambda}\left\{-F'(\psi) - 4(1-\nu)\left[c\cos(\lambda-1)\psi - d\sin(\lambda-1)\psi\right]\right\} \qquad (3.3.6)$$

$$U_r = \frac{1}{2\mu} r^{\lambda}\left\{-(\lambda+1)F(\psi) + 4(1-\nu)\left[c\sin(\lambda-1)\psi + d\cos(\lambda-1)\psi\right]\right\} \qquad (3.3.7)$$

In the above expressions μ is the shear modulus, and ν is the Poisson's ratio. The primes denote differentiation with respect to ψ.

Using the interface conditions at $\psi = 0$ and the equations (3.3.2), (3.3.4), (3.3.5), (3.3.6) and (3.3.7) the following four algebraic equations result,

$$b_1 + d_1 = b_2 + d_2 \qquad (3.3.8)$$

$$(\lambda+1)a_1 + (\lambda-1)c_1 = (\lambda+1)a_2 + (\lambda-1)c_2 \qquad (3.3.9)$$

$$4(1-\nu_1)c_1 = 4k(1-\nu_2)c_2 + (k-1)\left[(\lambda+1)a_2 + (\lambda-1)c_2\right] \qquad (3.3.10)$$

$$4(1-\nu_1)d_1 = 4k(1-\nu_2)d_2 - (k-1)(\lambda+1)\left[b_2 + d_2\right] \qquad (3.3.11)$$

where the subscripts 1 and 2 denote quantities belonging to material M_1 and M_2 respectively.

In the same way the boundary conditions at $\psi = -\pi/2$ lead to the following two equations

$$-a_2 \cos\frac{\lambda\pi}{2} - b_2 \sin\frac{\lambda\pi}{2} + c_2 \cos\frac{\lambda\pi}{2} + d_2 \sin\frac{\lambda\pi}{2} = 0 \qquad (3.3.12)$$

$$-a_2(\lambda+1)\sin\lambda\pi + b_2(\lambda+1)\cos\lambda\pi + c_2(\lambda-1)\sin\frac{\lambda\pi}{2} - d_2(\lambda-1)\cos\frac{\lambda\pi}{2} = 0 \qquad (3.3.13)$$

and two more equations are obtained from the conditions at $\psi = \pi$,

$$a_1 \sin\lambda\pi + b_1 \cos\lambda\pi + c_1 \sin\lambda\pi + d_1 \cos\lambda\pi = 0 \qquad (3.3.14)$$

$$-a_1(\lambda+1)\cos\lambda\pi + b_1(\lambda+1)\sin\lambda\pi - c_1(\lambda-1)\cos\lambda\pi + d_1(\lambda-1)\sin\lambda\pi = 0 \qquad (3.3.15)$$

the quantity k introduced in the above equations is defined as the ratio of the moduli of the two materials, i.e. $k = \mu_1/\mu_2$. The parameter λ does not require a subscript since it is common to the stress functions in both materials in order that r-stress variations match.

The equations (3.3.8) to (3.3.15) are eight homogeneous algebraic equations in the unknowns $a_1, a_2 \ldots d_1, d_2$. A non-trivial solution to these constants exists if the determinant of their coefficients is equal to zero. After necessary algebraic manipulation the determinant can be written in the following form,

$$\sin^2\frac{\lambda\pi}{2}\left[1+(2\alpha-4\beta+\alpha^2-2\alpha\beta)\sin^2\lambda\pi\right]$$
$$+(\beta+\beta^2-\lambda^2\alpha^2-2\lambda^2\alpha)\sin^2\lambda\pi-\lambda^2=0 \qquad (3.3.16)$$

where

$$\alpha=\frac{(k-1)}{2(1-\nu_1)}$$
$$\beta=k\frac{1-\nu_2}{1-\nu_1}$$

Equation (3.3.16) is the characteristic equation whose solutions define the parameter λ which in turn defines the stress distribution for the particular configuration considered. The solutions for λ can be real or complex. In order that a stress singularity may exist and the displacements be bounded at $r = 0$ it is necessary that a solution exists for equation (3.3.16) such that the real part of λ satisfies the condition $0 < \lambda < 1$.

Special Situation of the Nearly-Rigid Grip. In the case of the poker-chip experiment the grips, Material 1, are always constructed from a material whose elastic modulus is much higher than that of the poker-chip, Material 2. Therefore, the ratio of the shear moduli k is always very large compared to unity and in fact for the poker-chip experiments described in Section 2, k was approximately equal to 500. It is therefore of practical interest to investigate the characteristic equation (3.3.16) for the case $k >> 1$.

The characteristic equation (3.3.16) can be written in powers of k,

$$\left[\sin^2\lambda\pi\left(A\sin^2\frac{\lambda\pi}{2}+B\right)\right]k^2+\left[\sin^2\lambda\pi\left(C\sin^2\frac{\lambda\pi}{2}+D\right)\right]k$$

$$+\sin^2\frac{\lambda\pi}{2}+E\sin^2\lambda\pi\sin^2\frac{\lambda\pi}{2}+F\sin^2\lambda\pi-\lambda^2=0 \qquad (3.3.17)$$

where:

$$A=\frac{1}{4(1-\nu_1)^2}-\frac{1-\nu_2}{(1-\nu_1)^2}$$

$$B=\frac{(1-\nu_2)^2}{(1-\nu_1)^2}-\frac{\lambda^2}{4(1-\nu_1)^2}$$

$$C=\frac{-5+6\nu_1+6\nu_2-8\nu_1\nu_2}{2(1-\nu_1)^2}$$

$$D=\frac{1-\nu_2}{1-\nu_1}+\frac{\lambda^2(3-2\nu_1)}{2(1-\nu_1)^2}$$

$$E=-\frac{1}{1-\nu_1}-\frac{1}{4(1-\nu_1)^2}$$

$$F=-\frac{\lambda^2}{4(1-\nu)^2}-\frac{\lambda^2}{1-\nu_1}$$

Since k is large compared to unity the first approximation to equation (3.3.17) is obtained by considering the k^2 term only, that is

$$\sin^2\lambda\pi\left(A\sin^2\frac{\lambda\pi}{2}+B\right)=0 \qquad (3.3.18)$$

therefore

$$\sin\lambda\pi=0 \qquad (3.3.19)$$

or

$$A \sin^2 \frac{\lambda\pi}{2} + B = 0 \qquad (3.3.20)$$

The solutions to equation (3.3.19) are all real, and they are $\lambda = 0, \pm 1, \pm 2, \ldots$ etc. Since $\lambda = 0$ leads to a trivial solution for the stress function, $\chi(r, \psi)$, it is obvious that the above solutions for cannot produce singularity. Equation (3.3.20) can be written in the form

$$\sin^2 \frac{\lambda\pi}{2} = \frac{4(1-\nu_2)^2}{3-4\nu_2} - \frac{\lambda^2}{3-4\nu_2} \qquad (3.3.21)$$

It can easily be checked that there are real solutions to equation (3.3.21) for $0 < \lambda < 1$, these solutions have been evaluated for different values of ν_2 and are presented in Figure 3.13. The second approximation to equation (3.3.17) is obtained by retaining both the k^2 and k terms. This will modify the real solutions obtained for equation (3.3.21) by a small amount; the new solution is written

$\lambda = \lambda_o + \delta$ where: λ_o is obtained from equation (3.3.21).

By neglecting second order terms of δ it can easily be shown that

$$\delta = \frac{1}{k}\left[\frac{2\sin^2\frac{\lambda_o\pi}{2}(5-6\nu_1-6\nu_2+8\nu_1\nu_2)+4(1-\nu_1)}{\pi \sin\frac{\lambda_o\pi}{2}\cos\frac{\lambda_o\pi}{2}(4\nu_2-3)-2\lambda_o}\right.$$

$$\left. + \frac{\lambda_o(6-4\nu_1)-4\nu_1(1-\nu_1)}{\pi \sin\frac{\lambda_o\pi}{2}\cos\frac{\lambda_o\pi}{2}(4\nu_2-3)-2\lambda_o}\right] \qquad (3.3.22)$$

Values obtained for δ from equation (3.3.22) are plotted in Figure 3.14 for different combinations of ν_1 and ν_2. It can be seen that for k $>>$1 the value of λ_o is only changed very slightly by retaining the k term in the characteristic equation.

Investigation of Complex Roots. The next question to be answered is whether there are complex solutions to equation (3.3.21) which will also lead to stress singularities. It can be investigated as follows: the complex number $\lambda\,\pi/2$ is written as

$$\frac{\lambda\pi}{2} = x + iy$$

Introducing this into equation (3.3.21), we define a function of complex variable $f(\lambda\pi/2)$ as follows:

$$f\left(\frac{\lambda\pi}{2}\right) \equiv \sin^2\frac{\lambda\pi}{2} - \frac{4(1-\nu_2)^2}{3-4\nu_2} + \frac{\lambda^2}{3-4\nu_2}$$

$$= \frac{1}{2}\left[1 - \frac{8(1-\nu_2)^2}{3-4\nu_2} + \frac{8(x^2-y^2)}{\pi^2(3-4\nu_2)} - \cos 2x \cosh 2y + i\left\{\frac{16xy}{\pi^2(3-4\nu_2)} + \sin 2x \sinh 2y\right\}\right] \qquad (3.3.23)$$

If complex values of λ exist which will produce singularities then equation (3.3.23) has to have a solution whose real part satisfies the condition $0 < X < \pi/2$. To examine the existence of such a solution it has been found very convenient to make use of the following complex variable theorem*

> If f(p) is a function of a complex variable p and in a certain region f(p) has r zeros and s poles, then as the vector p moves around the periphery of this region in

* e.g. Introduction to Complex Variables and Applications by R. V. Churchill. McGraw-Hill, New York, 1948.

the clockwise direction, the vector representing f(p) performs r-s clockwise revolutions.

The above theorem is now applied to the function defined by equation (3.3.23). As the complex variable $\lambda\pi/2$ moves around the periphery of an infinite strip defined by $0 \leq \mathrm{Re}\,\lambda\pi/2 \leq \pi/2$, shown in Figure 3.15, then the complex function represented by the equation (3.3.23) generates the curve shown in Figure 3.15. In the curves of these two figures the numbered points correspond. It can be seen from Figure 3.16 that as the tip of the vector, joining the curve to the origin, moves along the curve in the direction shown by the arrows then the vector performs one complete clockwise revolution. Since it can easily be checked that the complex function $f(\lambda\pi/2)$ possesses no poles, therefore, by the above theorem of complex variables, $f(\lambda\pi/2)$ has one zero, that is one solution, which lies in the infinite strip of Figure 3.15. Furthermore it has already been established that there is one real solution in this region so that it easily follows that there cannot be any complex solutions.

Conclusions. It has thus been determined that a stress singularity exists at the upper and lower peripheries of the poker-chip and that the order of this singularity is given by $(1-\lambda)$ where λ can be obtained for different values of Poisson's ratio from Figure 3.13. Naturally the question arises as to why fracture has not been observed experimentally at the edge of the poker-chip. One very plausible explanation of this is that there are very high strains in the vicinity of the singularity, which make the classical elastic theory invalid and produce finite

rather than infinite stresses. Such a reduction of the stresses by the finite deformation is obviously sufficient to preclude fracture in this region, although additional quantitative analysis is required.

3.3.2 Matching of the Field and Singular Stresses

In the discussion of the different methods of analysis of the poker-chip in Sections 3.1 and 3.2, it was pointed out that these methods fail to predict the stress distribution in the vicinity of the corners. In view of the results of the previous section it is clear that the reason for this is the presence of stress singularities. In the vicinity of such singularities, the poker-chip solutions previously described possess extremely slow or no convergence and thus they do not predict the actual stress conditions. Consequently the question arises as to what is the stress distribution in the vicinity of the singularities. It has been shown in references 3.9 and 3.10, that, for wedge bodies, if the nature of the stress singularity is known then the stress distribution can be obtained in its vicinity.* The stress distribution obtained in this way is not, however, completely defined since the expressions for all the stresses contain a common unknown multiplying constant. To evaluate this unknown constant it is necessary to have a solution for the stresses away from the region of the singularity and match the stresses obtained from both of the solutions along some internal surface in the body. Such matching will determine the unknown multiplying constant.

In the case of the poker-chip a similar approach can be taken. From the previous section the nature of the stress singularities is

* Good accuracy has also been obtained using the multiplicative principle and satisfying force equilibrium. See M. L. Williams, J. Aero. Sci. 19, 9, 1952, p. 615.

known, and therefore the stress distribution in the vicinity of the corners can be evaluated. The unknown constant can be obtained by the matching of the stresses as described above. This approach will now be illustrated by obtaining the stress distribution for the poker-chip specimens analyzed by finite difference technique in reference 3.5.

From the singularity analysis of the previous section and the results of reference 3.11, the expressions for the stresses on the interface of the poker-chip and the grips can be obtained, and the results are

For Poisson's ratio $\nu = 0.4$

$$\sigma_z = \frac{C}{(a-r)^{0.35}} \tag{3.3.24}$$

$$\sigma_r = \sigma_\theta = C\,\frac{0.66}{(a-r)^{0.35}} \tag{3.3.25}$$

$$\tau_{rz} = C\,\frac{0.396}{(a-r)^{0.35}} \tag{3.3.26}$$

and for $\nu = 0.5$

$$\sigma_z = \sigma_r = \sigma_\theta = \frac{C}{(a-r)^{0.405}} \tag{3.3.27}$$

$$\tau_{rz} = C\,\frac{0.502}{(a-r)^{0.405}} \tag{3.3.28}$$

In the above equations the nomenclature of Section 3.2 has been used. The coefficient C is the unknown multiplying constant which has to be determined by the stress matching. This has been done, and the results obtained by matching the stresses in equations (3.3.24) to (3.3.28) to the interface stresses from reference 3.5 are shown in Figures 3.17 and 3.18.

The point at which the stresses should be matched is to some extent arbitrary and depends on the individual judgment of the analyst; however the quality of matching is indicated by the smoothness through the transition region. The point of matching in Figures 3.17 and 3.18 has been chosen to be at $r = 0.98$ and the corresponding values of the coefficient C are:

for $\nu = 0.4$ $\quad C = 10.0$

for $\nu = 0.5$ $\quad C = 22.3$

It is obvious from Figures 3.17 and 3.18 that for the case $\nu = 0.4$ the stresses are matched closely and for the case $\nu = 0.5$ the matching is also good with the exception of the shear stress. Any error in the matching could be attributed to the fact that in the region $r/a = 0.98$ the results of reference 3.5 are only approximate.

The procedure of matching two different stress fields near a singularity cannot only be used for defining the stress state in a poker-chip, but it also provides a useful criterion for determining when, in a finite difference technique, a sufficiently suitable grid size has been chosen. Obviously if a systematic reduction of the grid size leads to a stress state which is predicted by the singularity analysis,

then this indicates that a sufficiently fine grid has been achieved, and the numerical calculation can be terminated. Without the singularity analysis there has really been no way of knowing when to terminate a numerical technique in the neighborhood of a stress singularity, and the cut off point has always been chosen rather arbitrarily. *

3.3.3 Viscoelastic Effects on Tri-axial Failure

In the poker-chip tests the failure phenomena was observed to be strongly dependent on the rate of loading of the specimens. This indicates strong viscoelastic effects, and in view of this an extension of the elastic solutions of this report to include time dependent material behavior will be the next important theoretical phase of the present investigation. This subject will be discussed in detail in the subsequent progress reports; however, a brief comment is in order at this stage.

Under sufficiently high strain rates or low temperatures[3.15] most polymers exhibit viscoelastic effects. Given the viscoelastic properties, one can use approximate inversion methods[3.14] to calculate time-dependent stresses and displacements, for arbitrarily applied strain or load history, from numerical values of the elastic solutions. A consequence of one method is that under applied, time-wise step-loading of displacements, described in reference 3.14, a viscoelastic response is often approximately equal to the elastic solution, in which elastic moduli are replaced by corresponding viscoelastic relaxation moduli[3.14]. Assuming that such an approximation

* An expedient way of conducting a numerical solution would be to insert the singular terms into the analytical formulation, and then proceed to compute the residual (non-singular) solution which would of course converge.

is valid, we can readily determine the effect of viscoelasticity on the slab or disk response. For example, substitution of the uniaxial relaxation modulus into the apparent disk modulus, equation (3.2.35), and assuming that bulk modulus is elastic and constant, immediately provides an approximate representation of the apparent relaxation modulus. In order to illustrate the relative sensitivity of the disk's apparent modulus and uniaxial modulus to viscoelastic effects, we have shown one particular case in Figure 3.19. If it is assumed that the bulk modulus is essentially constant, it is clear from the graph that a small, or practically unobservable, change in the uniaxial relaxation modulus can often lead to a large change in the apparent modulus. This conclusion extends, of course, to the local stresses and implies that for a given time-scale, viscoelastic effects in the poker-chip or slab will often be much larger than obtained in simple uniaxial tension. Such a conclusion has an important bearing on the problem of obtaining a triaxial failure criterion with the poker-chip test.

REFERENCES

3.1 Pickett, G.: Application of the Fourier Method to the Solution of Certain Boundary Problems in the Theory of Elasticity. Journal of Applied Mechanics, Vol. 11, September 1944, p. A-176.

3.2 Gent, A. N.; Lindley, P. B.: The Compression of Bonded Rubber Blocks. Publication No. 324, Journal of British Rubber Producer's Association, Vol. 173, p. 111, 1959.

3.3 Williams, M. L.; Schapery, R. A.: Studies of Viscoelastic Media, Aeronautical Research Laboratories, Wright-Patterson Air Force Base, Ohio, ARL 62-366, June 1962.

3.4 Francis, E. C.; Cantey, D.: Structural Integrity of Propellant Grains, Lockheed Propulsion Company Report No. 556-F, January 1963.

3.5 Messner, A. M.: Stress Distribution in "Poker Chip" Tensile Specimens. Aerojet-General Corporation (Personal communication).

3.6 Timoshenko, S.; Goodier, J. N.: Theory of Elasticity, McGraw-Hill Book Company, New York, 1951.

3.7 Williams, M. L.: Surface Stress Singularities Resulting from Various Boundary Conditions in Angular Corners of Plates Under Bending. Proceedings First National Congress Applied Mechanics, June 1951.

3.8 Williams, M. L.: Stress Singularities Resulting from Various Boundary Conditions in Angular Corners of Plates in Extension. Journal of Applied Mechanics, Trans. ASME Vol. 74, 1952, p. 526. See also: Discussion JAM, Vol. 20, No. 4, December 1953. p. 590.

3.9 Williams, M. L.: The Stresses Around a Fault or Crack in Dissimilar Media. Bulletin of the Seismological Society of America, Vol. 49, No. 2, April 1959, pp. 199-204.

3.10 Zak, A. R.; Williams, M. L.: Crack Point Stress Singularities at a Bi-Material Interface. GALCIT SM 62-1, California Institute of Technology, January 1962.

3.11 Zak, A. R.: Stress Singularities in Bodies of Revolution. California Institute of Technology, GALCIT SM 62-29, July 1962.

3.12 Goodier, J. N.; Appendix to the paper by Barton, M. V. titled "The Circular Cylinder with a Band of Uniform Pressure on a Finite Length of the Surface." Journal of Applied Mechanics, Vol. 8, September 1941, p. A-97.

3.13 Sokolnikoff, I. S.: Mathematical Theory of Elasticity, McGraw-Hill Book Company, New York, 1956.

3.14 Schapery, R. A.: "Approximate Methods of Transform Inversion for Viscoelastic Stress Analysis." Proceedings of the Fourth U. S. National Congress of Applied Mechanics, Vol. 2, 1962, p. 1075.

3.15 Williams, M. L.; Blatz, P. J.; Schapery, R. A.: Fundamental Studies Relating to Systems Analysis of Solid Propellants. GALCIT SM 61-5, California Institute of Technology, February 1961, ASTIA Report No. AD 256-905.

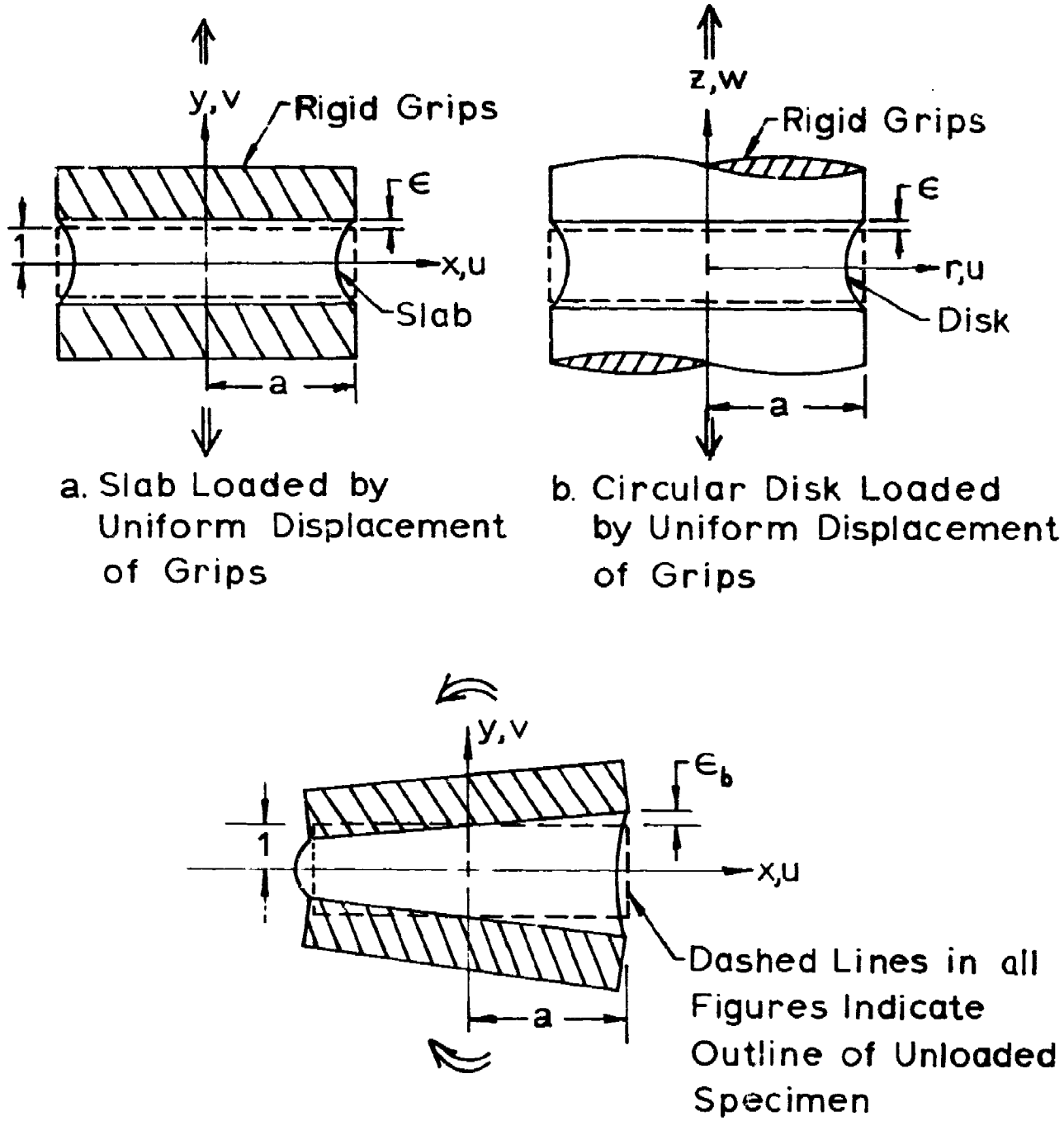

a. Slab Loaded by Uniform Displacement of Grips

b. Circular Disk Loaded by Uniform Displacement of Grips

c. Slab Loaded by Uniform Rotation of Grips

Fig. 3.1. Geometry and Notation Used in Slab and Disk Stress Analyses

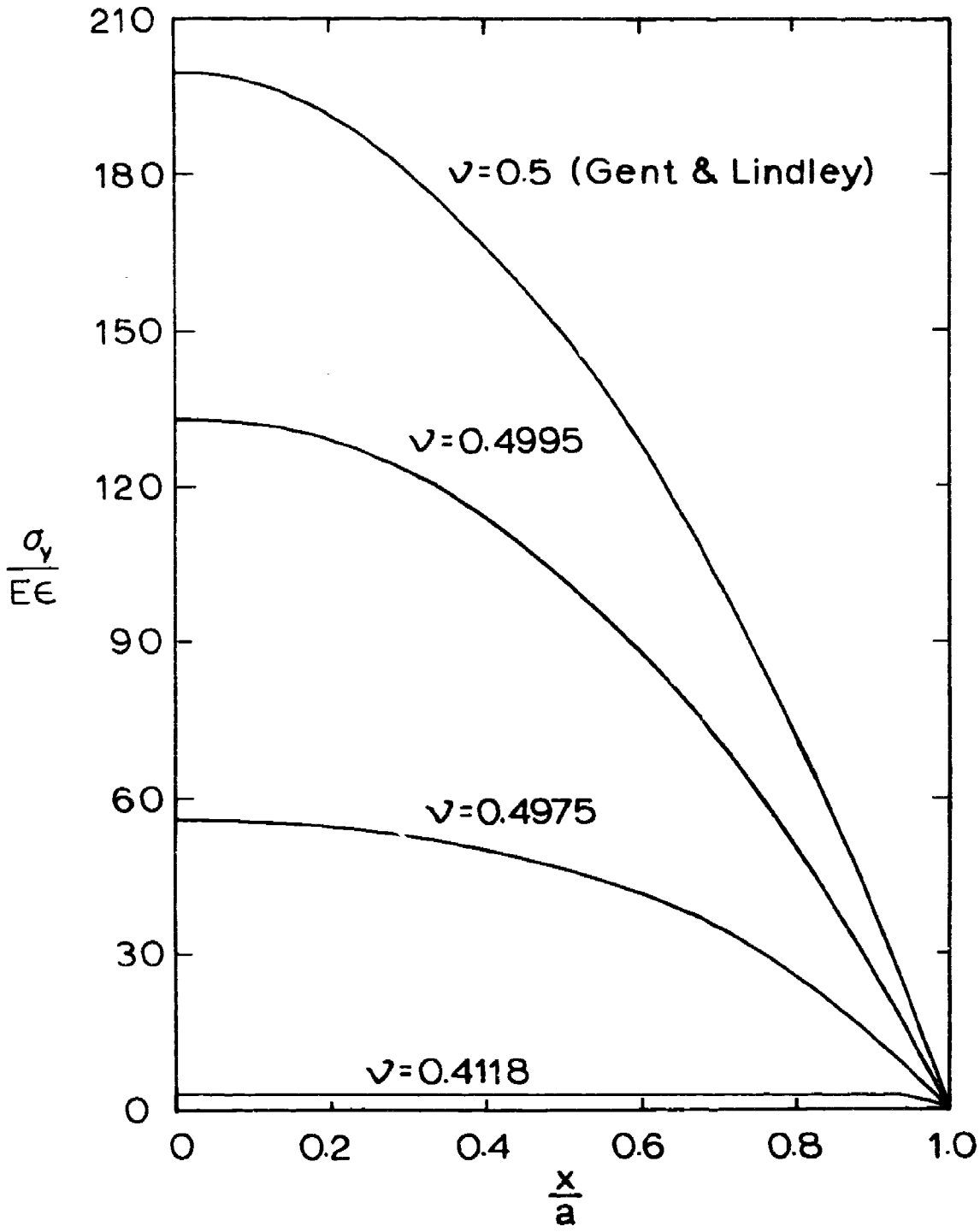

Fig. 3.2. Y-Normal Stress in Slab vs. x/a: a = 20 by Averaged Stress Method.

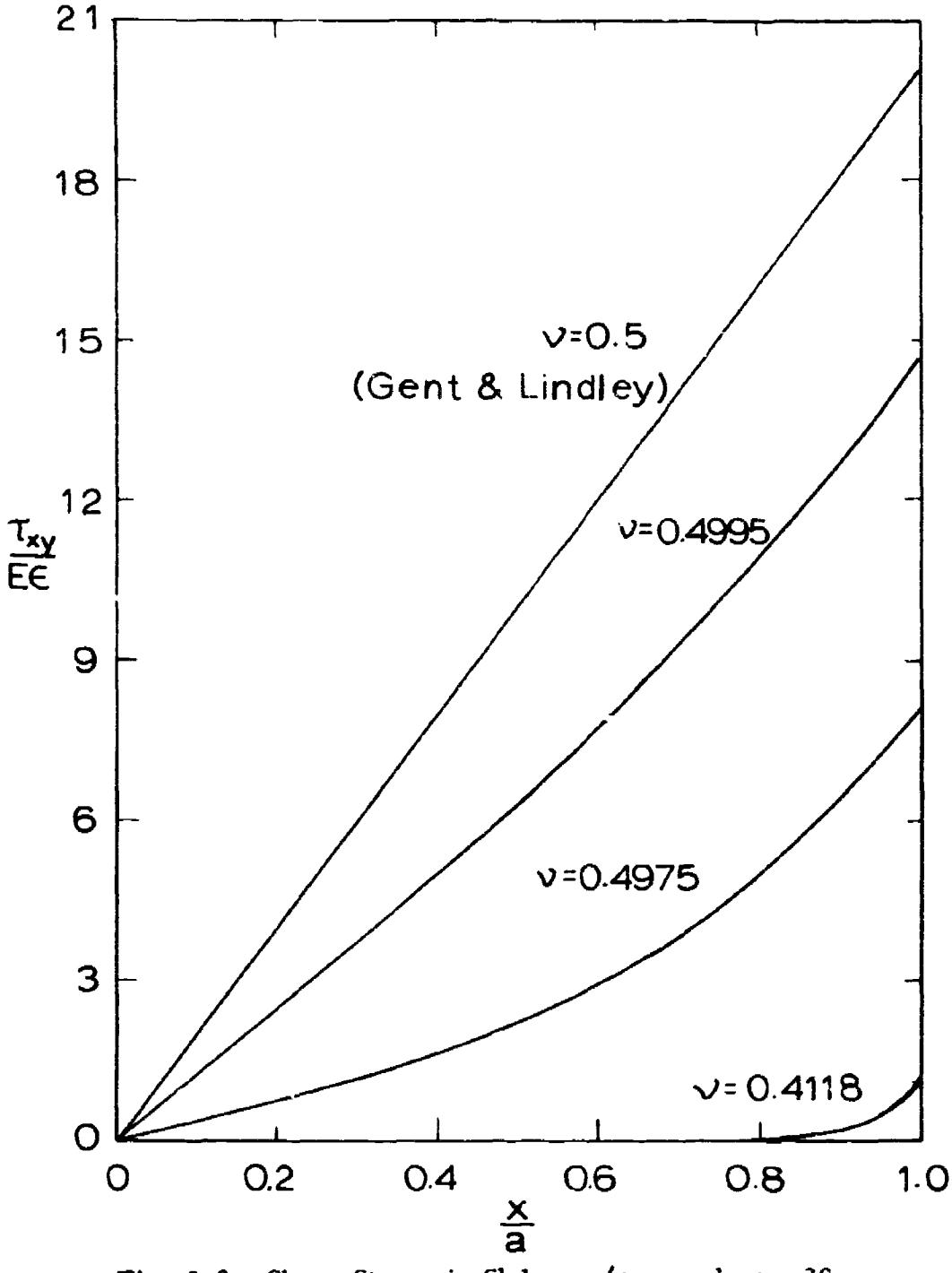

Fig. 3.3. Shear Stress in Slab vs. x/a: y = 1, a = 20. by Averaged Stress Method.

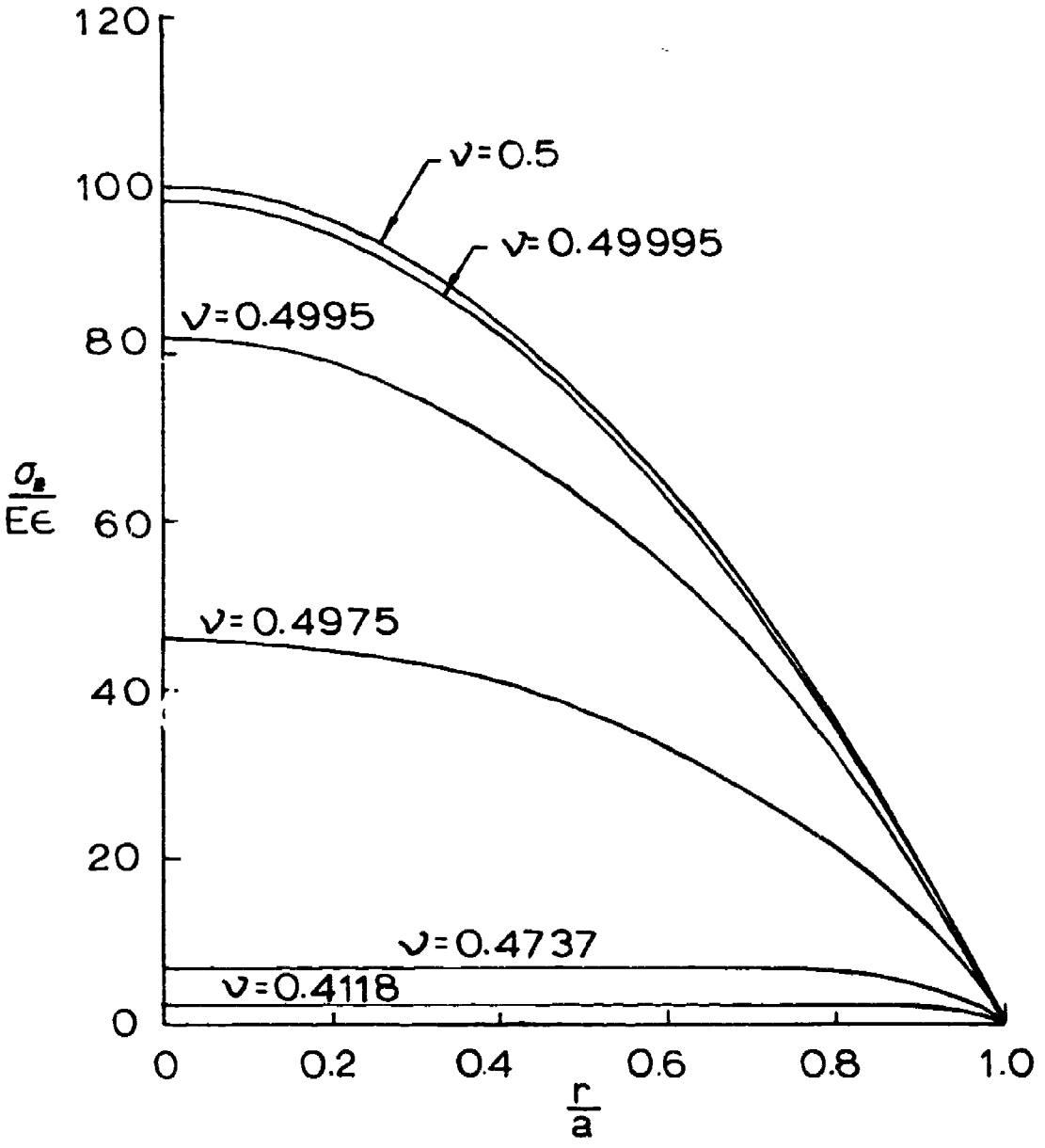

Fig. 3.4. z-Normal Stress in Disk vs. r/a: a = 20.

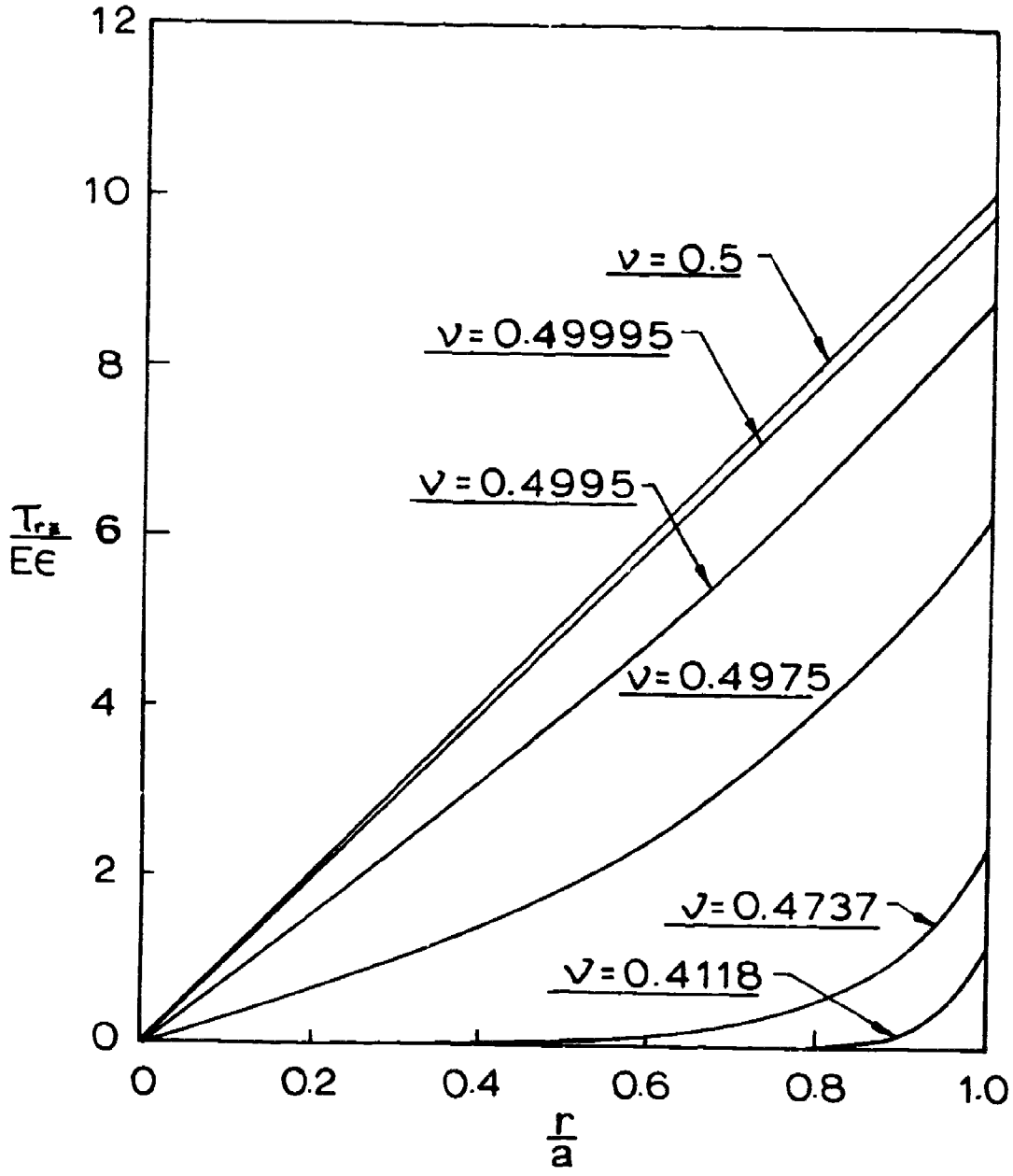

Fig. 3.5. Shear Stress in Disk vs. r/a: z = 1, a = 20.

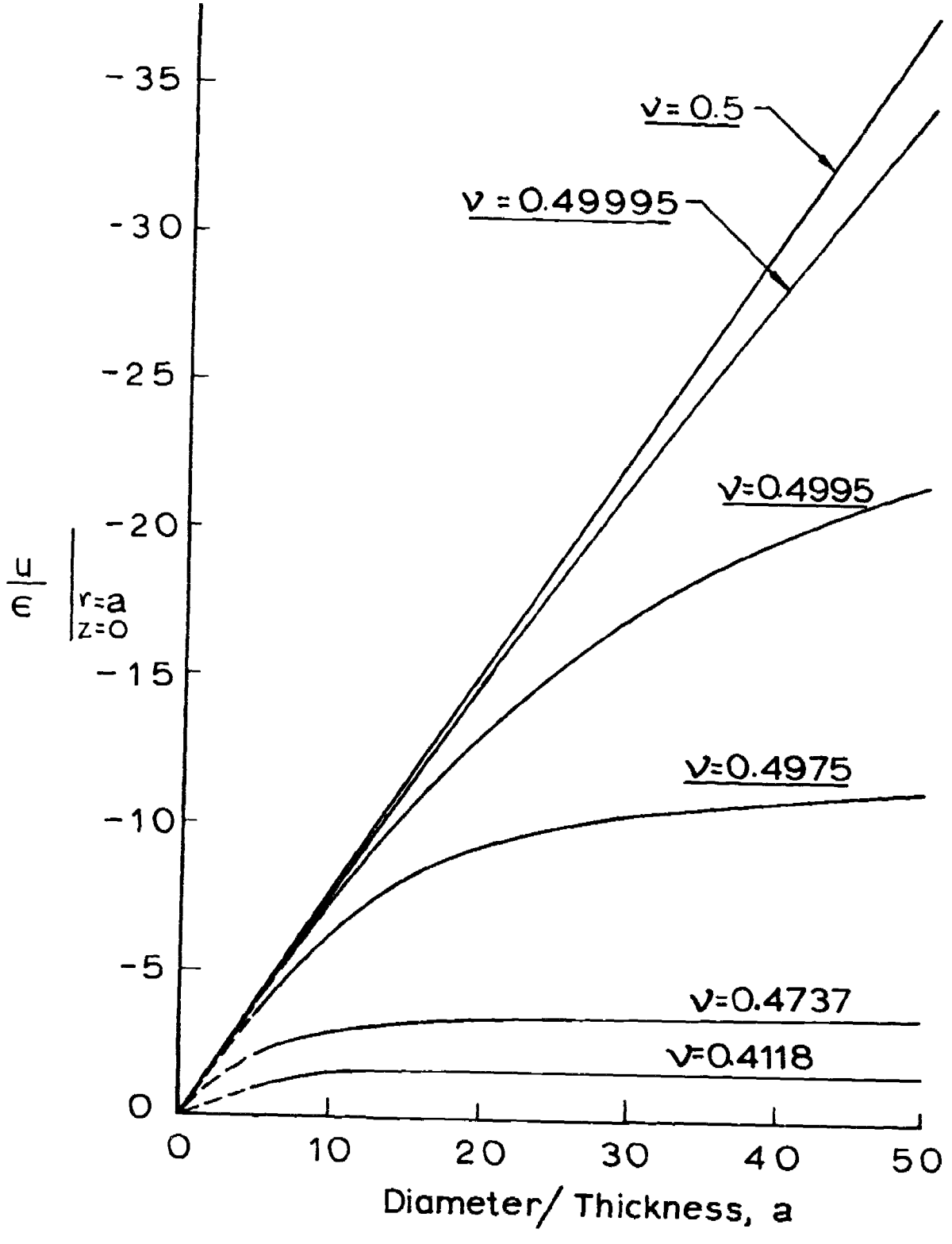

Fig. 3.6. Maximum Radial Displacement in Disk vs. a.

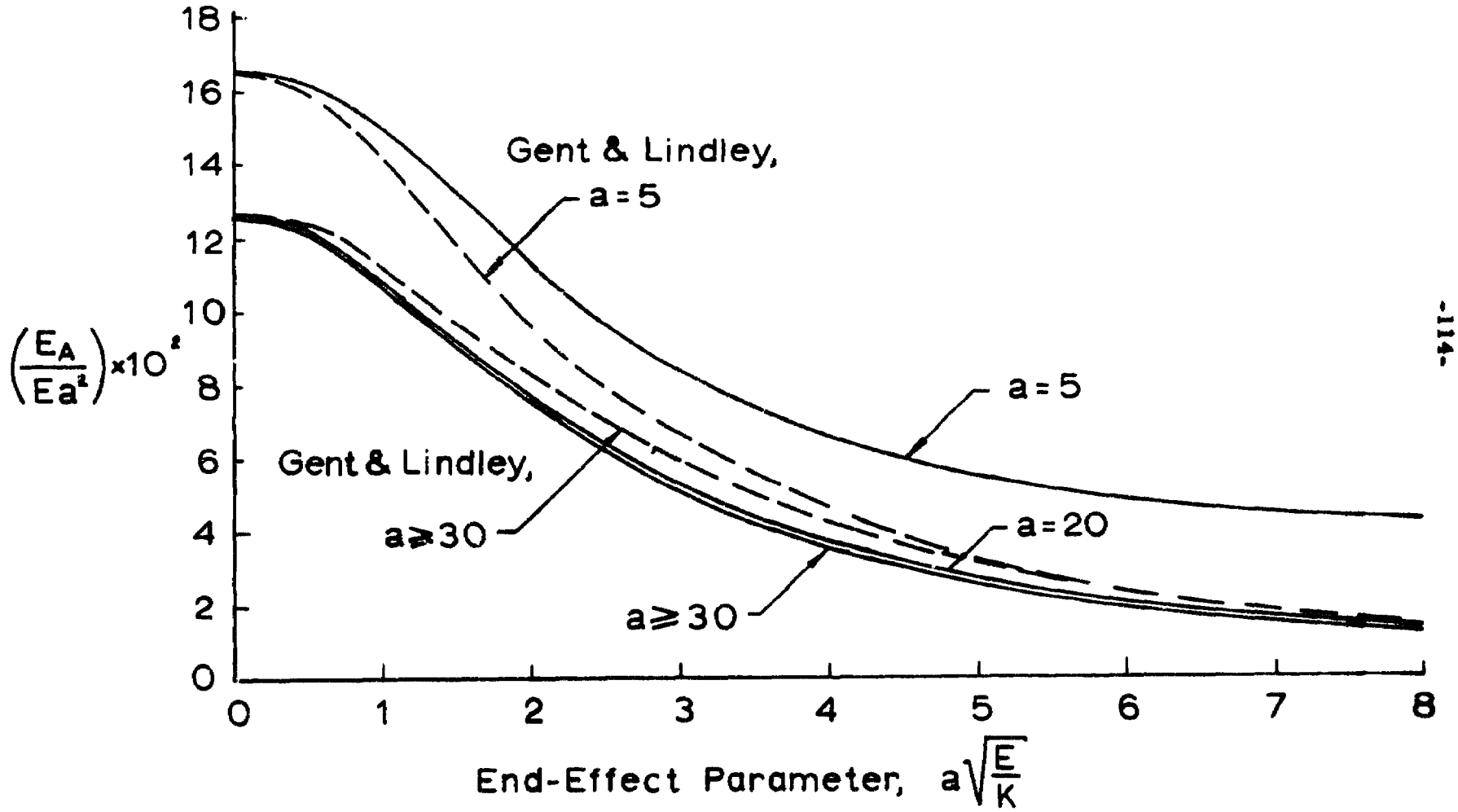

Fig. 3.7. Apparent Modulus of Disk vs. $\left[a\sqrt{E/K}\right]$. Note $E/K = 3(1-2\nu)$.

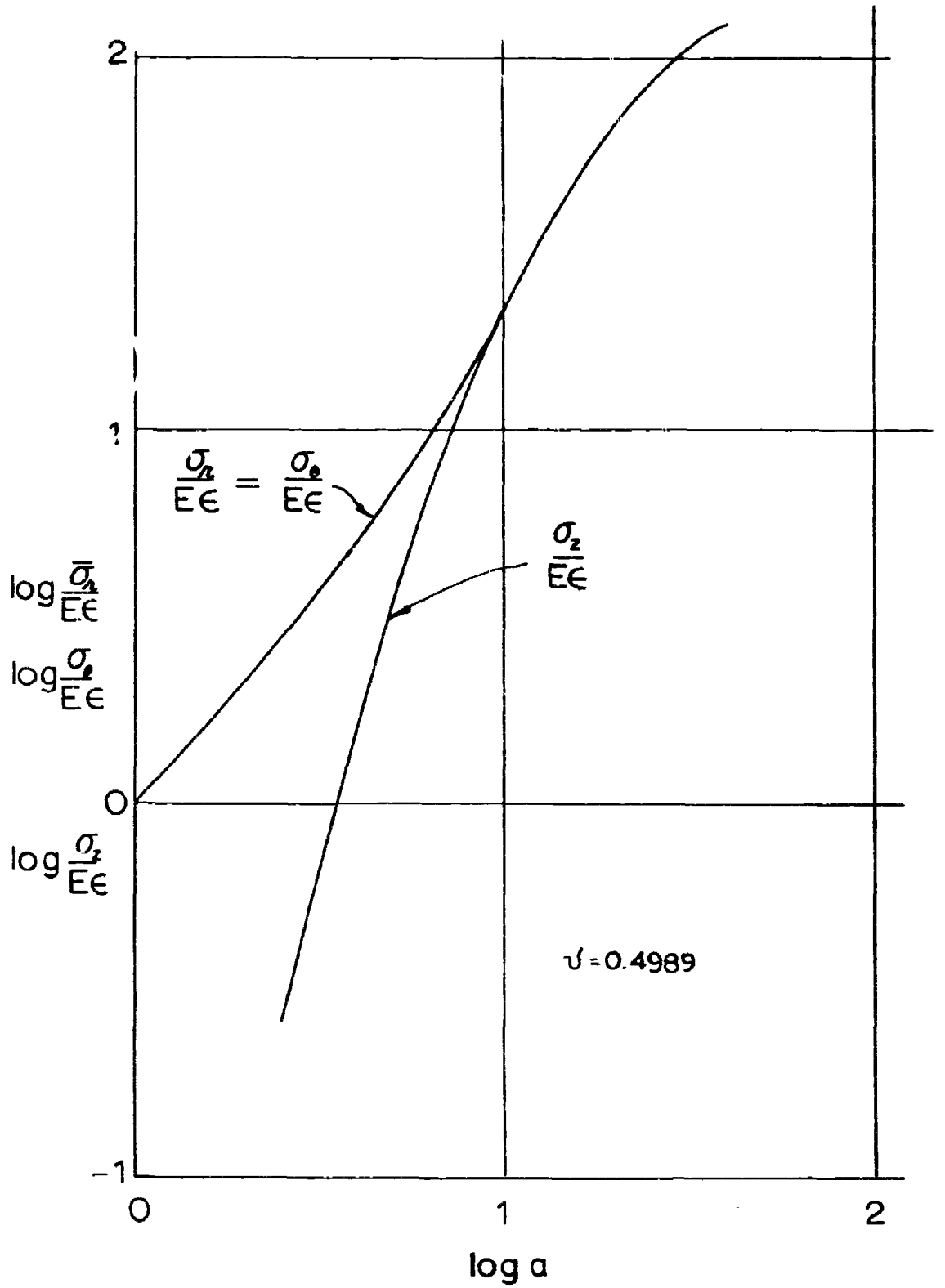

Fig. 3.8. Normal Stresses at the Center of the Poker-Chip versus the Aspect Ratio.

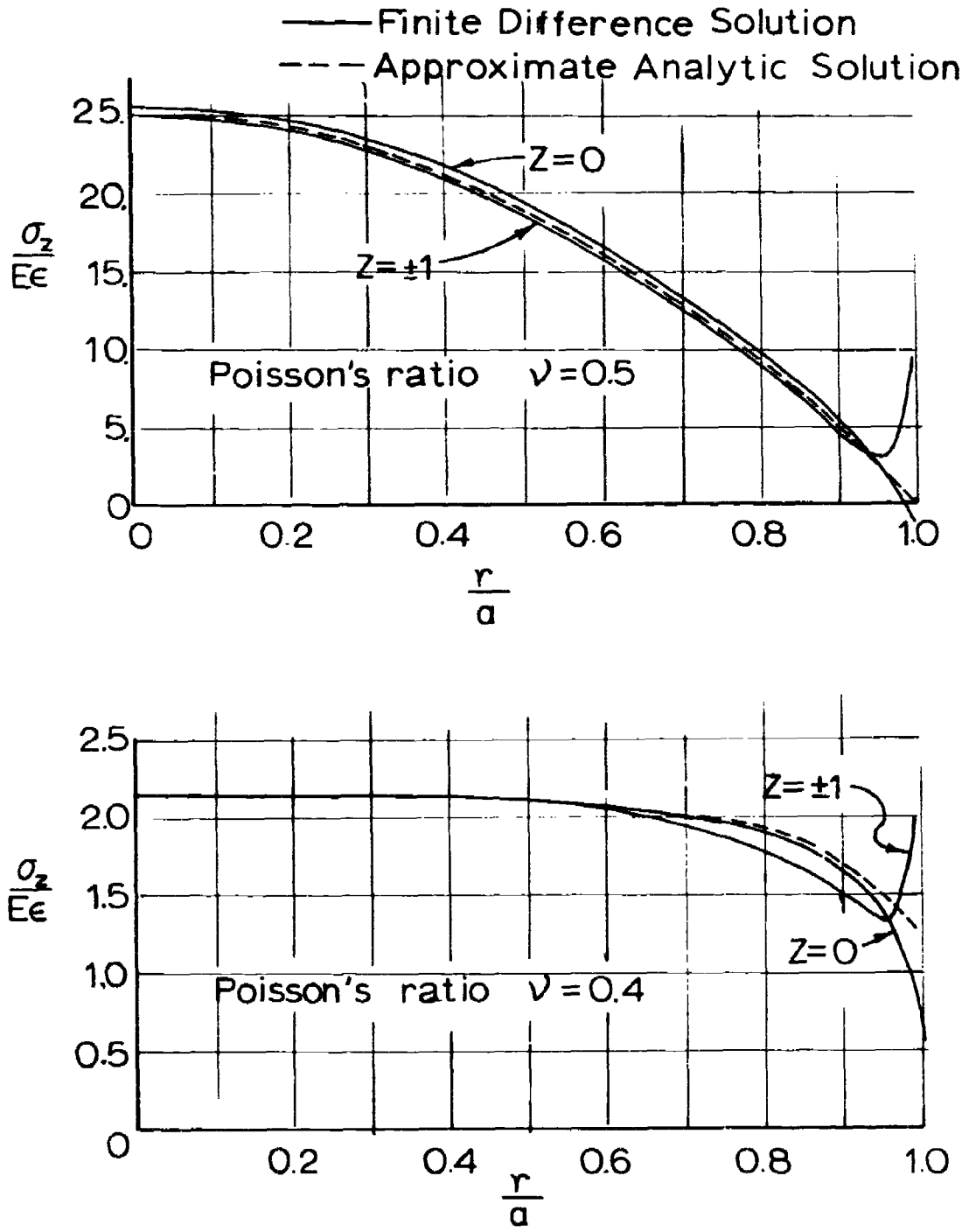

Fig. 3.9. Comparison of Axial Stresses Obtained from Two Different Methods of Solution.

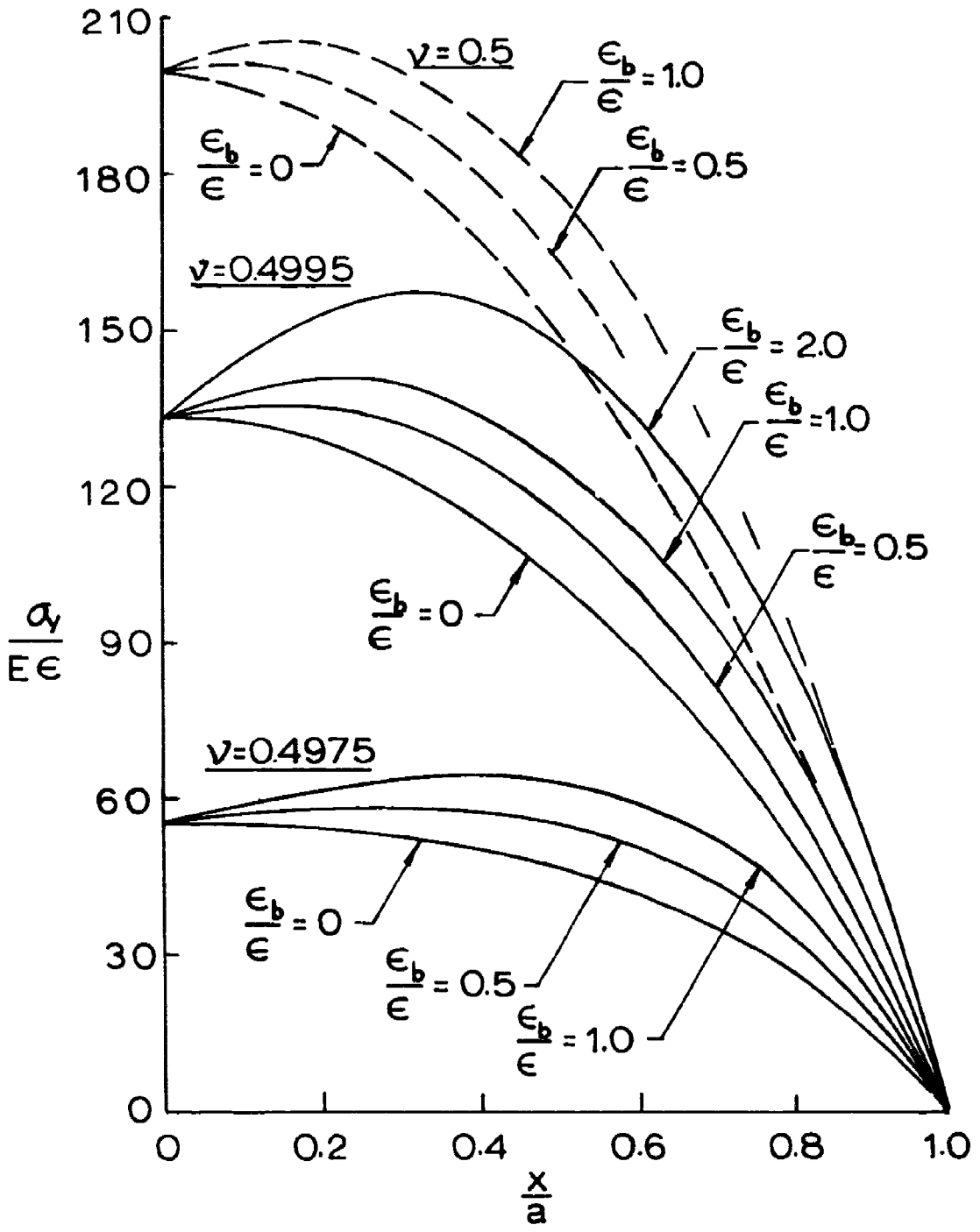

Fig. 3.10. y-Normal Stress in Slab vs. x/a, With Bending: a = 20.

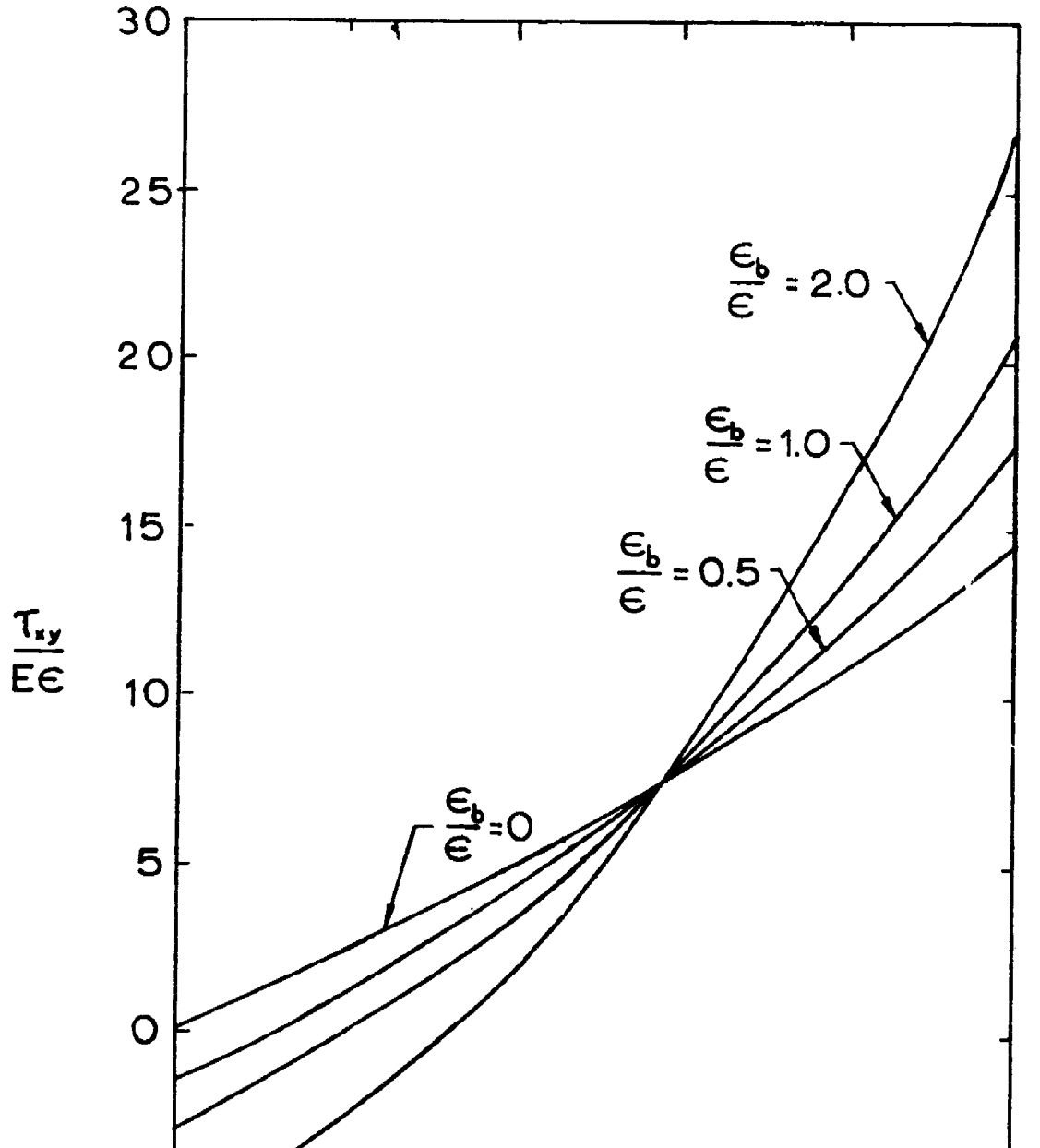

Fig. 3.11. Shear Stress in Slab vs. x/a, with Bending: $\nu = 0.4995$, y = 1, a = 20.

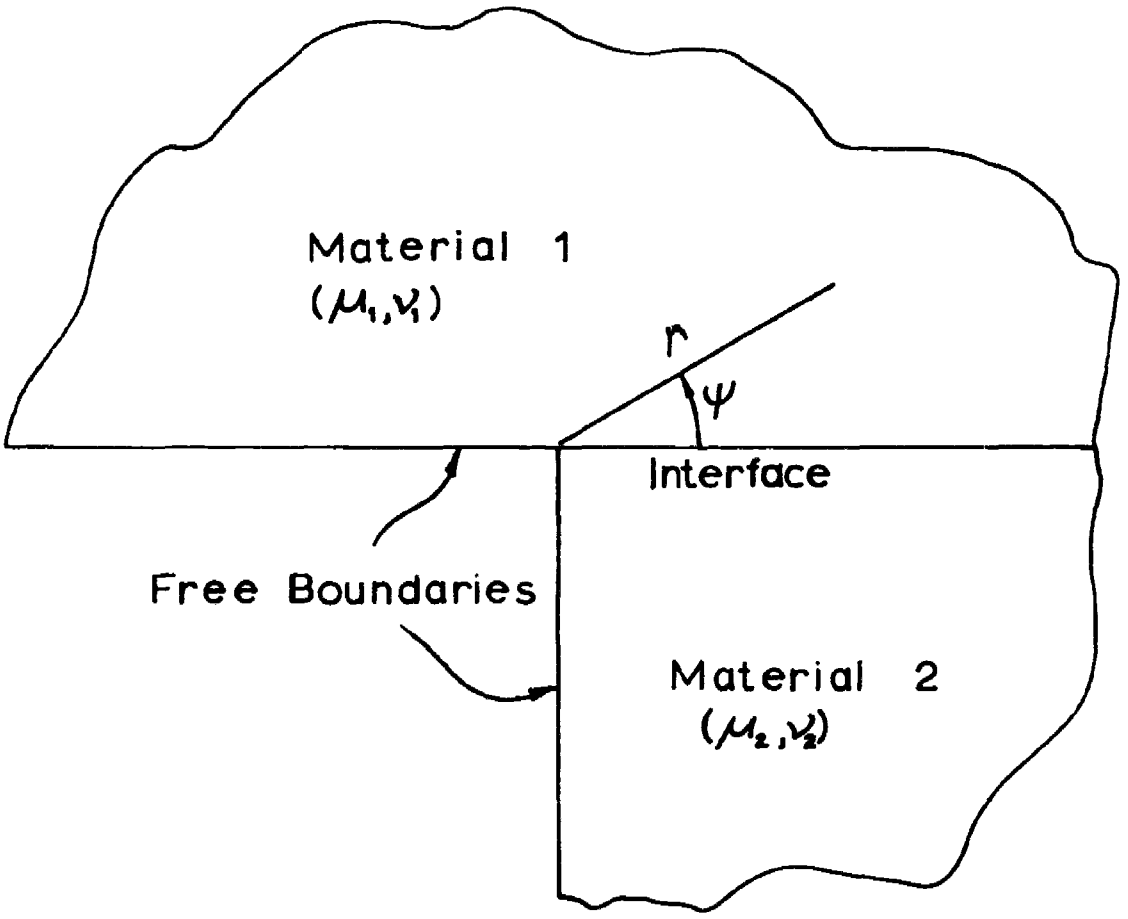

Fig. 3.12. Bi-Material Configuration and the Coordinate System.

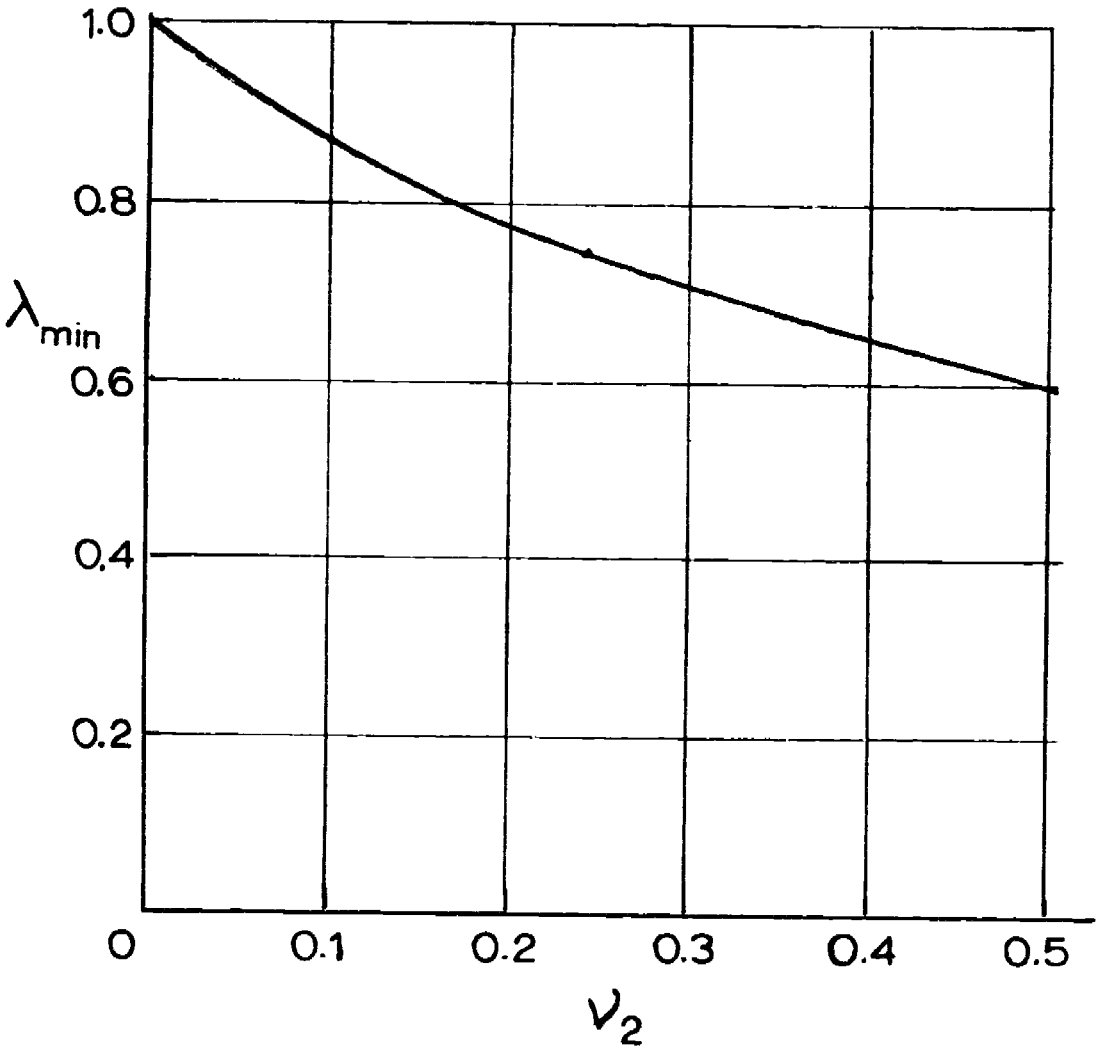

Fig. 3.13. Singularity-Producing Eigenvalue for the Bimaterial Combination. (M_1 assumed nearly rigid).

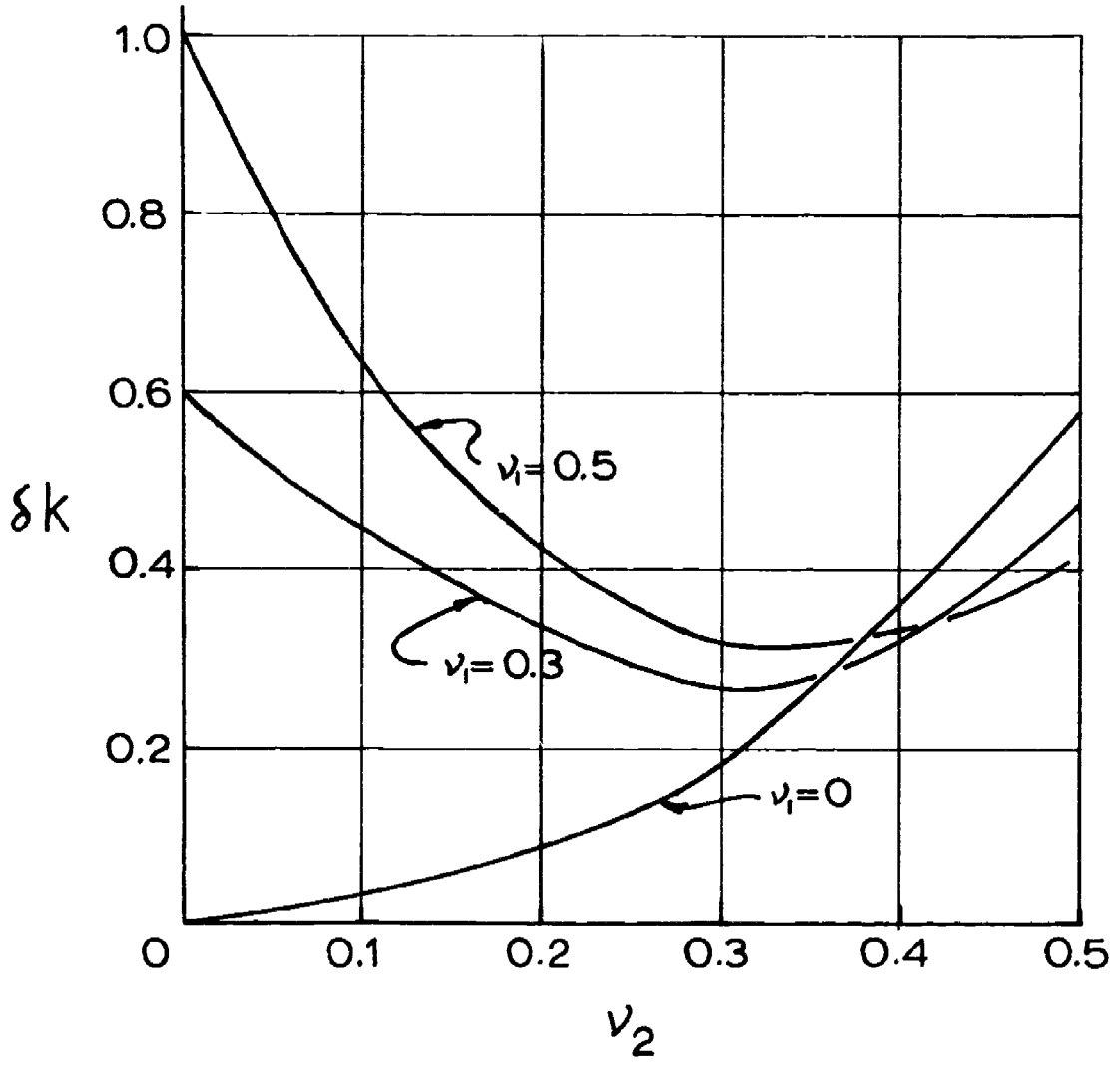

Fig. 3.14. Pertubation in the Singularity-Producing Eigenvalue Due to the Non-Rigidity of Material 1.

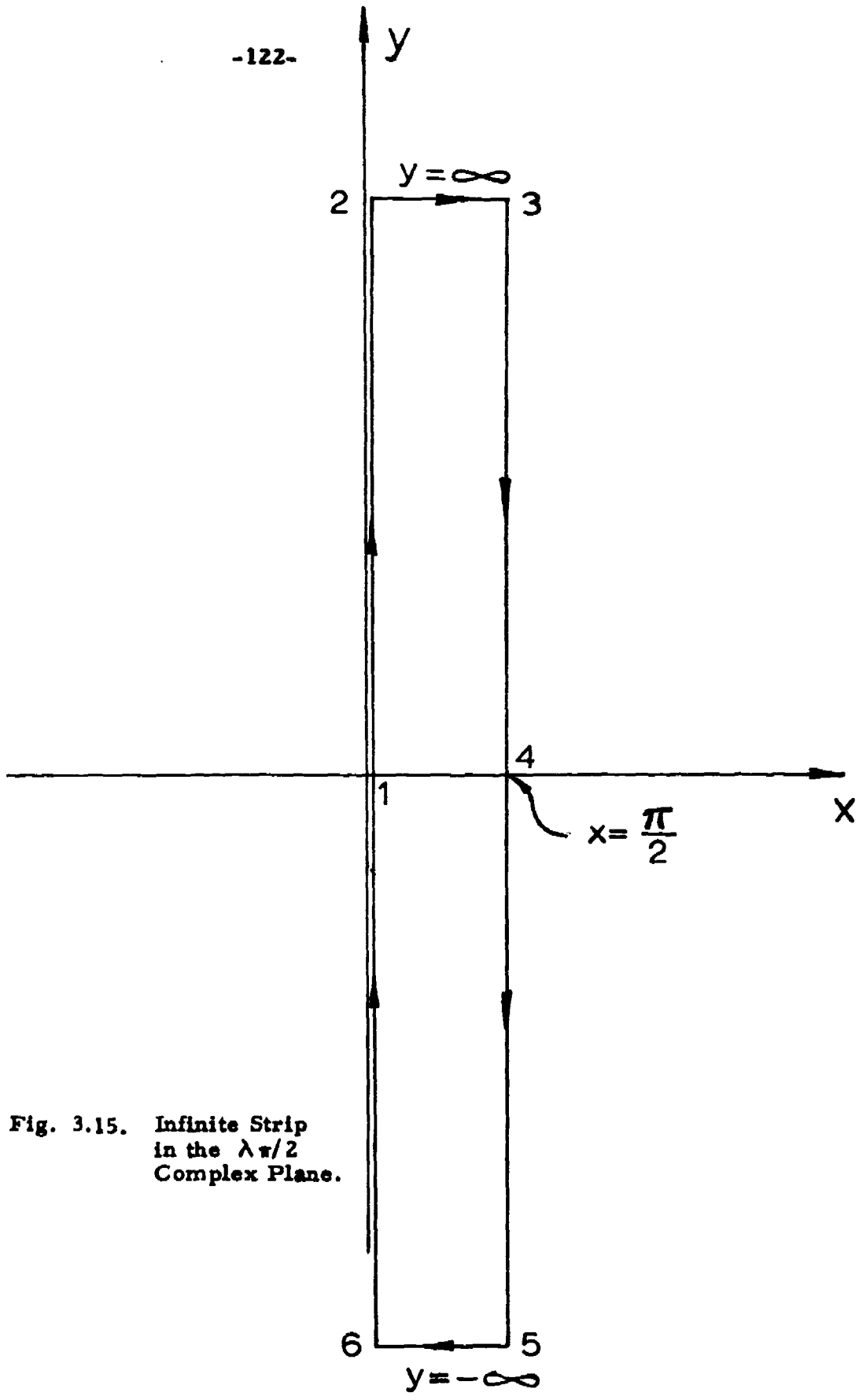

Fig. 3.15. Infinite Strip in the $\lambda\pi/2$ Complex Plane.

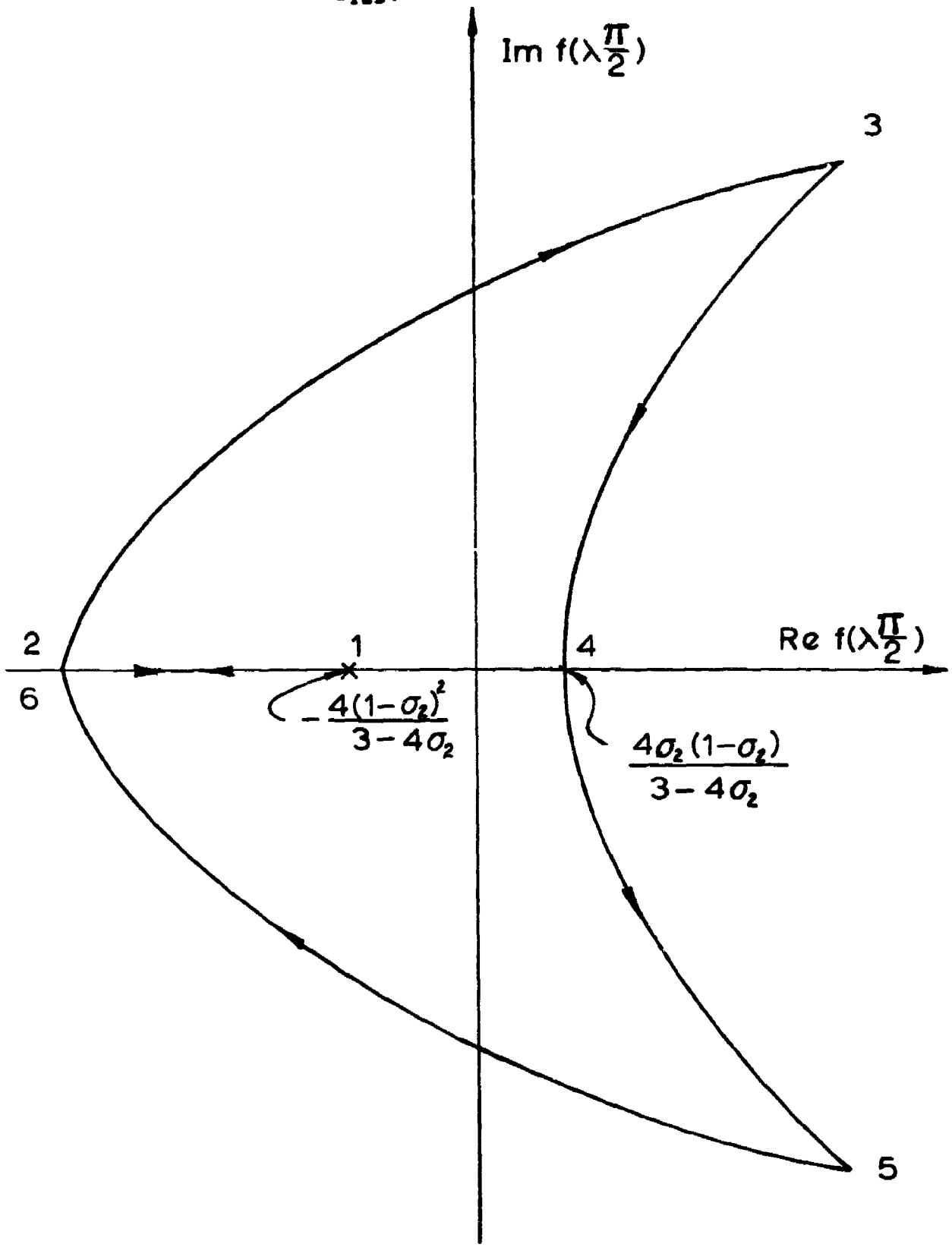

Fig. 3.16. Path Traced by the Vector Representing the Complex Function f (λ π/2).

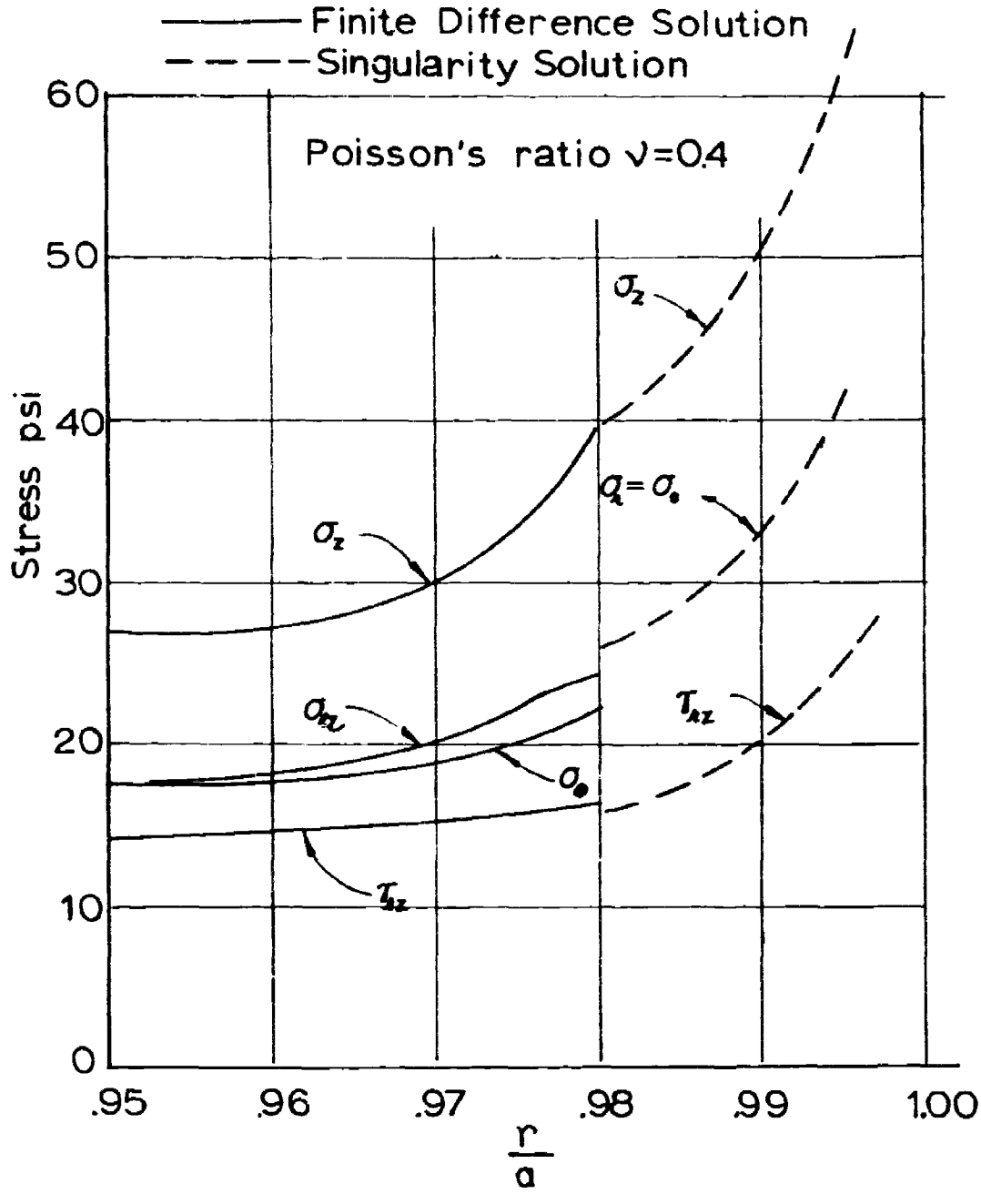

Fig. 3.17. Matching of Stresses from Finite Difference and Stress Singularity Solutions.

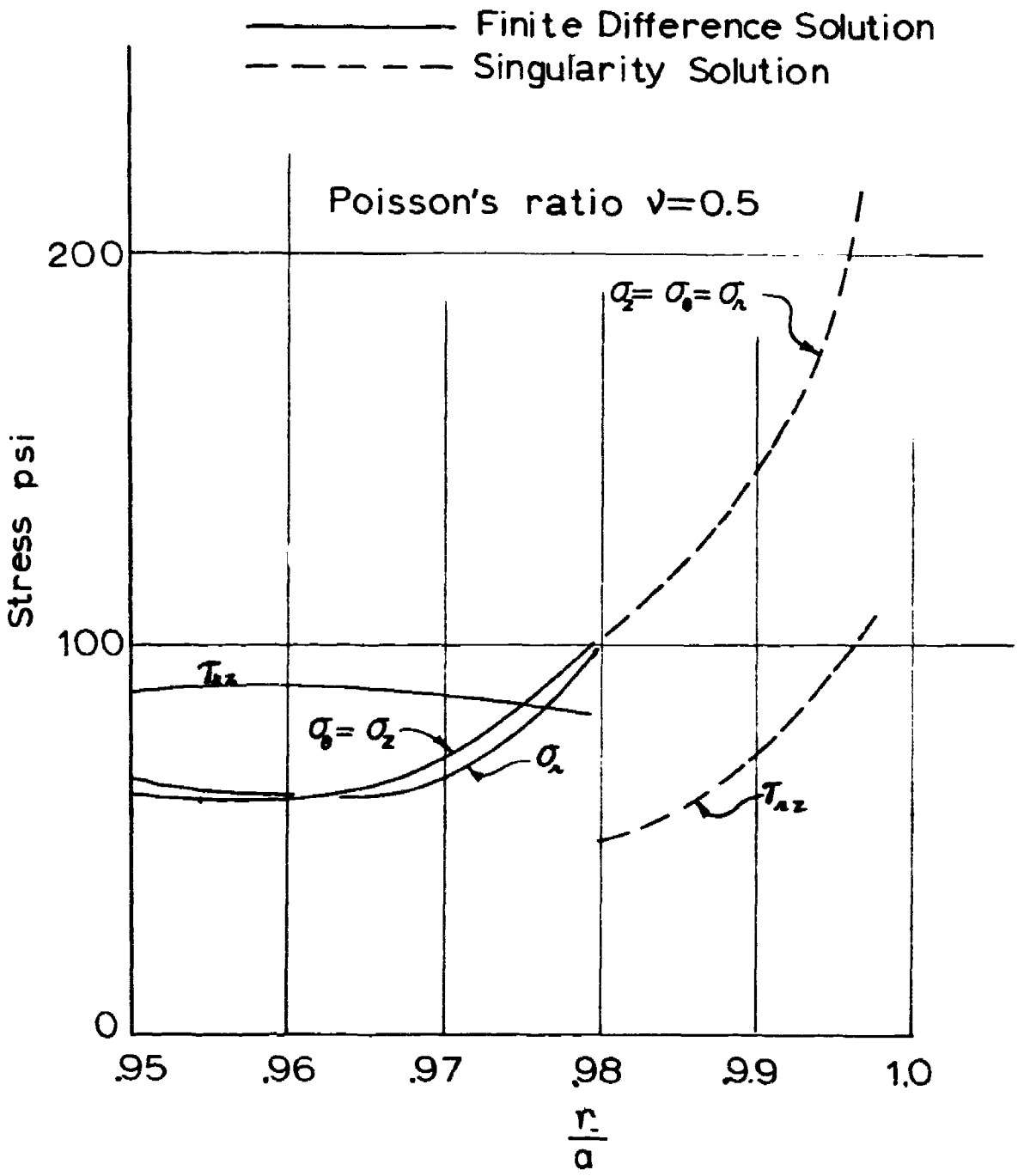

Fig. 3.18. Matching of Stresses from Finite Difference and Stress Singularity Solutions.

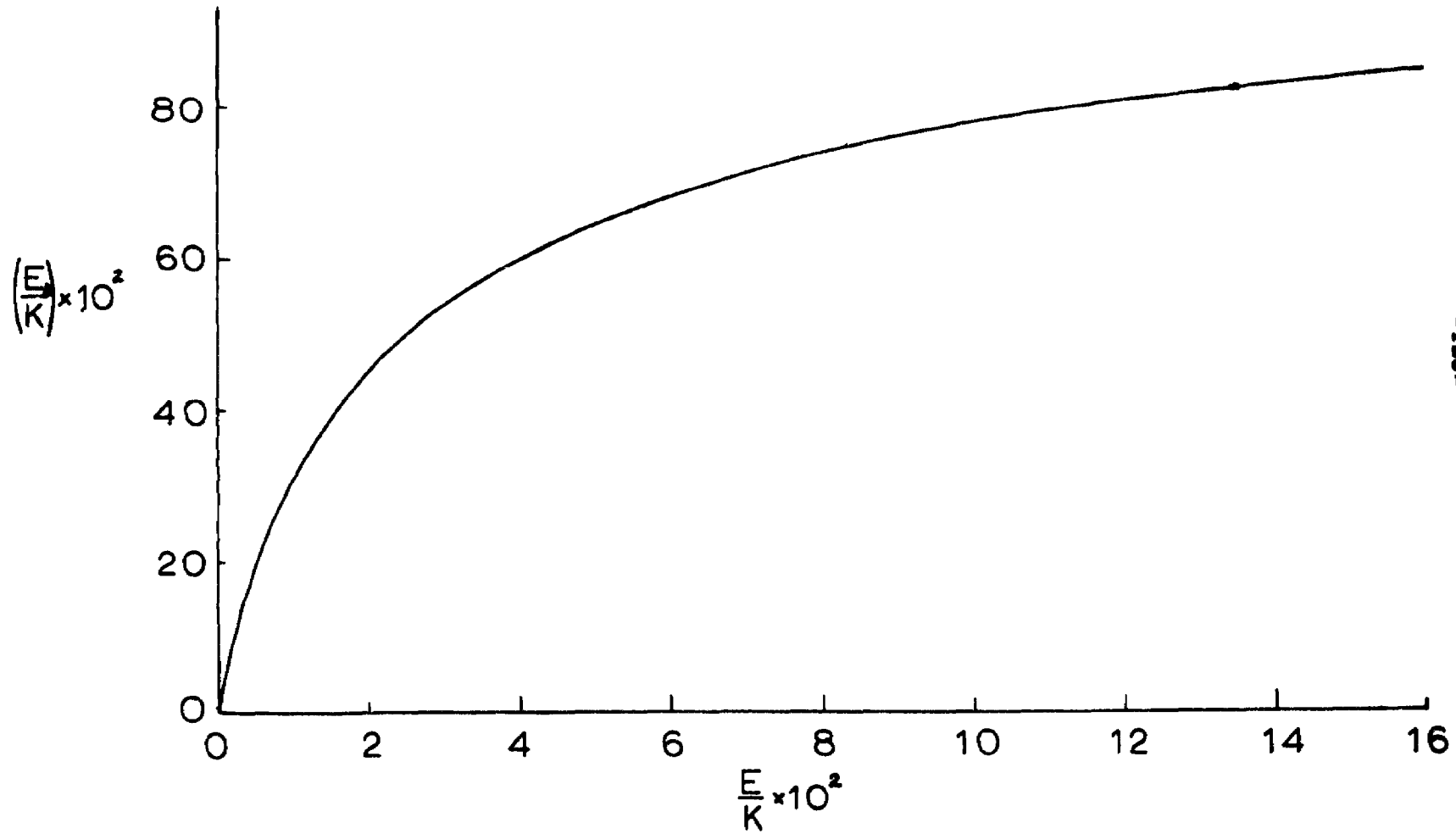

Fig. 3.19. Ratio of Apparent Modulus of Disk to Bulk Modulus vs. E/K: a = 20.

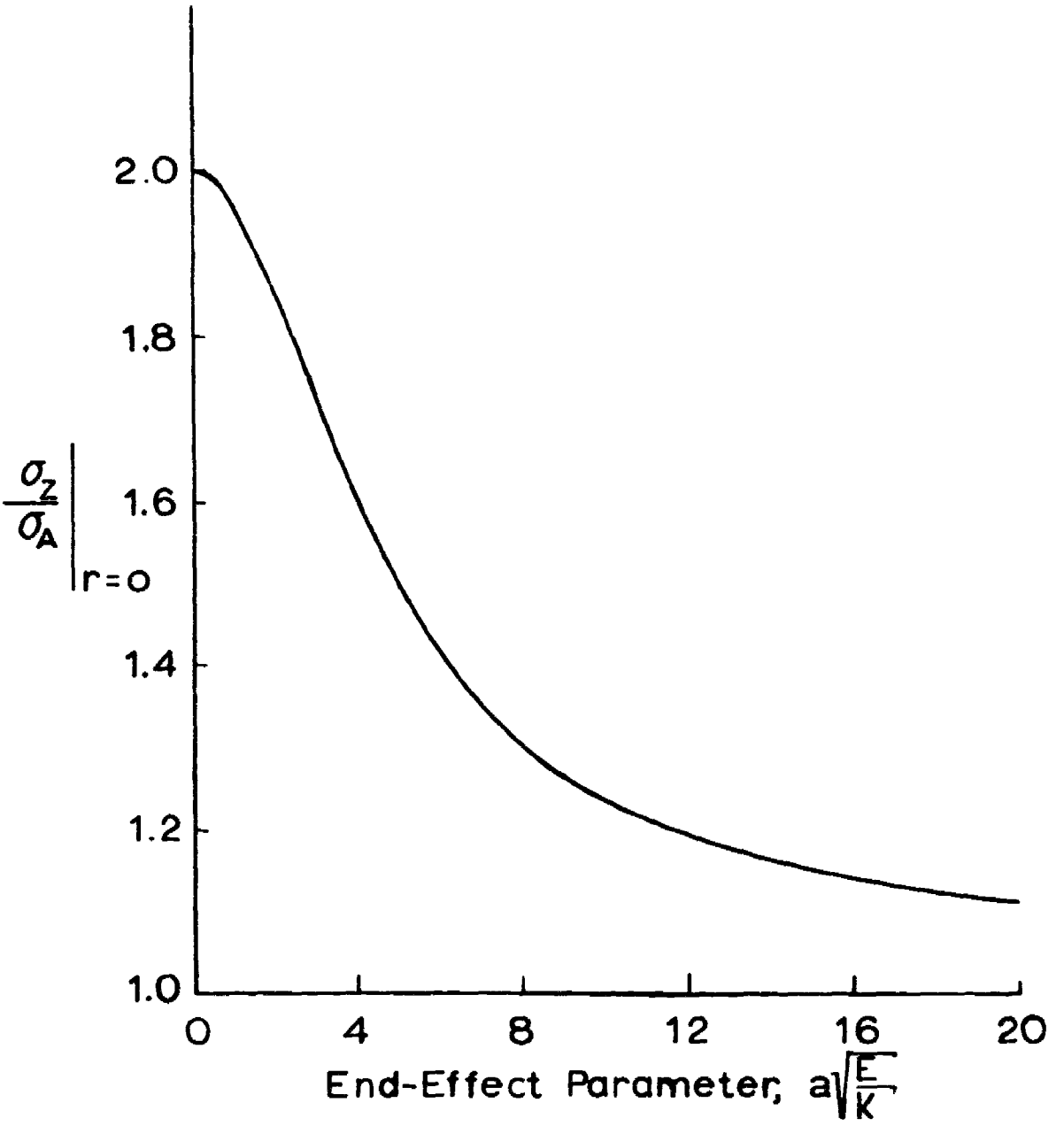

Fig. 3.20. Ratio of Maximum Normal Stress in Disk to Average (Applied) Stress vs. $a\sqrt{E/K}$: $E/K \ll 1$.

4.0 FRACTURE INITIATION FROM INITIAL SPHERICAL FLAWS

4.1 Introduction and Background Information

Since the conditions under which fracture is initiated are so important in engineering applications, it is necessary to understand them thoroughly. Even if one is mainly concerned with the mechanics of crack propagation, the initiation phase or triggering phenomenon is still an important consideration. It is appropriate, therefore, to use the theoretical description of the stress field in Section 3.0 in order to study the problem of flaw initiation and to postulate possible threshhold conditions.

Since the failures that we have observed emerge as sudden, catastrophic bursts in which a spherical void appears, one would suspect the existence of initial "residual" voids which grow under applied load until they reach a critical void size at which this burst occurs. We shall therefore postulate the presence of an initial void and idealize it as a spherical cavity of initial radius a_o imbedded in the center of a spherical medium of initial radius b_o as shown in the sketch below.

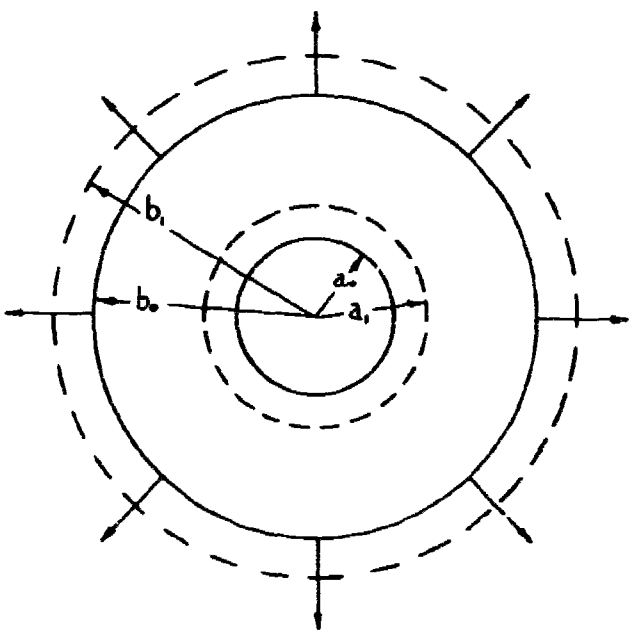

The outside of the medium will be assumed to be subject to a uniform hydrostatic tensile stress, p. Since these cavities will be considered to be small in comparison to the dimensions of the specimen, we will eventually approximate the problem as a spherical cavity in an infinite medium. This will be done in the subsequent analysis by making the ratio of the radii b_o/a_o to be very large compared to unity. In this limit the surface stress p acting at infinity will be assumed to be the local field stress in the poker-chip specimen. The above assumptions also imply that the voids are sufficiently small and isolated so as to have little interaction with each other. This assumption is therefore similar to the dominant flaw concept often invoked in brittle fracture.

When an external pressure is applied, the internal cavity size will increase in such a way that the energy balance between the applied work and the internally stored strain energy will be preserved. On the other hand, one can inquire for conditions under which it is possible for this energy balance to be achieved in an alternate way. In particular, one can visualize increased cavity area arising from the creation, at fracture, of additional surface, which phenomenon requires an incremental increase in surface energy. In the ensuing analysis, failure of the cavity will be associated with incremental energy transfers at some constant critical stress p_c between applied work, internal strain energy, and surface energy. Considerations similar to those used by Griffith[4.1] will be employed, but in addition finite strains will be permitted because of our desired application to rubbery incompressible media.

4.2 Determination of the Critical Pressure

To examine this critical condition a small change δa_o in the original radius a_o is assumed, and the failure condition is specified by the following energy balance equation

$$\delta(\text{External work}) = \delta(\text{Surface energy}) + \delta(\text{Strain energy}) \quad (4.2.1)$$

where in the above equation δ is to be interpreted as the variation with respect to a_o under condition of constant applied stress.

The deformed internal and external radii are respectively a and b, corresponding to two stretch ratios λ_a and λ_b defined as follows

$$\frac{a}{a_o} = \lambda_a \quad (4.2.2)$$

$$\frac{b}{b_o} = \lambda_b \quad (4.2.3)$$

In the present analysis it will be assumed that the medium in question is incompressible and therefore the volume will be conserved during elastic deformation. This relates λ_b to λ_a by the following relation

$$a_o^3(\lambda_a^3 - 1) = b_o^3(\lambda_b^3 - 1) \quad (4.2.4)$$

from which

$$\lambda_b^3 = 1 + \left(\frac{a_o}{b_o}\right)^3(\lambda_a^3 - 1) \quad (4.2.4a)$$

It may be noted that for the configuration with which we are concerned, one has $a_o/b_o \ll 1$ and also $a_o \lambda_a/b_o = a/b_o \ll 1$, so that we have, approximately

$$\lambda_b \doteq 1 + \frac{1}{3}\left(\frac{a_o}{b_o}\right)^3\left(\lambda_a^3 - 1\right) + \cdots \qquad (4.2.5a)$$

$$\lambda_b^2 \doteq 1 + \frac{2}{3}\left(\frac{a_o}{b_o}\right)^3\left(\lambda_a^3 - 1\right) + \cdots \qquad (4.2.5b)$$

The potential energy U_1 of the external load p is equal to the total load acting on the external boundary of the medium times the displacement of that boundary. Therefore

$$U_1 = 4\pi b^2 p\,(b - b_o)$$
$$= 4\pi p\, b_o^3\left(\lambda_b^3 - \lambda_b^2\right) \qquad (4.2.6)$$

or using (4.2.5)

$$U_1 = \frac{4\pi}{3} p a_o^3\left(\lambda_a^3 - 1\right) \qquad (4.2.7)$$

The internal strain energy in the material, U_2, is equal to total work done by the external surface force p during the deformation, assuming no new fracture surface is created. To calculate this energy, the relation between the external load and deformation is required, and this depends on the constitutive laws of the material. For the purpose of the present analysis, it is assumed that the material is Neo-Hookean, so that

it can be characterized by a strain energy function of the form

$$W = \frac{E}{6}\left(I_1 - 3\right) \tag{4.2.8}$$

where in this expression E is the tensile modulus as measured at small strains and I_1 is the first strain invariant

$$I_1 = \lambda_1^2 + \lambda_2^2 + \lambda_3^2 \tag{4.2.9}$$

written for this spherical configuration in terms of the local principal extension ratios

$$\lambda_1 = \lambda_r \quad ; \quad \lambda_2 = \lambda_\theta \quad ; \quad \lambda_3 = \lambda_\phi \tag{4.2.10}$$

where conditions of symmetry require $\lambda_\theta = \lambda_\phi$. The Neo-Hookean material assumption implies incompressibility, i.e.

$$\lambda_1 \lambda_2 \lambda_3 = 1 \quad \text{or} \quad \lambda_r \lambda_\theta^2 = 1 \tag{4.2.11}$$

so that, upon substitution into (4.2.8),

$$W = \frac{E}{6}\left[2\lambda_\theta^2 + \lambda_\theta^{-4}\right] \tag{4.2.8a}$$

Using this constitutive law one may deduce the relation between the radial pressure applied at infinity and the corresponding extension

ratio, at the surface of the cavity, λ_a, (see references 4.2 and 4.3)

$$p = \frac{E}{6}\left[5 - \frac{4}{\lambda_a} - \frac{1}{\lambda_a^4}\right] \tag{4.2.12}$$

which for small strains gives the appropriate limit value

$$p\,(\lambda = 1 + \epsilon_\theta) = \frac{4E}{3}\epsilon_\theta \tag{4.2.12a}$$

Therefore the strain energy stored in the medium is

$$U_2 = \int_1^{\lambda_b} p\, 4\pi b_o^3 \lambda_b^2\, d\lambda_b \tag{4.2.13}$$

Using relations (4.2.5) and (4.2.12), (4.2.13) can be written, assuming $a/b_o << 1$, as

$$U_2 = \int_1^{\lambda_b} 4\pi b_o^3 \frac{E}{6}\left[5 - \frac{4}{\lambda_a} - \frac{1}{\lambda_a^4}\right]\left(\frac{a_o}{b_o}\right)^3 \lambda_a^2\, d\lambda_a \tag{4.2.14}$$

carrying out the integration gives

$$U_2 = \frac{2}{3}\pi E a_o^3\left[\frac{5\lambda_a^3}{3} - 2\lambda_a^2 + \frac{1}{\lambda_a} - \frac{2}{3}\right] \tag{4.2.15}$$

The surface energy of the cavity U_3 is

$$U_3 = 4\pi a_o^2 T \tag{4.2.16}$$

where T is the surface energy per unit area. Physically the quantity

T, which was first introduced for crack problems by Griffith[4.1], can be interpreted as the energy required to perform the necessary molecular bond breaking in order to produce a unit area of new surface.

Using the criterion for the fracture of the cavity, equation (4.2.1), can now be written as

$$\delta(U_1) = \delta(U_2) + \delta(U_3) \tag{4.2.17}$$

where obviously the fact was used that the small change in work done by external force is equal to the change in its strain energy. Substituting into equation (4.2.17) from (4.2.7), (4.2.15) and (4.2.16) and recalling that the variation is carried out at constant pressure with respect to the unfractured radius a_o, it follows that

$$\delta\left[\frac{4\pi}{3} p a_o^3(\lambda_a^3 - 1)\right] = \delta\left[4\pi a_o^2 T\right] + \delta\left[\frac{2}{3}\pi E a_o^3\left(\frac{5\lambda_a^3}{3} - 2\lambda_a^2 + \frac{1}{\lambda_a} - \frac{2}{3}\right)\right] \tag{4.2.18}$$

From equation (4.2.12) it can easily be seen that p is a monotonically varying function of λ_a, and therefore the above variation under the condition of constant pressure implies that λ_a is also constant. Therefore varying (4.2.18) with respect to a_o gives

$$a_o\left[p_c a_o(\lambda_a^3 - 1) - 2T - \frac{E}{2} a_o\left(\frac{5\lambda_a^3}{3} - 2\lambda_a^2 + \frac{1}{\lambda_a} - \frac{2}{3}\right)\right] = 0 \tag{4.2.19}$$

which in addition to the trivial solution $a_o \neq 0$ gives a defining equation for a critical pressure p_c. Upon substituting for p from (4.2.12) and defining a new material parameter

$$k = \frac{6T}{E a_0} \tag{4.2.20}$$

equation (4.2.19) can be rewritten as follows

$$\lambda_a^6 - \frac{3}{2}\lambda_a^4 + \frac{1}{2} - \lambda^4 k = 0 \tag{4.2.21}$$

The above equation defines the critical extension ratio for a given value of the parameter k. The corresponding critical load p_c is related to the critical cavity extension ratio, λ_{ac} by (4.2.12).

4.3 Critical Flaw Sizes

Solutions to equations (4.2.21) will now be investigated. In general this equation can only be solved numerically, which has been carried out with the results presented in Figure 4.1, where the critical extension ratio λ_{ac} and the critical external load $6p_c/5E$ are plotted against the parameter k on a semi-log scale. For the two extreme ranges of k, that is for $k << 1$ and $k >> 1$, approximate analytic expressions can be obtained for the critical extension ratio and the load.

Criticality for Larger Cavities ($k << 1$). In this range where the surface tension is relatively small or the voids reasonably large,

it may be verified that equation (4.2.21) can be closely satisfied by $\lambda_{ac} \doteq 1$. To determine this root, write

$$\lambda_{ac} = 1 + \epsilon \tag{4.3.1}$$

where $\epsilon \ll 1$. Upon substituting (4.3.1) into (4.2.21) and neglecting terms of order ϵ^3 or higher it follows that

$$\epsilon = \sqrt{\frac{k}{6}} = \sqrt{\frac{T}{Ea_o}} \tag{4.3.2}$$

from which

$$\lambda_{ac} = 1 + \sqrt{\frac{k}{6}} \tag{4.3.3}$$

The associated value of the critical pressure, using (4.2.12), is

$$p_c = \frac{4}{3} E \sqrt{\frac{k}{6}} = \frac{4}{3} \sqrt{\frac{ET}{a_o}} \tag{4.3.4}$$

which is valid for infinitesimal strains.

One may first observe that this expression has the familiar form of the Griffith critical stress, wherein the radius a_o plays the part of the half crack length, c in an infinite sheet. For reference, this latter situation gives

$$p_c = \sqrt{\frac{2}{\pi} \frac{ET}{C}} \tag{4.3.5}$$

so that the numerical factor on the critical pressure differs by only 50 percent, reflecting the curvature and biaxial stress field at the flaw. Note further that it is possible to obtain an excellent estimate of the importance of small vs. large strain theory by examining

the departure of the actual extension ratio from the infinitesimal estimate*, (4.3.3) .

Criticality for Smaller Cavities ($k >> 1$). At the other end of the scale, where the surface tension is large compared to the modulus or there exist very small flaws, it is also possible to obtain the approximate root of (4.2.21) as

$$\lambda_{ac} = \sqrt{k} = \sqrt{\frac{6T}{E a_o}} \tag{4.3.6}$$

and the corresponding expression for the critical load is

$$\frac{p_c}{E} = \frac{5}{6}\left[1 - \sqrt{\frac{8}{75}\frac{E a_o}{T}}\right] \tag{4.3.7}$$

The error in equation (4.3.7) is 2.5 percent at $k = 50$ and it decreases as k increases.

Remembering that $k = 6T/Ea_o$ the above results indicate an interesting point. For a given value of $E/6T$ it can be seen from equation (4.3.6) that as the initial radius a_o decreases, the critical extension ratio λ_{ac} increases, and it becomes infinite for vanishingly small cavity radius, although at a finite critical applied pressure of $5E/6$. It can be noted that the high stretch ratios obtained for small voids at fracture confirms the need for finite elastic theory for such geometries.

---

* In the more general case of a compressible material the direct calculation of the critical applied stress for a spherical cavity in an infinite medium can be readily calculated using infinitesimal theory. The result is

$$p_c = \frac{4}{3}\sqrt{\frac{3/2}{1+\nu+6(1-2\nu)}\cdot\frac{ET}{a_o}}$$

In conclusion, it is important to note that the above asymptotic approximations are valid on either end of a 6-decade band, $10^{-3} \lesssim 6T/Ea_o \lesssim 10^{3}$, as can be readily seen in Figure 4.1. For the intermediate transition region the values of critical applied pressure and associated cavity strain may be obtained from the curve.

4.4 Preliminary Remarks on a Triaxial Failure Criterion

It has been shown that in an incompressible material of modulus E and surface energy T there exists a potential critical field stress p_c at which a small internal cavity of radius a_o may grow in size. Because the relation between the field stress and the stress and strain state at the cavity has also been determined, a knowledge of the local conditions at the point of fracture is available to examine the validity of various theories of failure, such as those enumerated in the first section.

At the cavity, the significant quantities are radial and tangential strains

Circumferential strains : $\lambda = \lambda_a$

Radial strain (4.2.11) : $\lambda_r = \frac{1}{\lambda_\theta^2} = \frac{1}{\lambda_a^2}$

and using the constitutive law (4.2.8a), one can find[4.3] the expression for the circumferential stress σ_θ at the cavity surface

$$\sigma_\theta = \frac{E}{3}\left[\lambda_a^2 - \frac{1}{\lambda_a^4}\right] \qquad (4.4.1)$$

Since at the condition of failure the critical extension λ_a is related to p_c and the parameter $\sqrt{6T/Ea_o}$, as shown in Figure 4.1, equation (4.4.1) can be used to relate the circumferential stress at failure to

the same quantities. This has been done and the results are shown in Figure 4.1. For the two limiting values of k the circumferential stress can be explicitly related to p_c and k.

For $k << 1$,

$$\lambda_a = 1 + \sqrt{\frac{k}{6}}$$

and therefore from equation (4.4.1)

$$\sigma_\theta = E\sqrt{\frac{2}{3}k} = \sqrt{\frac{4TE}{a_o}} \tag{4.4.2}$$

and using relation (4.3.4) it follows

$$\sigma_\theta = \frac{3}{2}p_c \tag{4.4.3}$$

This last result can easily be verified from classical elastic theory.

For $k >> 1$,

$$\lambda_a = \sqrt{k}$$

and therefore from equation (4.4.1)

$$\sigma_\theta = \frac{2T}{a_o} \tag{4.4.4}$$

Using the relation (4.3.7) and combining with (4.4.4) it follows

$$\frac{p_c}{E} = \frac{5}{6}\left[1 - \frac{4}{5}\left(\frac{E}{3\sigma_\theta}\right)^{\frac{1}{2}}\right] \tag{4.4.5}$$

or inversely

$$\frac{\sigma_\theta}{E} = \frac{(16/75)}{\left(1 - \frac{6P_c}{5E}\right)^2} \qquad (4.4.6)$$

The asymptotic expressions are also shown in Figure 4.1.

In the experimental phase, mechanical property measurements on one variety of Solithane 113 prepared at its particular curing time and temperature gave a uniaxial tensile modulus of 510 psi and an apparent modulus during the poker-chip test of approximately 17,500 psi. Using the results of the theoretical analysis for this ratio $E_a/E = 34.3$, with an aspect ratio $a = 20$, one finds from Figure 3.7 that

$a\sqrt{E/K} = 1.65$, for which the associated mechanical properties are

$$K = 73,500 \text{ psi} \quad ; \quad \nu = 0.4989$$

With this value of Poisson's ratio we see from Figure 3.4 that the normal stresses are maximum and are virtually constant out to $r/a = 0.2$ or for our specimens ($a = 1$ in) $r = 0.2$ in. Thus within a central ring of 0.4 in. diameter, random, initial failures would be expected to occur, as they have been observed to do.[4.5] However, if there is bending in the test, Figure 3.9 indicates that failure should not initiate in the central region, but rather somewhere in the neighborhood of $r = 0.4$ in., depending upon the relative amount of bending present. This position of initial failure has also been observed.

For the same material formulation, the applied stress, σ_A, at failure for many tests was of the order of 300 psi. (By σ_A stress is meant the applied load divided by the area of the poker-chip as if it were a uniaxial tensile bar.) From Figure 3.19 we find that near the center of the specimen the maximum local field stress is 1.89 σ_A.

Thus $p_c = (1.89)(300) = 566$ psi and therefore using the value of $E = 510$ psi given above it follows that for our specimen, approximately

$$\frac{6p_c}{5E} = 1.332 \qquad (4.4.7)$$

However according to the elastic failure analysis presented previously the value of the parameter $6p_c/5E$ should not exceed unity. In view of the observed strong dependence of failure of poker-chip specimens on rates of loading it is quite possible that this discrepancy is due to viscoelastic effects in the vicinity of the voids. These viscoelastic effects will not be discussed in the present report since, as indicated in Section 3.3.3, they are being further investigated and the results will be presented in subsequent reports.

Comparative Failure Criteria. Having made some investigations into the localized stress and strain state at the point of failure, we now proceed to examine on a global scale the applicability of the various failure criteria outlined in Section 1.1. Our basis of computation will be the field stress in the poker-chip and the true stress in the uniaxial test specimen. The typical failure stresses in the poker-chip have been tabulated above on the basis of the approximate analysis, and the ultimate strength in uniaxial tension was measured on ring specimens as outlined in Section 1.3 at a corresponding strain rate and temperature as the poker-chip. Numerical values given are for room temperature and 0.2 in/min strain rate in both uniaxial and triaxial tests.

(1) Maximum Principal Stress — Qualitatively the experimental results yield support to the maximum principal stress theory, where for equal triaxial tension the failure stress (σ_f) is given by

$$\sigma_f = \sqrt{\sigma_1^2 + \sigma_2^2 + \sigma_3^2} = \sqrt{3}\ \sigma_u$$

where σ_u is uniaxial failure stress and it is found to be 300 psi for our material. Therefore

σ_f = 520 psi

This compares favorably with the average failure stress in poker-chips of 560 psi.

(2) Maximum Principal Strain. From expressions (3.2.19) (3.2.25) and (3.2.26) the strains at failure may be calculated, and for r = 4.0 and ν = 0.4989, we have

$$\epsilon_r = 0.725\epsilon, \quad \epsilon_\theta = 0.725\epsilon \quad \epsilon_z = \epsilon$$

Experimental results yielded failures at values of $\epsilon \doteq .01$; thus, the field strains are the order of infinitesimal theory in the poker-chip. In contrast to this, the strains in uniaxial tension are 0.60 to 0.75, which eliminates maximum principal strain as the failure criterion, since it would require the strains in the poker-chip to be larger than those in the uniaxial case.

(3) Maximum Principal Stress Difference. In the limit of incompressible materials and infinite aspect ratio, there is no principal stress difference, which indicates that shearing stress is not an important factor in the failure if these

limit conditions are approached in any substantial degree in the laboratory. To illustrate that this is not the criterion which is valid, we compare values from (3.2.28)

$$\sigma_1 = \sigma_2 = 1.02\,\sigma_3$$

Thus $\Delta\sigma_{max} = .02\,\sigma_3 = 11.32$ psi, where for uniaxial tension, $\Delta\sigma_{max} = 300$ psi, and there is no failure correlation.

(4) Maximum Principal Strain Difference. Similar remarks to those made for maximum principal stress difference can be made here. The strain in the uniaxial specimen is much larger than in the poker-chip and this discrepancy is further magnified when differences are taken. It is therefore appropriate to delete maximum principal strain difference as a possible criterion.

(5) Maximum Total Strain Energy. By equating the tal strain energy in a uniaxial tensile specimen to that of . poker-chip, we find from (3.2.32)

$$\sigma_u^2 = \frac{1}{3}\left\{(1+\nu)\left[(\sigma_1-\sigma_2)^2\ (\sigma_2-\sigma_3)^2\ (\sigma_1-\sigma_3)^2\right]+(1-2\nu)\left[(\sigma_1+\sigma_2+\sigma_3)^2\right]\right\}$$

where σ_u is ultimate strength in uniaxial tension.

For Solithane we find,

$$\sigma_1 = 13\,\sigma_u$$

which does not conform to observed results and can be eliminated as a failure criterion.

(6) Maximum Distortional Strain Energy. The maximum distortional strain-energy criterion (1.1.1) can be quickly checked for the poker-chip test by assuming

$$\sigma_3=\sigma \qquad \sigma_1=C_1\sigma \qquad \sigma_2=C_2\sigma$$

where $C_2 = C_1 + b \qquad C_1 = C$

and ϵ is small compared to 1. Substituting in (1.1.1) and neglecting quantities of order ϵ^2

$$\sigma_u=\sigma(C-1)\sqrt{1+\frac{\epsilon}{C-1}} \tag{4.4.8}$$

Expanding the radical in a binomial series, and neglecting terms of order ϵ^2

$$\sigma_u=\sigma\left|C-1+\frac{\epsilon}{2}\right|$$

Substituting the appropriate values for C and ϵ

$$\frac{\sigma}{\sigma_u}=\left|\frac{2}{(C_1-C_2)-2}\right| \tag{4.4.9}$$

From equation (3.2.28) for failure at a typical radial location

$$\sigma_1=\sigma_2=1.02\,\sigma_3 \Rightarrow C_1=1,\ C_2=1.02$$

which predicts the failure stress in the poker-chip to be much too high. On the basis of preliminary results, we can dispose of all of the criteria except maximum principal stress. More than likely some more general surface will be required to specify the failure for general stress state and work is already in progress to accurately define the failure surface at room temperature and fully relaxed strain conditions. In addition, it is planned that a complete

relation ship between uniaxial tension and triaxial tension be obtained for a wide range of temperature and strain rates.

In discussing comparative failure, it is important to recognize that there are two important considerations: (1) the overall three dimensional stress field with their association to the various failure theories, and (2) the interpretation of failure as a local, flaw instability, phenomenon. In this latter situation further study is also needed, especially in comparing for example results obtained from tests on sheet materials with those in the poker-chip. At this time our preliminary correlations are not deemed sufficiently conclusive to report.

REFERENCES

4.1 Griffith, A. A.: The Phenomena of Rupture and Flow in Solids. Philosophical Transactions of the Royal Society (London) Series A, Vol. 221, 1921.

4.2 Gent, A. N.; Lindley, P. B.: "Internal Rupture of Bonded Rubber Cylinders in Tension." Proceedings of the Royal Society A. Vol. 249, 1959, p. 195.

4.3 Green, A. E.; Zerna, W.: Theoretical Elasticity, University Press, Oxford.

4.4 Timoshenko, S.; Goodier, J. N.: Theory of Elasticity, McGraw-Hill Book Company, New York, 1951.

4.5 Williams, M. L.; Schapery, R. A.: "Studies of Viscoelastic Media." Aeronautical Research Laboratories, Wright-Patterson Air Force Base, Ohio, ARL 63-366, June 1962.

4.6 Knauss, W. G.: Personal communication.

4.7 Bueche, A. M.; Berry, J. P.: "The Mechanisms of Polymer Failure." Conference on Fracture, National Academy of Sciences, 1957.

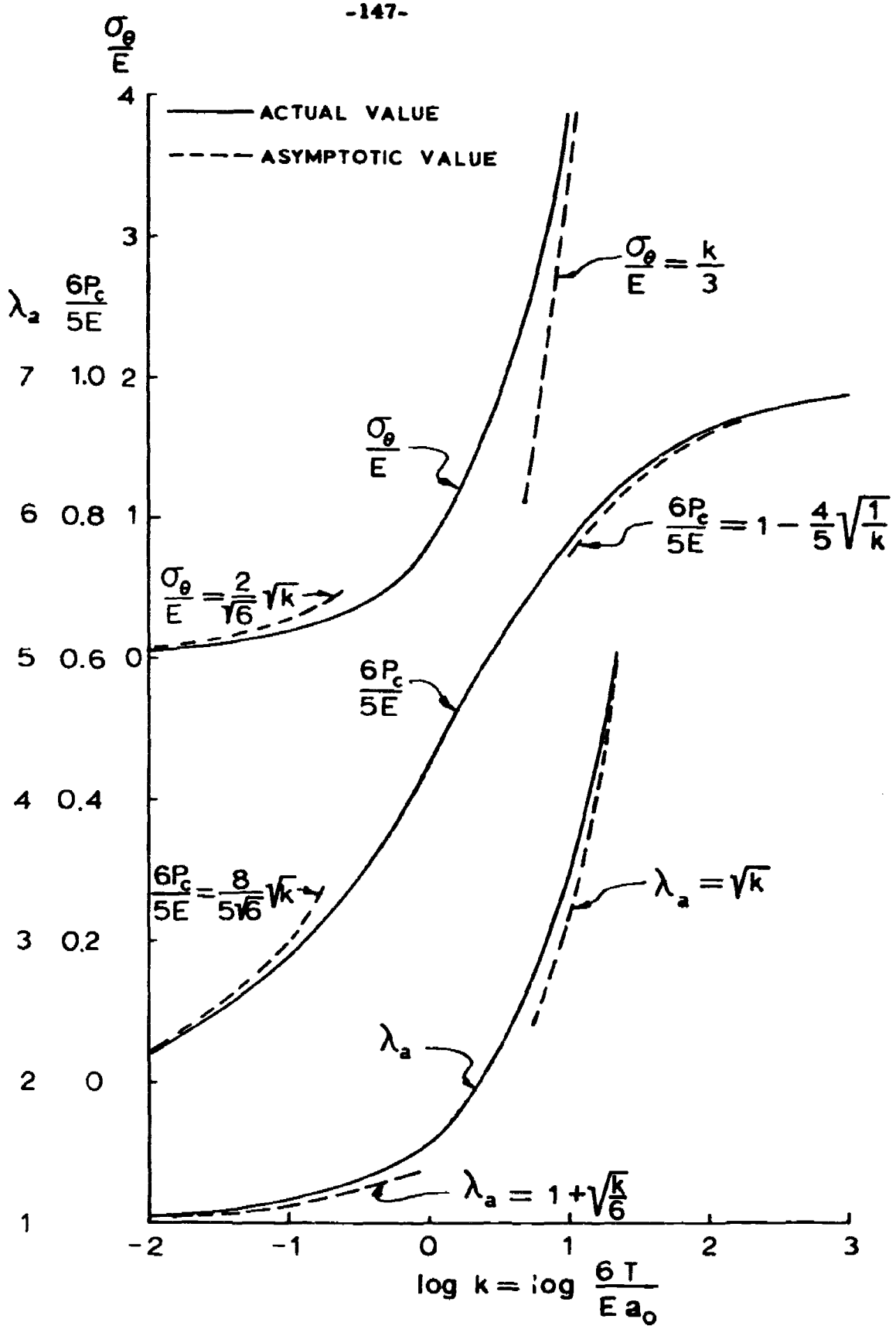

Fig. 4.1. Critical Conditions for Instability of an Initial Spherical Cavity.

5.0 CONCLUSIONS

While the work reviewed in this report in effect reports current results in a continuing study, it is worth emphasizing that several specific points have been established.

1. There has been little work in determining multiaxial failure criterion for viscoelastic material as a function of strain rate and temperature.

2. The triaxial poker-chip specimen can be a satisfactory tool for determining fracture under triaxial tensile stress.

3. A relatively simple stress analysis of the poker-chip configuration has been presented. The results are internally consistent and agree well with a more precise and extensive numerical analysis; moreover, in conjunction with the singular stress evaluation which is valid near the edges, a quantitative assessment of the state of stress throughout the entire geometry can be obtained.

4. A multiaxial failure criterion has not yet been fully established for the material tested; however with further experimental data, this will soon be possible.

5. An instability criterion for the catastrophic growth of small spherical flaws has been obtained. It is important to note that this criterion includes large as well as small strain effects, and as such can be applied to any initial void size.